NOVEL CONCEPTS IN PIEZOHYDRAULIC PUMP DESIGN

A Thesis
Presented to
The Academic Faculty

By

Charles Anderson Keller

In Partial Fulfillment
Of the Requirements for the Degree
Master of Science in Mechanical Engineering

Georgia Institute of Technology

May, 2004

NOVEL CONCEPTS IN PIEZOHYDRAULIC PUMP DESIGN

Approved by:

Dr. Christopher S. Lynch, Advisor

Dr. Kenneth A. Cunefare

Dr. Yves H. Berthelot

Date Approved: March 26, 2004

ACKNOWLEDEMENT

I would like to thank my advisor, Dr. Christopher Lynch for his insight into the subject matter and for teaching me the steps to perform meaningful research.

I thank the thesis reading committee, Dr. Yves Berthelot and Dr. Kenneth Cunefare, for taking the time to speak with me and review my thesis.

I thank my wife for her devotion and continuous support of my endeavors.

I thank my parents for always teaching me to reach for the highest goals.

I thank my fellow graduate students for their willingness to listen and pleasant company.

TABLE OF CONTENTS

Acknowledgement iii

List of Tables viii

List of Figures ix

Summary xiii

Chapter 1 Introduction/ Literature Review 1

1.1 Introduction 1

1.2 History of Piezoelectricity 3

1.3 Mechanics of Piezoelectric Materials 5

1.4 Poling Characteristics and Switching 6

1.5 Constitutive Laws and Characteristic Response 10

1.6 Piezoelectric Transducers 14

1.7 Actuator Types 15

1.7.1 Composite Unimorph 15
1.7.2 Ultrasonic Motors (USM's) 16
1.7.3 Piezo Stack Actuators 16

1.8 Piezoelectric Hydraulic Pump 17

Chapter 2 Aluminum Piezoelectric Hydraulic Pump Using Check Valves 20

2.1 Introduction 20

2.2 Background 20

2.3 Pump System Design 23

2.4 Experimental Setup/ Testing of the System 28

2.5 Experimental Results 30

2.6 Discussion 34

Chapter 3 Introduction to Fluid Resonator Systems 37

3.1 Introduction 37

Chapter 4 Head Mass Resonator 40

4.1 Introduction 40

4.2 Resonator Design Requirements 40

4.3 Calculations Using Chosen Hardware 43

4.4 Testing and Results 45

4.5 Discussion 47

Chapter 5 Design of Piezo Driven 20kHz Fluid Cavity Resonator 48

5.1 Introduction 48

5.2 Diaphragm Design 49

5.2.1 Diaphragm Design Characteristics 49
5.2.2 Diaphragm Construction 50
5.2.3 Diaphragm Finite Element Analysis 51

5.3 Piezoelectric Driving System 54

5.4 Fluid Cavity Design – 20 kHz Operation 57

5.5 Experimental Setup – Closed Chamber 58

5.6 Results – Closed Chamber 61

5.7 Rectification Investigation for Use in Piezohydraulic Pump 63

5.7.1 Introduction 63
5.7.2 Reed Valve – Frequency Response 63
5.7.3 Reed Valve – Fatigue Investigation 65
5.7.4 Reed Valve – Discussion 68
5.7.5 Vortex Fluid Diode 69
5.7.6 Flow Testing 72
5.7.7 Nozzle/ Diffuser Rectification 73

5.8 Results – 20 kHz Operation Using Fluid Diodes 74

5.9 Discussion – 20 kHz Resonator 75

Chapter 6 Design of 1 kHz Fluid Resonator 77

6.1 Introduction 77

6.2 Resonant Frequency Calculations 77

6.3 Reed Valve Design – 1 kHz Operation 78

6.3.1 Reed Valve Fatigue Investigation 79

6.4 1 kHz Resonator Construction 80

6.5 Experimental Setup 83

6.6 Results and Discussion – 1kHz Resonator 84

Chapter 7 Non-resonant Pump Utilizing High Speed Reed Valves 86

7.1 Introduction 86

7.2 Reed Valve Pump Design 86

7.3 Experimental Setup 90

7.4 Experimental Results 92

7.5 Discussion 95

Chapter 8 Concluding Remarks and Recommendations 97

Appendix A Check Valve Pump Dimension Drawings 100

Appendix B Head Mass Resonator Dimension Drawings 111

Appendix C 20 kHz Fluid Resonator Dimension Drawings 114

Appendix D Vortex Fluid Diode Dimension Drawings 119

Appendix E 1 kHz Fluid Resonator Dimension Drawings 121

Appendix F Reed Valve Dimension Drawing 129

Appendix G Reed Valve Pump Dimension Drawings 131

Appendix H Finite Element Result for Aluminum Diaphragm 134

Appendix I Spread Sheet Data 136

References 139

LIST OF TABLES

Table 2.1 Blocked Pressure Readings with Varying Bias Pressure Driven at 150V 34

Table 5.1 Natural Frequency Calculations for 10kHz and 20kHz 65

Table 5.2 Properties of 1095 Carbon Steel Q&T at 200°F 66

Table 5.3 Measured Flow Rates for Vortex Diodes 72

Table 5.4 Percent Reduction in Flow Versus Free Flow 73

Table 6.1 Maximum Valve Lengths 79

LIST OF FIGURES

Figure 1.1 Cubic and Tetragonal Crystal Structures for PZT 6

Figure 1.2 Description of Pole Switching 8

Figure 1.3 Domain Polarization 10

Figure 1.4 Electric Displacement vs. Electric Field for Representative PLZT 12

Figure 1.5 Typical Longitudinal Strain vs. Electric Field Response 14

Figure 1.6 Early Generation Piezo Pump 18

Figure 2.1 Fluid Flow Diagram 23

Figure 2.2 Spool Valve Solid Model 24

Figure 2.3 Spool Valve Photograph 25

Figure 2.4 Three Epcos Stacks 26

Figure 2.5 PZT Housing 26

Figure 2.6 Piston and Cylinder Using O-ring Seal 27

Figure 2.7 Wireframe of Top Half of Cylinder Head 28

Figure 2.8 Experimental Setup of Aluminum Check Valve Pump 29

Figure 2.9 Photograph of PZT Pump System 29

Figure 2.10 Flowrate vs. Frequency: 150V Drive, Various Bias Pressures 31

Figure 2.11 Check Valve Pump Flowrate Measurements 33

Figure 4.1 PZT Resonator Assembly 41

Figure 4.2 Three Stack PZT Resonator 45

Figure 4.3 Experimental Setup of Laser Vibrometer 46

Figure 4.4 Velocity Magnitude at First Natural Frequency 46

Figure 5.1 Aluminum Diaphragm 51

Figure 5.2 Finite Element Model of Diaphragm 53

Figure 5.3 EPCOS Stack Actuator Top and Side View 56

Figure 5.4 EPCOS PZT Array 56

Figure 5.5 Fluid Resonator Assembly 57

Figure 5.6 Resonating Fluid Cavity 58

Figure 5.7 Schematic of Closed Chamber 20 kHz Resonator 59

Figure 5.8 Resonator Assembly (side view) 60

Figure 5.9 Resonator Assembly (end view) 60

Figure 5.10 Pressure vs. Frequency for Closed Chamber 61

Figure 5.11 Pressure Sensor Location Data for .10 in. Diaphragm 62

Figure 5.12 Vortex Fluid Diode 70

Figure 5.13 Dimensional Drawing of Fluid Diode (Dimensions in Inches) 71

Figure 5.14 Large Vortex Fluid Diode 72

Figure 6.1 End Cap, Valve Cover Removed 81

Figure 6.2 Inlet Port and Valve Cover 82

Figure 6.3 Reed Valve Detail 82

Figure 6.4 Experimental Setup of 1kHz Resonator 83

Figure 7.1 Cylinder Head Base 88

Figure 7.2 Cylinder Head Top 88

Figure 7.3 Reed Valve 89

Figure 7.4 Reed Valve Pump Subsystem 89

Figure 7.5 Schematic of Experimental Setup 90

Figure 7.6 Reed Valve Pump Assembly 92

Figure 7.7 Flow Rate vs. Frequency for various reed valve thickness; 150V, .082in. diaphragm 93

Figure 7.8 Flow Rate vs. Frequency, Diaphragm Thickness Variation; 150 V, .010in. Valves 95

Figure A.1 Pump Body Assembly 101

Figure A.2 Backing Plate 101

Figure A.3 End Screw Cap 102

Figure A.4 PZT Housing 103

Figure A.5 Cylinder Head Base 105

Figure A.6 Cylinder Head Top 106

Figure A.7 Spool Valve Body 108

Figure A.8 Spool Valve Rod 110

Figure B.1 Head Mass Resonator Assembly 112

Figure B.2 Head Mass 112

Figure B.3 Tail Mass 113

Figure C.1 20 kHz Resonator Fluid Cavity 115

Figure C.2 O-ring 116

Figure C.3 Rear PZT Housing 117

Figure D.1 Large Fluid Diode 120

Figure D.2 Small Fluid Diode 120

Figure E.1 Resonator Body 122

Figure E.2 Resonator Body End Cap 124

Figure E.3 Inlet Valve Cover 125

Figure E.4 Outlet Valve Cover 127

Figure F.1 Reed Valve 130

Figure G.1 Pump Head Base 132

Figure G.2 Pump Head Top 133

Figure H.1 Finite Element Result of .10 in. Diaphragm 135

Figure I.1 Reed Valve Frequency Response for Fluid Resonators 137

Figure I.2 Reed Valve Fatigue Calculations (All Applications) 138

SUMMARY

Over the past several years, there has been significant development in the field of applications for piezoelectric materials. This thesis focuses on using these materials in a piezohydraulic pump system. Piezopump systems typically operate by pushing fluid through check valves to produce positive fluid flow. The accompanying hydraulic system utilizes a control valve, hydraulic accumulator, and hydraulic actuator. The function of the piezopump is to convert the very small displacements of the piezoelectric stack actuators into useful work. This paper details the design, construction, and testing of four such possible pumping systems.

The first system was a thin diaphragm piezo pump which utilized conventional check valves to rectify the flow. This pump was the next generation system in a series of piezopumps designed at Georgia Tech. Its peak performance with a driving voltage of 150V was a flowrate of 140 cc/min with a blocked pressure of 1.38 MPa (200 psi.). The key features of this system were its aluminum construction and ease of assembly.

A new technology was developed which used a resonant fluid cavity to build usable pressure for a pumping system. Two half wave resonators were build to operate at frequencies of 20 kHz and 1 kHz. These systems produced good pressure during resonance, but attempts to rectify these high frequency pulses were unsuccessful. Rectification methods such as reed valves, vortex fluid diodes, and nozzle/ diffuser arrangements were discussed. A reed valve system was developed and tested. A fourth piezoelectric system was developed which used the driving elements and the reed valves originally designed for the resonant systems. This non resonant reed valve pump

produced good results. This pump systems produced 338cc/min at a frequency of 400 Hz. It also produced a blocked pressure of 250 psi. There are many applications for these miniature high flow pumping systems. The technology in the reed valve pump is scalable, and the size of this particular system may be reduced dramatically to offer even more space saving potential.

CHAPTER 1

Introduction/ Literature Review

1.1 Introduction

The use of piezoelectric materials in a fluid pump system is discussed in this thesis. The research performed in this area includes methods for pumping fluid, valving techniques, and use of fluid resonance. The objective was to design a high power density piezoelectric system suitable for applications where small size and high force are primary requirements.

An investigation into the history of piezoelectric pumps showed a development of systems and concepts for this application. Mauck and Lynch (1999, 2000) developed several generations of piezohydraulic pump systems under the DARPA Smart Wing Phase II program. These systems used a reciprocating piston to force fluid through passive check valves. The early systems achieved a flow rate of 86 cc/min at a driving voltage of 1000V (Mauck and Lynch 1999). Further development at Georgia Tech produced systems capable of 250 ccm at a drive voltage of 800V and frequency of 50 Hz (Oates 2001). The first generation systems were large in size and required driving voltages close to 1000V to operate. Following these developments, companies such as Kinetic Ceramics began developing systems for commercial use under the Compact Hybrid Actuators program (CHAP). Kinetic Ceramics produced a pump system capable of producing pressures up to 10 MPa and flow rates of 240 cc/min (Kinetic Ceramics 2002). The developments under these programs produced working systems, however

their size and drive voltages hindered them from many applications where small and light actuation systems were desired.

Most of the systems utilized passive check valves to rectify flow. The use of an active valve system has been a topic of research for piezohydraulic pump systems. Active valves would allow much more control of the fluid flow and allow the system to operate at higher frequencies. This higher operation frequency would increase power output of the system (Tan et al. 2002). Some active valve systems consist of a piezo material bonded to a metal disk that flexes when energized thus opening and closing the valve (Lee et al. 2002). Lee et al. developed an active valve pump system that operated at frequencies up to 1kHz with a flow rate of 204 cc/min (2002). A blocked pressure of 8.3 MPa was also attained.

Some piezoelectric hydraulic actuation systems may compete with traditional hydraulic systems typically consisting of a large and heavy motor driven pump. To compete with these systems, a piezohydraulic actuation system must be small in size and lightweight. Smaller and lighter systems will have an added effect of being able to operate at higher frequency as well. High operation frequency is generally desired to increase output because the overall strain of the material is very small. The development of a high force hydraulic actuation system would be of great value to applications in the aerospace and unmanned aircraft applications where size and weight are heavily scrutinized.

This thesis deals with the development of small scale pump systems and concepts which produce compact fluid pump systems. The progress in development of this application has resulted in smaller and more efficient piezoelectric pump systems. Part of

the reason for this is the use of more advanced materials. This thesis focuses on utilizing cofired piezoelectric actuators as the primary driving element. The systems developed are capable of producing high pressure and high flow rates with minimum space and weight impact. This produces a system with high power density, which may allows these systems to compete with traditional motor driven hydraulic systems. Many concepts and systems were developed in this thesis which built upon past research. These systems were designed not only to increase performance, but to also explore new methods that may be possible with piezoelectric materials. The piezoelectric driving element is what makes pumping possible with these systems. The following section describes the basic characteristics and history of this unique material.

1.2 History of Piezoelectricity

Pierre and Jaques Curie first discovered the phenomenon of piezoelectricity in 1880 (Piezo Systems, Inc. 2002). Their published paper described how crystals such as tourmaline, quartz, topaz, and Rochelle salt exhibited a surface charge when mechanically loaded. This discovery was called piezoelectricity. The roots of the word piezoelectricity are from the Greek word *piezein*, which means, "to press tight" (The American Heritage Dictionary 2000). The brothers also discovered that changes in temperature would also produce these electrical effects. While the Curie brothers were known for their discovery of the direct piezoelectric effect (electricity from applied stress), it was Lippmann in 1881 who made the realization of the converse piezoelectric effect (stress in response to electric field). Once this effect was known, the Curie brothers continued to develop applications where this new technology would be used.

Over the next few decades the piezoelectric community grew its knowledge of the asymmetric crystal structure behind the materials that exhibited the piezoelectric effect (Piezo Systems, Inc. 2002). The first and one of the most important applications of piezoelectric materials came during World War I. Until this time the subtle strains exhibited by these materials did not call as much attention as the technology being developed in the field of electromagnetism. In 1917, a French scientist named P. Langevin began development of an ultrasonic submarine detector. The transducer consisted of quartz crystals bonded between two steel plates with a resonant frequency of around 50 KHz. This transducer emitted an underwater chirp and measured the return echo to measure depth and presence of other vessels. This achievement was the first use of sonar, which revolutionized the detection of underwater entities, and development of this technology still exists today.

Development in the following years consisted of the formulation of classes of piezoelectric materials which were tailored to a specific application, including development of the barium titanate and lead zirconate titanate (PZT) families of ceramics (Piezo Systems, Inc. 2002). Applications of these materials extended to phonograph cartridges, ignition systems, and microphones. One of the main applications developed in recent years is magnifying the motion of the piezoelectric ceramics in the presence of electric field. This has been performed using systems such as composite unimorph actuators. These actuators consist of a composite panel which bends when energized due to an imbedded piezo ceramic. These actuators may be used in smart skins of aircraft to deflect when needed as well as detect defects. Other systems such as piezohydraulic pumps have been developed as a lightweight alternative to traditional hydraulic pumping

mechanisms. These high specific output systems have a high theoretical efficiency, and are capable of producing high pressures for high force applications.

1.3 Mechanics of Piezoelectric Materials

A discussion of the response of piezoelectric materials begins with a definition of ferroelectricity. Piezoelectricity is a subclass of ferroelectricity. Jaffe, B. et al. (1971) define ferroelectricity as "the presence of a spontaneous electric moment in a crystal which can be changed in its orientation between two or more distinct crystallographic directions by applying an external electric field". This same work also states three key concepts for understanding piezoelectricity in ceramics. First is that these materials have a high dielectric constant; second is that the high dielectric is a result of the material's ferroelectric properties. Finally, the poling process is critical to its behavior.

The response of a microscopic unit cell of a piezoelectric material is discussed to explain how it affects the bulk material. An example of a widely used piezoelectric material used in this discussion is lead zirconate titanate (PZT) $Pb(Ti,Zr)O_3$. After the ceramic manufacturing process, this material is cured above its Curie temperature, above which no piezoelectric characteristics exist. The crystal structure above this temperature is an isotropic body centered cubic. Figure 1.1(a) shows this cubic structure above the Curie temperature with the titanium atoms in the middle, lead ions at the corners, and oxygen ions centered on the faces (Hopkinson 2003). As the ceramic cools, its piezoelectric properties emerge. When the material falls below its Curie temperature, the central titanium ion shifts above the plane of the face centered oxygen ions. This results in a net dipole arrangement and a tetragonal crystal structure. This crystal arrangement

has a net charge difference across the dimension parallel to this ion shift. Figure 1.1(b) shows this structure for PZT, with the top of the cell having a positive charge and the bottom with a negative charge. The direction of the positive charge is known as the poling direction.

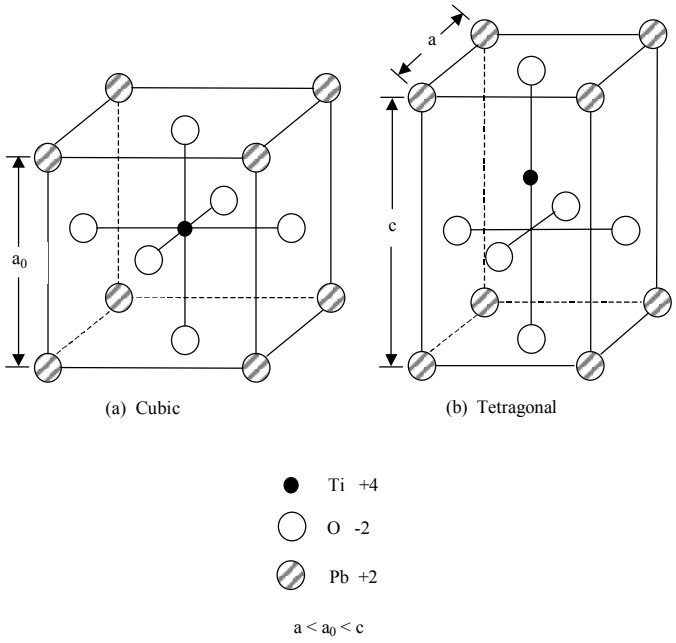

Figure 1.1: Cubic and Tetragonal Crystal Structures for PZT

1.4 Poling Characteristics and Switching

With an understanding of the elementary unit cell, the primary piezoelectric properties may now be explained. Stress or electric field may act upon the unit cell discussed above. Figure 1.2(a) shows the poled unit cell and direction of polarization (Hopkinson 2003). When an electric field is applied in the direction of poling, the field pulls the titanium ion further from its central axis, causing the unit cell to elongate, as shown in Figure 1.2(b). This is an example of the converse piezoelectric effect. Electric field may be applied in this direction until the unit cell saturates; saturation occurs when

the elongation per unit additional applied electric field approaches zero. This elongation of the cell causes bulk material deformation and is the core response that applications for piezoelectric materials are designed around. If the electric field is applied in the direction opposite the poling direction, the titanium atom is forced towards the center of the cell. As a result, the unit cell will shrink and become more cubic. When a field value known as the coercive field is reached, an important event occurs. When the center titanium ion gets sufficiently close to the center, it will suddenly flip to the other side of the element. This event is known as 180° switching. This type of switching, shown in Figure 1.2(c), results in a switch of the polarity by 180°. As the field is increased in the negative direction, the element will elongate and saturate as before, except the polarity is reversed.

Switching may occur in two ways, either 180° or 90°. Either stress or electric field may induce 90° switching. If a compressive stress is applied in the direction parallel to the initial poling direction, it will force the titanium atom closer to the center of the crystal. When the stress level reaches the coercive stress it will suddenly undergo a 90° switch, as shown in Figure 1.2(d). Similarly, if a tensile stress is applied in a direction perpendicular to the initial poling direction, a similar switch will occur, as shown in Figure 1.2(e). The same switching can occur if sufficient electric field is applied in a direction 90° to the initial polarization, as shown in Figure 1.2(f). A thorough discussion of the microscopic unit cell promotes a further understanding of how the material behaves macroscopically.

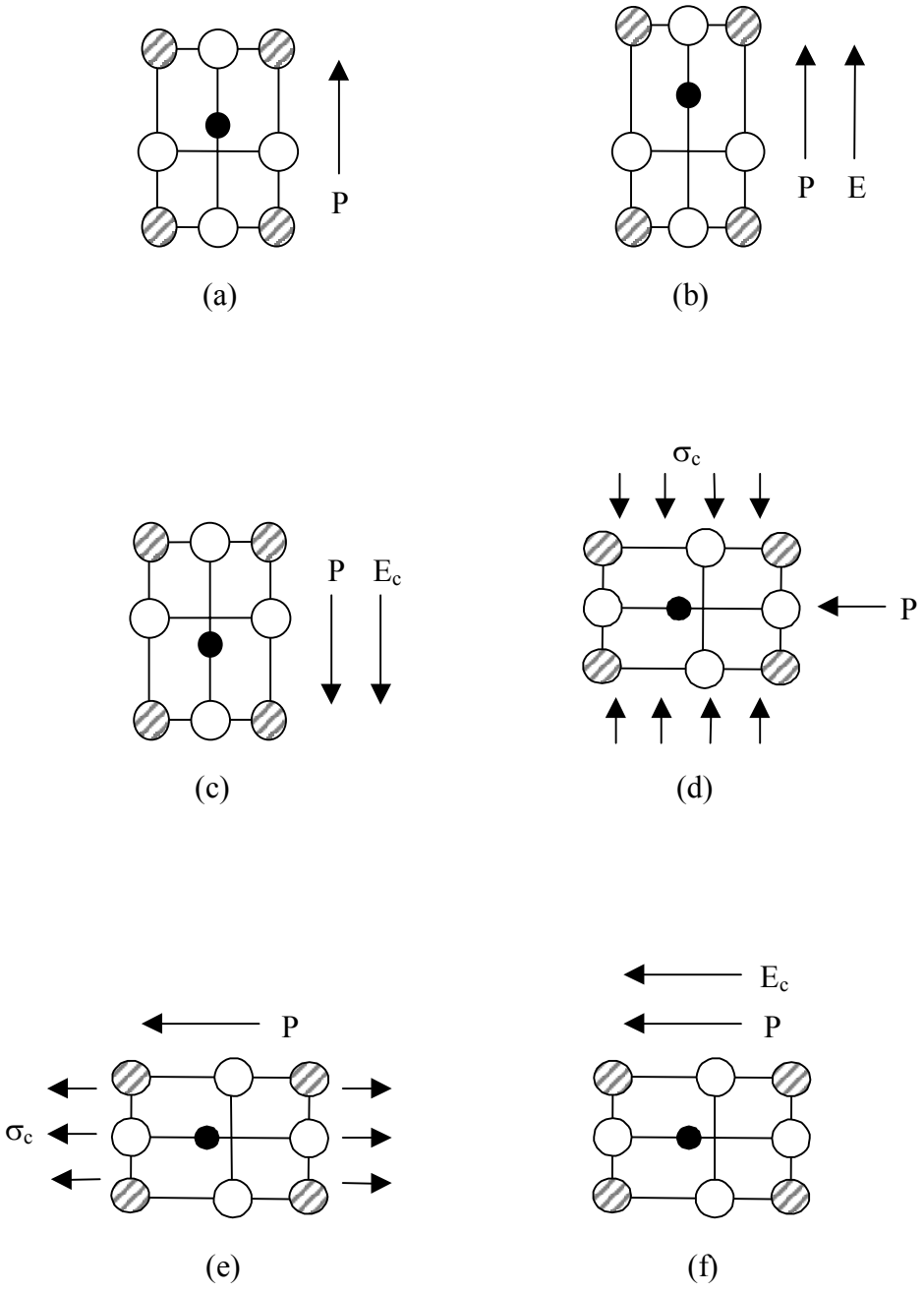

Figure 1.2: Description of Pole Switching

Whenever a bulk material is manufactured, the unit cells do not spontaneously pole in the same direction. Collections of identically poled unit cells, called domains, develop within the material; the polarity of these domains is arranged in random directions. Therefore, an unpoled ferroelectric material cannot produce useful deformations because the bulk expansion and contraction of the domains will cancel. In order for the material to be useful in engineering, the domains must be poled in the same direction. The same principles of pole switching in the unit cell discussed earlier apply to the poling of domains. An electric field higher than the coercive field is applied to the material and the domains switch and become poled in the direction of the field. When the field is removed, there is some relaxation of the poling directions, but the net poling direction remains. After the material has been poled, application of electric field in the poling direction will cause the domains to expand in the same direction, producing a net deformation of the material. Figure 1.3 shows an illustration of the poling of a piezoelectric material, where the black arrows represent the polarization directions of the domains (Physik Instrumente, 1996).

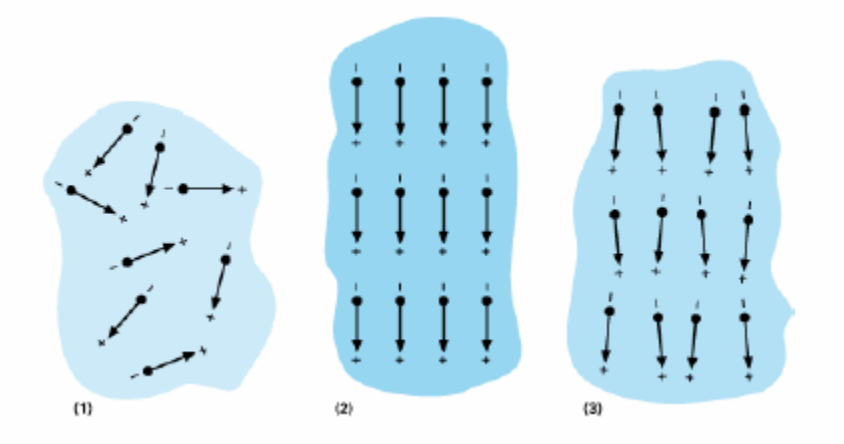

Figure 1.3: Domain Polarization 1) Before Polarization 2) During Polarization 3) after Polarization

1.5 Constitutive Laws and Characteristic Response

The response of a piezoelectric material to applied fields and stresses is important to designing systems that utilize the ceramic. Therefore, it was important to develop a set of equations that use the characteristic properties of the ceramic as well as the conditions the material is under to predict its response. These equations are known as the constitutive laws for piezoelectric materials, shown in Equations 1.1-i through 1.1-iv.

$$S_{ij} = s^{E}_{ijkl} T_{kl} + d_{kij} E_k \qquad (1.1\text{-i})$$

$$D_i = d_{ikl} T_{kl} + \varepsilon^{T}_{ik} E_k \qquad (1.1\text{-ii})$$

$$T_{ij} = c^{E}_{ijkl} S_{kl} - e_{kij} E_k \qquad (1.1\text{-iii})$$

$$D_i = e_{ikl} S_{kl} + \varepsilon^{S}_{ik} E_k \qquad (1.1\text{-iv})$$

In these equations S_{ij} are the strain components, T_{ij} are the stress components, E_k are the electric field components, D_i are the electric displacement components, s^{E}_{ijkl} are the compliance components at a given electric field, d_{kij} are piezoelectric components, ε^{T}_{ij} are

dielectric permittivity components at fixed stress, c^E_{ijkl} are stiffness components at fixed electric field, e_{kij} are piezoelectric components, and ε^S_{ij} are dielectric permittivity components at fixed strain. These equations may be used to characterize the linear response of ferroelectric materials to certain stimuli.

Typical values measured during testing are electric displacement, electric field, stress, and strain. If we are only concerned with the response of the piezoelectric material in the poled direction, denoted by a subscript "3" in the components of the constitutive law, then the characteristic response takes certain predictable shapes. Figure 1.4 shows typical graphical values of electric displacement, D_3 vs. electric field E_3 (Lynch 1996). When a material starts out in an unpoled state, it has zero electric displacement with zero electric field applied; this is represented by point *A* on the graph. As electric field is applied for the first time the switching of the dipoles may be seen as a large jump in electric displacement as the graph travels to point *B*. This jump occurs at an electric field value near the actual coercive field, but it is slightly different when starting with an unpoled specimen. As electric field continues to be applied in the positive direction, the material saturates and no longer increases its electric displacement with added electric field. If the electric field is decreased to zero, represented by point *C*, one can see that there is a remnant polarization because the material still has a positive electric displacement. If the electric field is now increased in the negative direction, another pole switch will occur at the negative value of the coercive field, as indicated by the steep slope from point *C* to point *D*. This represents a 180° switch, and the material is now poled in the negative direction. If a larger negative field is applied, the material will saturate as before. When the electric field is returned to zero, there still exists a

remnant polarization, only now with a negative electric displacement. If the electric field continues to be applied in the positive direction, another 180° shift will occur at the coercive field value and the material will return to point *B*. At this point the full hysteresis curve is completed and varying the electric field will cause the response to follow this curve.

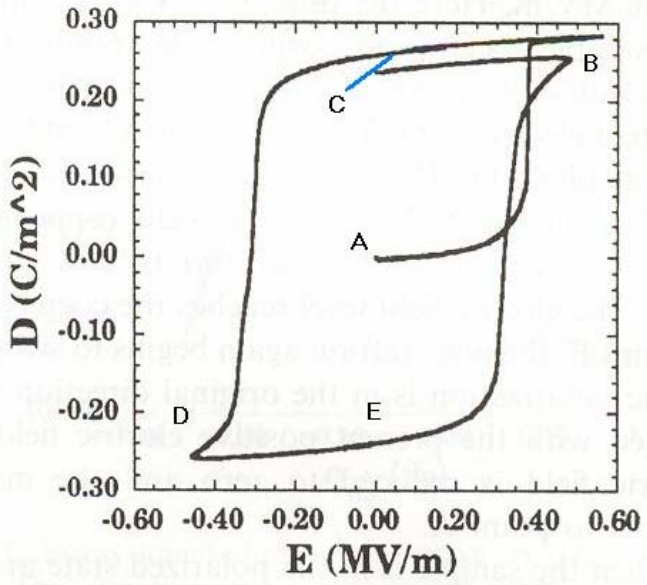

Figure 1.4: Electric Displacement vs. Electric Field for Representative PLZT

There is a similar type response when longitudinal strain and electric field are investigated. A typical representation of this graph is shown in Figure 1.5 (Lynch 1996). The response begins with a material with zero strain and zero electric field applied. As the electric field is applied, there is a large jump in strain as the poles of the crystal structure align themselves in the direction of the applied field. Continuing to apply electric field past this coercive field value will not result in much increased strain and the material will saturate, as represented by point *B* on the figure. If the electric field is

reduced to zero, represented by point *C*, there exists a positive remnant strain. The response in this region is nearly linear, and can be represented by a simplified form of the constitutive law, shown in Equation 1.2. Most actuators operate in this region because the response is very linear, and there is not much self heating present due to pole switching.

$$\varepsilon_{33} = d_{333} E_3 \tag{1.2}$$

If the electric field is driven in the negative direction, however, a pole switch will occur. As the field becomes more negative, the central titanium ion is driven towards the middle of the crystal, making it more cubic. Once the negative value of the coercive field is reached, the specimen experiences a negative strain before the Ti ion flips to the other side of the crystal, causing a positive strain and approaching point *D* on the figure. At this point a 180° switch has occurred and the specimen is poled in the negative direction. When the electric field is reduced to zero there is still the same amount of remnant strain, but the slope of the remnant polarization is negative. As the electric field is again applied in the positive direction, another 180° pole switch occurs and the material returns to point *B*, completing the loop. The material is now poled in the original direction with a positive electric field.

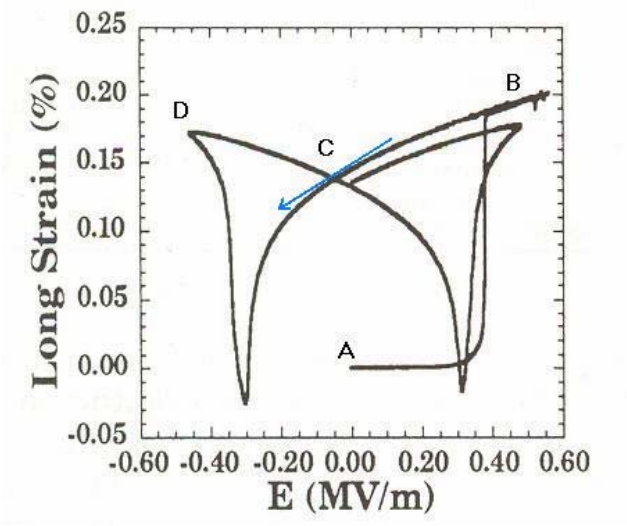

Figure 1.5: Typical Longitudinal Strain vs. Electric Field Response

Most piezoelectric actuators operate in the linear region between the positive and negative coercive fields. In this region the response is most predictable using the linear constitutive laws. Operating outside this region is advantageous because of the large strains associated with switching the poling direction of the material. Each time the titanium ion is switched to another poling direction, heat is generated. If the switching occurs frequently this heat can degrade the material. This is the reason operating in this manner is generally avoided.

1.6 Piezoelectric Transducers

With the knowledge of how piezoelectric ceramics work, their implementation into engineering design may now be discussed. As stated, the current state of the art in applications of piezoelectric ceramics includes transducers and systems that produce useful mechanical work. This means applying a voltage to a system and getting useful motion out. Using this type of material presents certain advantages and disadvantages in

these systems. The disadvantages are that the material strains are very small with applied electric field; the motion is not even visible. Another is that the piezoceramic is inherently brittle and cannot sustain substantial tensile loading without fracture. Also, some of the materials produce some self-heating losses that may elevate the temperature of the material to the point of becoming unusable. Some advantages of the material are that the material is capable of producing very high stresses at high frequency. With piezoelectric transducers, the amount of usable work is directly proportional to the operating frequency. This presents a challenge to system design because every component of the system must perform at the high operating frequency. Another advantage is that with the proper amplifier, the electrical work put into energizing the material may be almost completely regained when deenergized, less the mechanical work performed. The theoretical efficiency possible with these materials is large when compared to traditional actuation systems.

1.7 Actuator Types

1.7.1 Composite Unimorph

A composite unimorph transducer is a piezoelectric ceramic embedded in a composite matrix of differing coefficients of thermal expansion and bonded together at high temperature. When the material cools, the difference in thermal expansion produces a curvature in the composite and places the ceramic in residual compression. When the ceramic is energized, its change in length causes the composite to flex and change curvature, therefore multiplying the motion of the ceramic. These actuators may be used in active skins on the wings of aircraft to mold the wing shape to the most efficient form,

and to also eliminate the seams in wings that cause drag. Piezo-ceramics may also be embedded in composite layers and send and receive signals to detect a hole or delamination in the composite.

1.7.2 Ultrasonic Motors (USM's)

Ultrasonic motors are piezoelectric devices that utilize the material to produce travelling waves between a stator and rotor. The piezoelectric material on the stator has finger-like protrusions that grab the rotor and pull it in a circular direction. This type of motor is widely used in power lenses of cameras. Its small size allows it to be used in these miniature applications. Where the main advantage is their size, the disadvantages of these mechanisms are that the travelling wave and finger-like stator cannot produce a high torque motor. This type of motor would not be a viable system in a high load system.

1.7.3 Piezo Stack Actuators

The work performed in this thesis uses primarily piezo stack actuators. The stack actuator consists of many layers of piezoelectric material stacked on top of one another and wired together in parallel. This type of actuator amplifies the minute deformation of one piece of ceramic by multiplying the deformation by the number of layers in the actuator. A much higher deformation is possible using this type of actuator. The only consequence is an increase in capacitive load on the driving circuitry. These actuators are manufactured in two ways, cut-and-bond and cofired methods. The cut and bond method simply slices the material from a large piece and glues the slices on top of each other, separated by an insulating layer and electrode. These types of actuators were used on the early generation piezo pumps designed at Georgia Tech. The layers of ceramic

were quite thick because very thin cuts of ceramic are not possible by slicing. This resulted in the stack actuators requiring a very high voltage to operate at full capacity, on the order of 1000V. The actuators themselves were very large and bulky, some being 12 inches long. The cofired method of manufacturing stack actuators is when the piezo material is deposited in thin sheets on the actuator. The electrodes are screened on to the ceramic material before they are cured. This type of process allows much thinner layers, which results in smaller actuators that may be run at full voltage without the need for a high voltage amplifier; these stacks run on voltages around 150V. The piezoelectric stack actuator is the key to designing high specific output pumping systems.

The advent of single crystal piezo stack actuators has been a step forward in piezoelectric technology. Single crystals have a much higher piezoelectric coefficient and a lower modulus of elasticity. They do not have the self heating problems associated with soft PZT, which make them ideal for high frequency applications. Single crystal stacks are still a new technology at the time of this thesis publication, therefore they are only made using the cut and bond method of manufacture.

1.8 Piezoelectric Hydraulic Pump

Another application of piezoelectric materials that has been developed over the past several years is the use of these materials in a fluid pumping system. A high speed, high pressure piezo-hydraulic pump has been in development at Georgia Tech for several years and is the main focus of this study. There have been several generations of the piezo-hydraulic pump developed at Georgia Tech. Mauck, Oates, and Lynch (2001) developed a piezo-hydraulic pump which drives a hydraulic actuator at 7cm/sec using a

drive frequency of 60Hz. Testing on these systems involves varying the drive voltage, drive frequency, and bias pressure. The basic construction of these systems consists of a series of stack actuators pushing against a piston or diaphragm in a reciprocating motion. Fluid motion is rectified using check valves installed in a cylinder head. Each generation was designed to be smaller and lighter. Figure 1.6 shows one of the larger early generation pump systems utilizing a 12 in. stack actuator. The pump shown in the figure is over two feet long and is quite heavy.

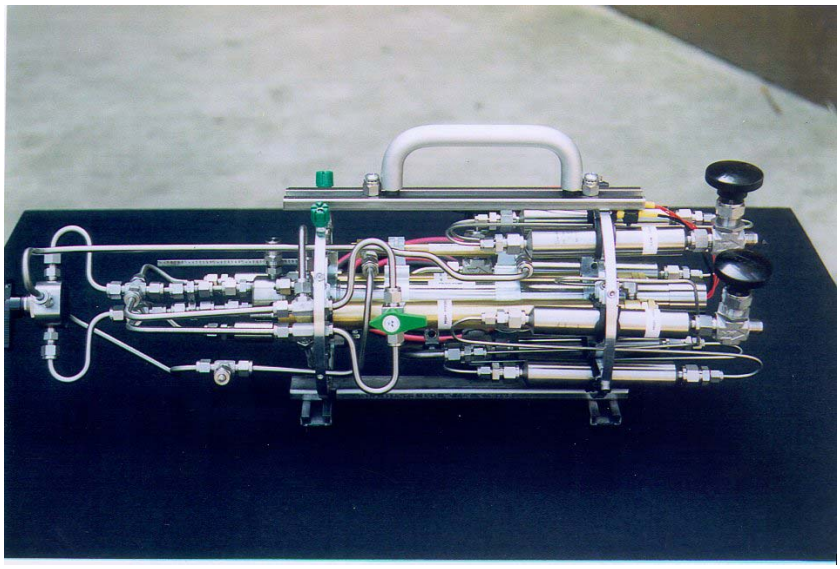

Figure 1.6: Early Generation Piezo Pump

Other types of pump systems designed have included piezo driven pumps with a valveless design. Some systems utilize a nozzle/ diffuser cone arrangement to simulate the function of ordinary check valves (Ullman and Fono 2002). Other research performed by Pan, et al. (2001) dealt with the fluid–membrane coupling which exists in

valveless micropumps. A further discussion of past research performed in the area of piezohydraulic pump systems is performed in Chapter 2.

New piezo driven pumps are under development using conventional poppet style check valves, systems using a resonating fluid cavity to boost pressure, and systems utilizing high speed reed valves. All these systems utilize the high frequency capabilities of the piezoelectric material. All new systems developed at Georgia Tech are currently using EPCOS 30mm cofired stack actuator. These stack actuators are far superior to their cut and bond counterparts because the layers are much thinner, which allows a maximum electric field to be applied with minimum voltage. This lower voltage requirement will have many advantages, including a smaller and lighter power supply. The development of these new pump systems is discussed in the following chapters.

CHAPTER 2

Aluminum Piezohydraulic Pump Using Check Valves

2.1 Introduction

A small hydraulic pump driven by cofired piezoelectric actuators and an associated control system was developed and tested. This type of pump will be well suited for driving small actuators in unmanned air vehicles where size and weight are of concern. It consists of a piezoelectric stack actuator used to deflect a diaphragm that pushes fluid through two poppet check valves in a cylinder head. This reciprocating system produces flow rate proportional to frequency. Several technical challenges have arisen with reducing the size of piezo pumps that are addressed. Pump characterization and performance results are presented.

2.2 Background

Piezoceramic driven hydraulic pumps have been developed for driving hydraulic actuators. These systems consist of a series of stack actuators pushing against a piston or diaphragm to produce a reciprocating motion. Fluid motion is rectified using check valves installed in a cylinder head. Mauck, Oates, and Lynch (2001) developed a piezo-hydraulic pump which drives a hydraulic actuator at 7cm/sec using a drive frequency of 60Hz. The operating frequency and amplitude of the stack actuators was limited by self heating. These pumps produced a maximum flow rate of 250 ccm at a drive voltage of 800V and frequency of 50 Hz (Oates 2001).

Other designs have included piezo driven pumps with either valveless or active valves. The valveless systems utilize a nozzle/ diffuser cone arrangement to simulate the function of ordinary check valves. Ullman and Fono (2002) have presented a dynamic model that details the arrangement of a nozzle and diffuser. While this type of fluid rectification system has no moving parts, a system based on fluid losses to create positive flow has certain drawbacks. Ullman and Fono (2002) predict pump systems using this method would have an efficiency on the order of 1%. Research performed by Pan, et al. (2001) discusses fluid–membrane coupling which exists in valveless micropumps. They found that the response of a system is highly dependent on the dimensions of the pump and the fluid medium used (Pan et al. 2001). Non-linearity in the response of the fluid/ vibrating membrane interface was found to be important (Pan, et al. 2001).

Research has also been performed on developing systems that use active valves to rectify the fluid flow. Lee et al. (2002) and Tan et al. (2002) have developed systems which use piezoelectric material integrated into the valving system to control the flow at higher frequencies. Oates (2001) shows, however, that the use of off the shelf, miniature passive check valves provides a simple, compact, and proven rectification system that operates well with frequencies into the hundreds of hertz.

Mauck and Lynch (1999), Mauck et al. (2000), and Mauck et al. (2001) have developed several generations of piezo-hydraulic pumps at Georgia Tech over the past several years utilizing miniature check valves to rectify the fluid motion. As each generation of pump became smaller, technical challenges arose that had to be addressed. One challenge was the process of evacuating the air from the system. Another challenge was that the stacks were driving a piston that used o-rings to seal the fluid chamber. The

o-ring compliance introduced losses that were degrading pump performance. Other design challenges included minimizing pump body deflection. Addressing each of these challenges in the design stage results in improved pump designs and performance. The main goals of the piezohydraulic pump developed are shown below.

1. Design a fluid cavity which resists the entrapment of air
2. Develop a system that separates the fluid from the PZT using a static instead of a dynamic seal
3. Provide a method of controlling position and direction of the hydraulic actuator being driven by the pump
4. Adapt the pump geometry to use EPCOS cofired stack actuators.

The EPCOS cofired actuators use lower voltage than other stack actuators due to their manufacturing process and design. The EPCOS actuators consist of 6.7mm x 6.7mm layers of PZT potted in a rubberized plastic to protect the ceramic. Use of the EPCOS stack actuators allows more flexibility in the system design due to their small size. Three 30mm long stack actuators were bonded end to end to provide the driving system of the directly driven piezo pump. Because of the smaller overall displacement of these actuators, the construction of the pump must be stiffer than previous systems; the early systems had 12 inch stack actuators operating at 1000V, producing much more overall strain than with the new materials. Because this larger displacement is not available with the small cofired stacks, the stiffness of the new system must be increased to reduce any losses due to deflection of the pump body.

2.3 Pump System Design

The major components of the piezo-hydraulic system are the pump assembly, spool valve, high and low pressure accumulators, and a hydraulic actuator. The major design changes performed in the development of this check valve pump over early generation systems were the spool valve to control flow, pump body design, and cylinder head design. A diagram of the fluid flow through the system components is shown in Figure 2.1.

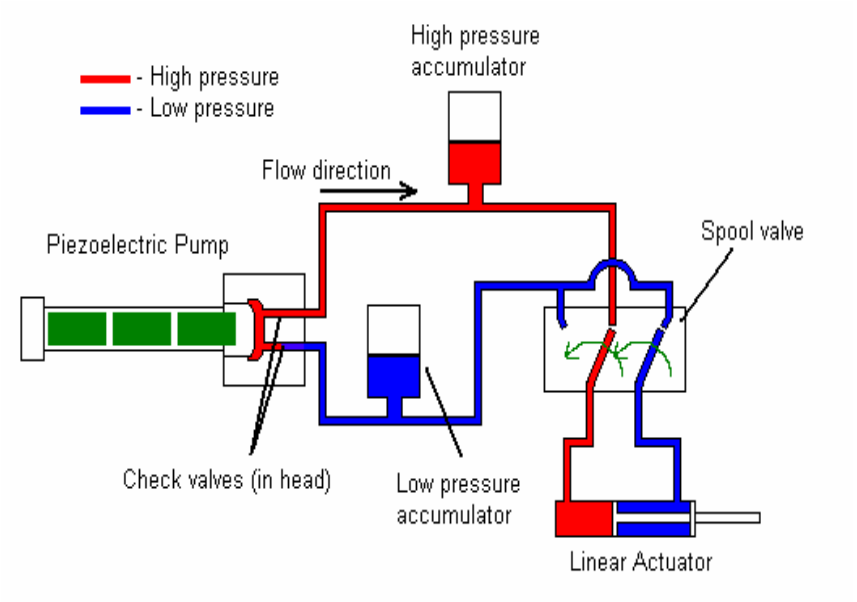

Figure 2.1: Fluid Flow Diagram

The high pressure accumulator is a high pressure fluid storage device and was optional at this point; one was not used in testing. The high pressure accumulator allows the pump to build up a reserve of fluid pressure if the actuator is in the locked position. The low pressure accumulator was used to apply a bias pressure on the fluid to prevent cavitation at high frequency and also to help with cylinder head filling.

The spool valve, depicted in Figure 2.2 and 2.3, was designed to replace the four way valve used in previous designs. It consisted of six o-rings placed at the proper locations to allow pressurized fluid to flow to the hydraulic cylinder and actuate it. This pump system was the first pump designed at Georgia Tech to employ the use of a spool valve based position control device. The valve employs three positions, forward, locked and reverse. When switched, the spool valve directs pressurized fluid to the desired inlet on the hydraulic actuator to drive the actuator in a particular direction, all while bleeding the low pressure fluid to the low side of the system. An important feature of the spool valve is the inclusion of a locked position. This middle position on the spool valve locks both the inlet and outlet of the hydraulic cylinder. This allows the user to lock the actuator in a desired position without having to use the pressure from the pump.

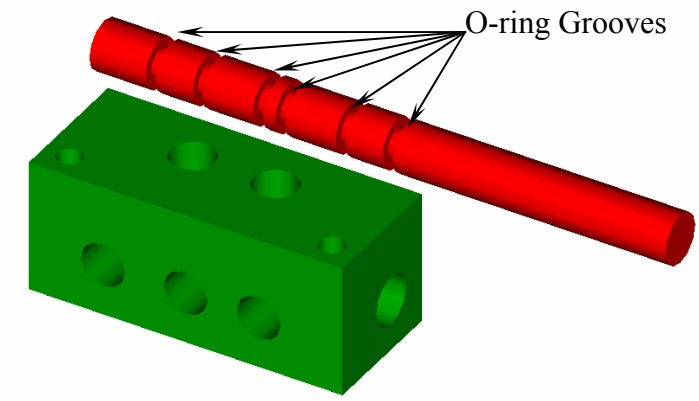

Figure 2.2: Spool Valve Solid Model

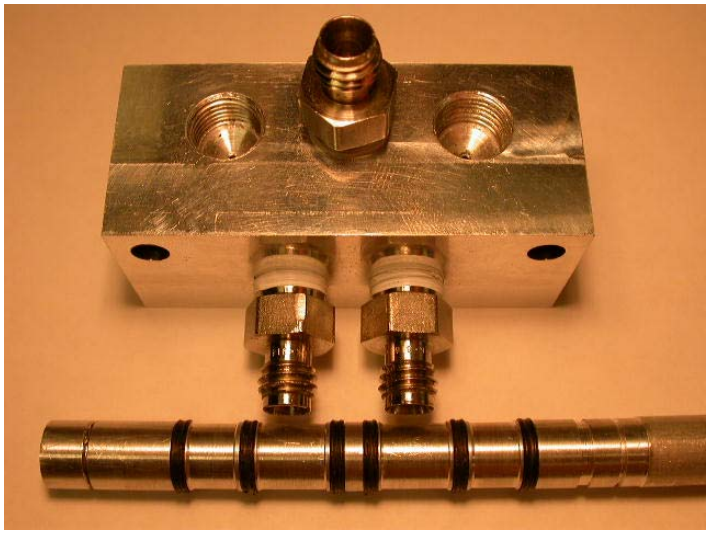

Figure 2.3: Spool valve photograph

The other design changes were directly related to the reciprocating pump subsystem. The first change to the pump was the material. The pump was fabricated entirely of aluminum. This material was chosen over steel, used previously, due to its light weight and ease of machining. The overall size of the pump body decreased as a result of using the EPCOS PZT stack actuators. Figure 2.4 shows the EPCOS driving actuator. The stacks were placed end to end to multiply the displacement of the end of the stack assembly. Spherical washers were placed at the ends of the actuators to prevent any bending moment of the driving element. The drive system was placed inside a housing that consists of a housing tube, backing plate, and screw cap, as shown in Figure 2.5. Detailed drawings of the PZT housing are shown in Appendix A. The PZT housing provides a solid foundation for the stacks to press against while allowing the wires to extend from the backing plate. The left end of the housing screws into the cylinder head during operation. This allows the stack housing to be removed as a complete unit to protect the PZT from damage and allow for quick reassembly. This design coupled with

the changes to the cylinder head allows complete disassembly of the drive system without discharging the fluid side of the system.

Figure 2.4: Three EPCOS stacks

Figure 2.5: PZT housing

The cylinder head was the component that received the most changes over the earlier systems. The most important change dealt with sealing the fluid. Previous designs actuated a piston that used an o-ring seal, similar to Figure 2.6. This design experienced difficulty sealing the fluid chamber, but more importantly, reduced the stiffness of the system through the compliance of the o-ring. The major design change was to convert to a static sealing system instead of dynamic. This was accomplished by using a thin metal diaphragm to separate the fluid chamber from ambient pressures. The diaphragm was clamped between the two halves of the cylinder head using a cork gasket.

The gasket was confined outside of the fluid chamber such that the gasket material was not in direct contact with the fluid, thus compliance was not introduced to the system. The diaphragm was stamped out of .2032mm (.008 in.) stainless steel shim stock and cut to a diameter of 31.75mm (1.25 in.). A 12.7mm (.5 in.) circle was stamped into the center of the diaphragm to a depth of 1.78mm (.070 in.).

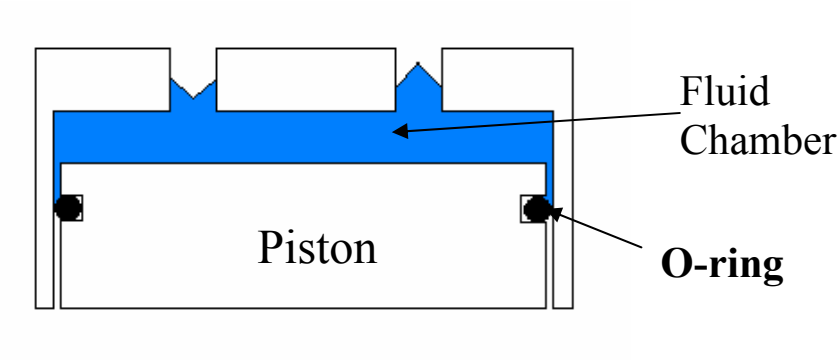

Figure 2.6: Piston and Cylinder Using O-ring Seal

The cylinder head was designed around several key characteristics. Figure 2.7 shows a wireframe of the cylinder head, which illustrates these features. The first characteristic was that the head was machined to have a smooth hemispherical fluid chamber. This aided in the bleeding of air from the system. The compression chamber was also designed to minimize the volume of fluid being compressed to reduce compliance losses. With the small displacements the PZT produces, any loss in stiffness of the system in the form of air bubbles significantly reduces the total system performance. The bleed port was angled in the head so that it enters at the apex of the compression chamber. When oriented upright, all the air collects at this point. An automotive type brake bleed screw was installed on the outside to facilitate expelling air

from the system. The inlet and outlet valves were placed close to the apex of the fluid chamber to aid in bleeding air from the head.

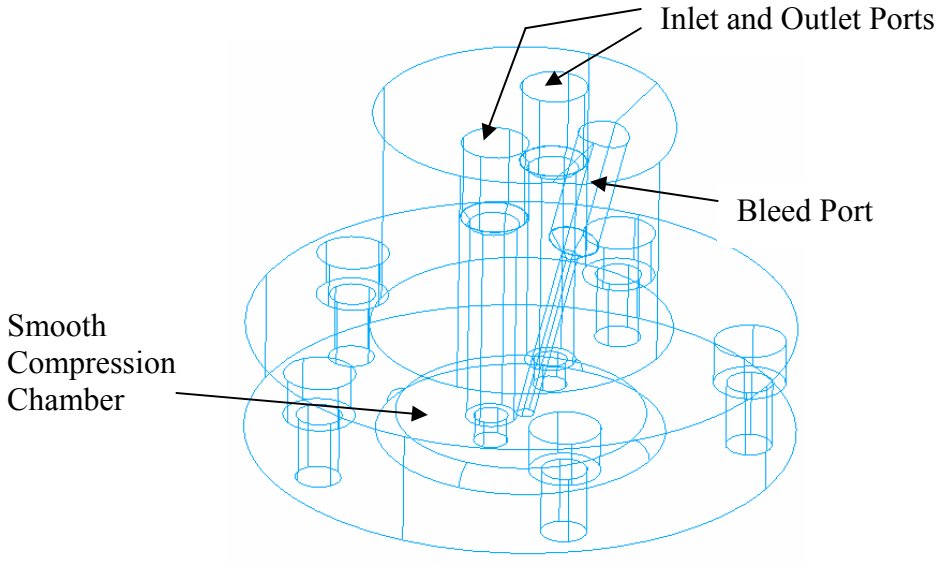

Figure 2.7: Wireframe of Top Half of Cylinder Head

2.4 Experimental Setup/ Testing of the System

The schematic of the experimental setup is shown in Figure 2.8. Figure 2.9 shows a photograph of the aluminum pump system. Two amplifiers were used during testing. For low frequencies, a Krohn-Hite (model 7500) 625mA amplifier was used. For higher frequencies where more current was required, an Instruments, Inc (model L6) amplifier was used. The working fluid for the experiments was Dow Corning 200 silicone oil with a low viscosity of .65cSt.

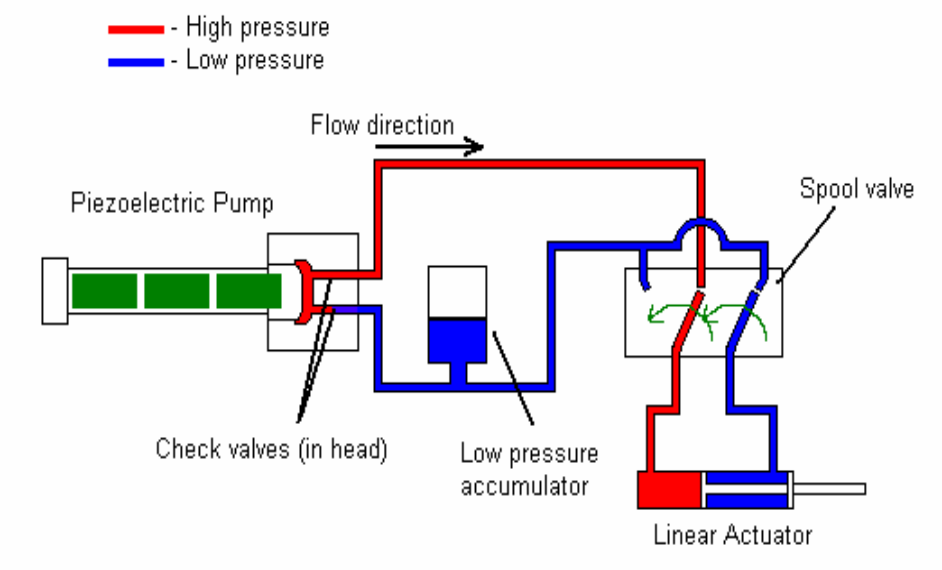

Figure 2.8: Experimental Setup of Aluminum Check Valve Pump

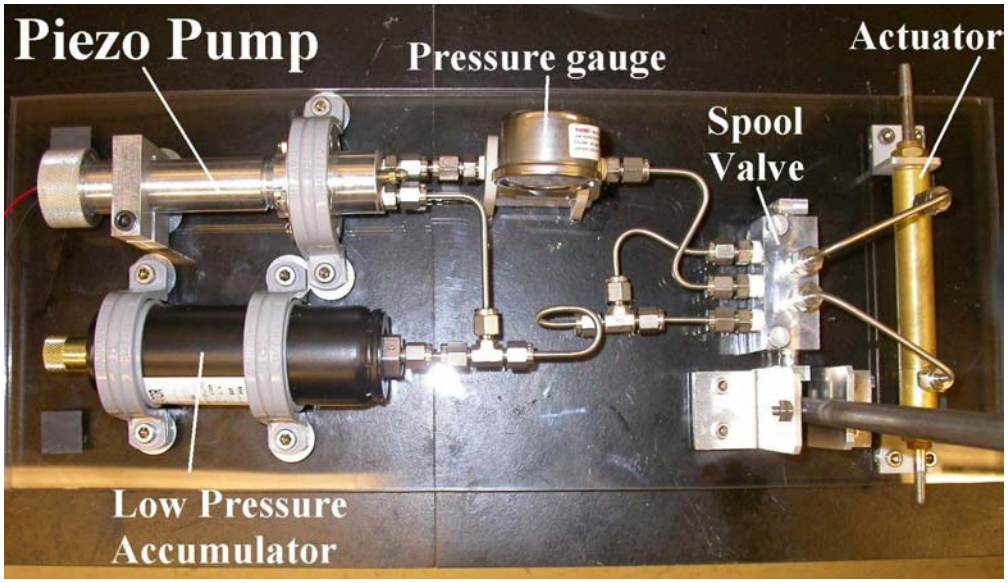

Figure 2.9: Photograph of PZT Pump System

After assembly and bleeding of the system, the low pressure accumulator was pressurized to preload the stacks and apply bias pressure to the fluid. The input voltage was a sine wave with a peak voltage of 150 V and a positive bias of 75 volts. The PZT can only be driven with positive voltages to avoid polarity switching, hence the voltage offset. The bias voltage for the Krohn-Hite amplifier was set up by inputting an offset sine wave from a function generator. The bias voltage for the Instruments, Inc. amplifier was attained by connecting nine-volt batteries in series with the output of the amplifier to attain the desired bias. The pump was attached to a double rod hydraulic cylinder (Clippard model H9D-1D) with an effective piston area of 128.6 mm^2 (.1994 in^2) and a stroke of 25.4mm (1 in.). These dimensions correspond to an inner fluid volume of 3.268 cm^3 (.1994 in^3). Measurements of flow rate were calculated using a stopwatch and the known fluid volume of the hydraulic cylinder. Pressure was measured using a gauge that was mounted inline with the high pressure side of the system. Experiments were performed at different bias pressures and at varying frequencies. The time required for the hydraulic actuator to traverse its entire range was recorded and later processed to determine flowrate.

2.5 Experimental Results

In order to characterize the aluminum pump system, several types of measurements were taken. Flowrate measurements were taken at various frequencies and bias pressures. The effect of bias pressure on flow rate was of concern, as well as the blocked pressures attained during operation, which were used to calculate actuator force.

The first set of experiments investigated the effect of bias pressure on flow rate. The accumulator that was used in the system could be charged using an external gas tank to any user defined pressure. Various bias pressures were applied and the pump was run. The driving voltage was kept at a constant $150V_{pp}$. The driving frequency was varied and the elapsed time for the actuator to travel its full range was recorded. These times were used to calculate flow rate. Figure 2.10 shows the flowrate data taken in these experiments. There were approximately two readings taken for each data point represented. An error of plus or minus .2 seconds was assumed because the times were measured by hand using a stop watch. This error corresponds to an error of plus or minus 4cc/min. A statistical analysis was not performed on the measurements taken and no confidence interval was calculated.

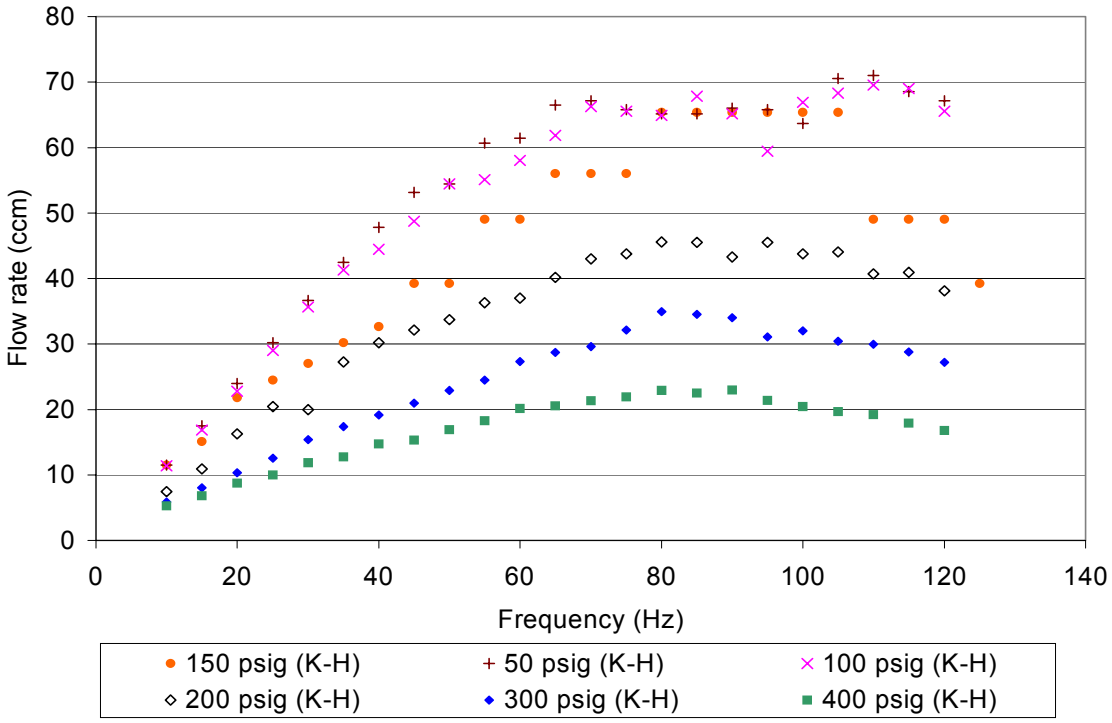

Figure 2.10: Flowrate vs. Frequency: 150V Drive, Various Bias Pressures

Assuming an effective piston diameter of 19.1mm (.75 in.), the bias pressures exerted the following preload on the stack actuators. Listed from lowest to highest, the preloads were 3.9 MPa, 7.9 MPa, 12 MPa, 16 MPa 24 MPa, and 31 MPa. It was found that an increase in bias pressure actually hurt pump performance. Although an increase in bias pressure was thought to aid in cylinder filling, the flow rate decreased. An increase in friction at the hydraulic actuator was observed with higher bias pressures. This was noticed while manually moving the hydraulic actuator. The decrease in pump performance was attributed to this increase in friction, most likely due to the type of seals used where the rod exits the actuator body. Therefore, the minimum bias pressure which prevents cavitation should be used for maximum performance. A different hydraulic actuator may also be used that has low friction seals.

The low viscosity silicone oil also may have an effect on the seals of the actuator. The fluid did not lubricate the moving parts of the system, but seemed to strip the grease from the actuator rod and seals. An increase in friction in the actuator was observed as the pump system continued to be tested after these experiments were performed. A working fluid with more lubricity may be beneficial to system performance.

The check valve pump system was also tested for maximum flowrate by increasing driving voltage and frequency. This testing was performed using the more powerful Instruments, Inc. model L6 amplifier. Figure 2.11 shows the results of this experiment. The results shown in Figure 2.10 are included for comparison. The figure also indicates which data sets were taken at increased voltage. All other data sets were performed with 150V driving. The increased voltage sets were measured once an optimum frequency range was determined. The error in measurement was the same as

the other experiments, 4cc/min. The maximum pump flow rate recorded occurred with a 100 psig bias pressure and a maximum flow rate of 140 cc/min. This reading was taken using the model L6 at a peak voltage of 220V. The blocked pressure at this condition was 260 psig. With the hydraulic actuator installed, this would correspond to a blocked force of 231N (52lb). The blocked pressure reading was taken when the hydraulic cylinder reached the end of its travel. There were slight variations in the blocked pressure with varying bias pressures, as shown in Table 2.1 for 150V driving voltage. From this table, it was observed that the maximum blocked force occurred at a bias pressure of 200 psig, using a 150V driving voltage. The blocked force value was calculated from the difference between the blocked pressure and the bias pressure, because the pressure above the bias pressure was what forced the actuator to move.

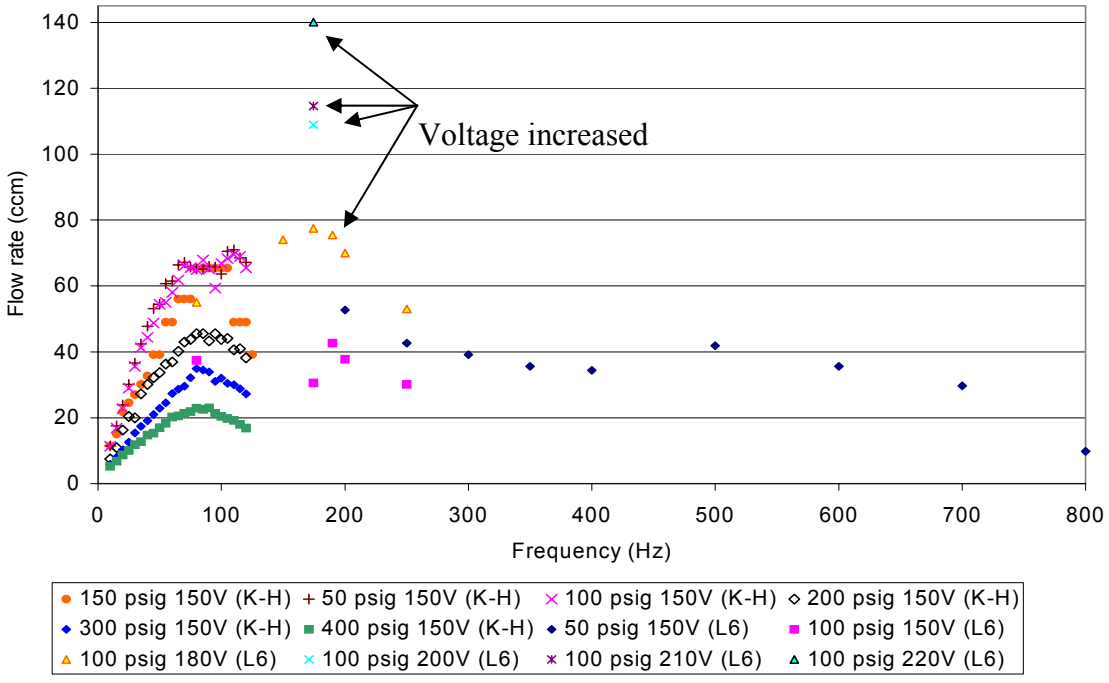

Figure 2.11: Check Valve Pump Flowrate Measurements

Table 2.1: Blocked Pressure Readings with Varying Bias Pressure Driven at 150V

Bias Pressure (psig)	Blocked Pressure (psig)	Blocked Pressure less Bias Pressure (psig)	Blocked force (lb)
50	240	190	38
100	280	180	36
200	400	200	40
300	460	160	32
400	560	160	32

2.6 Discussion

The maximum flow rate observed was approximately 140 cc/min. This flow rate was lower than the previous generation pumps, however there were notable differences between the system described here and earlier designs. The current generation had a maximum tested voltage input of 220V, which is much lower than the cut-and-bond driving actuators used in the past; the older actuators pumped approximately 250 cc/min at a voltage of 800V using 12 inch stack actuators (Oates 2001). These results represent a 53% reduction in flowrate but with a 72% reduction in voltage and much smaller stack actuators. This performance increase becomes ever more significant when the system weight and materials are considered.

The aluminum construction of the current pump is many times lighter than the stainless steel used in previous generations. Its small size contributes to its reduced weight of 625g without accumulator. Utilizing the EPCOS stacks provided a pressure of 1.38 MPa (200 psig) over the bias pressure using only 150V. The light chassis weight and low voltage requirements allow these pumps to be used in parallel to provide

necessary flow requirements. The small size of the pump body allows the pump to be placed closer to the load, therefore reducing fluid line loss.

Another interesting result of this investigation is that the maximum flowrate occurred at the minimum bias pressure. This result is attributed to the seal design in the hydraulic actuator. The actuator became harder to move manually as the bias pressure increased, most likely because the increased pressure pushed the seals tighter against the rod. As the pump system operated for an extended period after the data was taken, the grease that lubricated the rod in the actuator was stripped away. This could have also been a reason for increased friction in the actuator, although no direct tests were performed to verify this theory. An alternative hydraulic fluid should be investigated because the silicone oil used did not appear to lubricate the moving mechanisms.

The piezoelectric material represents a capacitive load on the amplifier system. With this type of load, the current draw is proportional to the driving frequency of the system. The three EPCOS stack actuators had a combined capacitance of 8.9 microfarads. This load could be impedance matched with an inductor to reduce the current draw, however the impedance matching is made at a specific frequency and does not work well at other frequencies. Impedance matching is performed by placing an inductor with a particular value in series with the capacitor. Once a peak performance frequency for the pumping system was found, then an impedance matched electrical system could be specified to reduce the power requirements of the amplifier system. Impedance matching was not performed in testing of the aluminum check valve pump.

The design of the current generation piezohydraulic pump was an evolution of earlier designs performed at Georgia Tech. The design discussed here incorporated new

technology in the form of the EPCOS cofired stack actuators, as well as design improvements that refine the maintainability and assembly of the miniature fluid system. Improvements such as the cylinder head redesign and pump housing construction give the experimenter more flexibility with the assembly and testing of the pump system by making the bleeding and inspection of the piezoelectric material easier than before. The added control of the spool valve increases the ease of use and demonstrates the ability to accurately position the actuator using this system.

CHAPTER 3

Introduction to Fluid Resonator Systems

3.1 Introduction

This chapter introduces a new concept in the development of piezoelectric hydraulic pumps. The new concept proposes using fluid and mechanical resonance to produce high pressure fluid flow. A system that operates at its resonant frequency would not only have an increased output due to a higher driving frequency, but it would also benefit from the higher amplitudes experienced during resonance. This chapter describes the similarities the resonant system has with existing piezo pumps, as well as the differences in form and function. Three resonant systems were designed. A head mass resonator was designed to investigate the response of a mechanical resonance. Two fluid resonance systems were designed to operate at two different frequencies, 20 kHz and 1 kHz. A method of rectifying the pressure pulses, such as through high speed check valves, was devised.

The resonant pump systems are similar to the previous pump system described in Chapter 2 in that they have an accumulator, control valve, and hydraulic actuator. The primary difference from the previous systems is in the pump itself. Previous piezo pump systems were designed to minimize the fluid in the compression chamber to reduce the effects of compressibility. These effects became important because the overall stroke of the piezoceramic is very small. A reduction in the volume of fluid being compressed results in less power loss to fluid compliance. A resonant fluid system instead uses fluid compliance to its advantage. The system resonates a column of liquid like a spring,

sending pressure waves back and forth inside a slender tube. Once resonance is achieved, the pressure within the fluid chamber is much higher than if the piezoelectric drivers were used without resonance. Once this pressure wave is created, a steady flow of fluid must be realized for any useful work to be performed.

When resonance is achieved, the high frequency, high pressure fluid waveform will have to be rectified through some type of valve system to produce positive fluid flow. Rectification alternatives such as reed valves, vortex diodes, and nozzle/diffuser configurations were explored. The rectification of the fluid pressure proved to be the toughest challenge in developing a pump system of this type. The pressure pulses have a very short duration on the order of 50μs for 20 kHz operation. A fluid rectification system must be devised which can bleed off some of the output as usable pressure flow. When this fluid resonance is then coupled with a mechanical resonant system, the output should be even greater.

A piezo driven head mass resonator was designed to investigate the mechanical resonance portion of the system before taking into account the nonlinearities associated with fluid resonance. This system consists of a series of stack actuators pushing against a head mass and preloaded against the mass with a threaded rod. The main goal of this investigation was to find what amount of mass is necessary to resonate at the desired operating frequencies. Also, one objective was to find what effect the mass of the stacks and hardware had on designing a head mass for a particular frequency. This understanding of mechanical resonance lead into a discussion of the fluid resonant systems.

The fluid resonant systems were designed to investigate and characterize fluid resonance. Each resonator is a half-wave resonant system with three stacks arranged in parallel and pushing against a thick aluminum diaphragm. A 20 kHz resonant fluid cavity was designed first, and tests on voltage and frequency variation were performed. It was found that an elaborate rectification system must be developed for 20 kHz operation. A 1 kHz resonator was also designed and fabricated. This system allowed the use of high speed reed valves, and tests were performed to explore the use of a lower frequency, although much larger, system. The following chapters detail the design and development of these three resonant systems, the head mass, 20 kHz, and 1 kHz resonators.

CHAPTER 4

Head Mass Resonator

4.1 Introduction

A head mass resonator was designed using cofired piezoelectric actuators. The resonator may be used in the future as a driving mechanism in a resonant fluid pump. The system consists of a head mass, three cofired stack actuators, a tail mass, and connecting hardware. The goal was to characterize the dynamic response of the mechanical system before adding the complexity of the resonant fluid section of the system. This was accomplished by first stating the design requirements for a resonant system; next, materials were chosen and the requirements applied to the selections. Lastly, the mechanical resonance system was constructed and tested.

4.2 Resonator Design Requirements

The design of the PZT resonator centered on a desired resonant frequency of 20kHz. An overview model of the system is shown in Figure 4.1. The system was viewed as a spring mass system, with a preload bolt and PZT stacks as the springs. The system consists of a tail mass, head mass, three EPCOS cofired stacks, a threaded rod, and assorted spacers and washers.

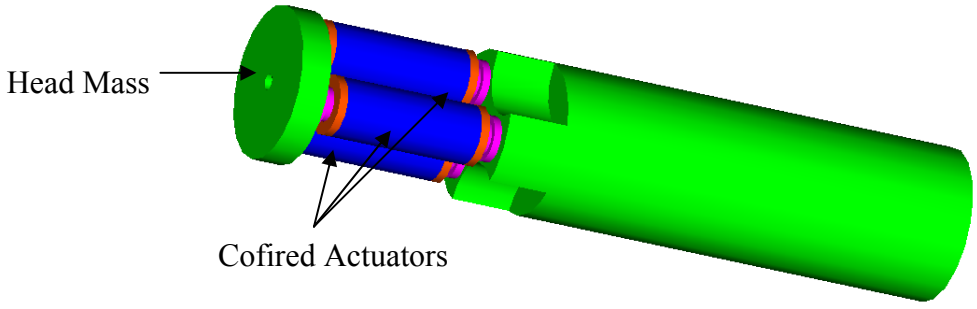

Figure 4.1: PZT Resonator Assembly

The requirements of the resonant system are complex, but can be narrowed down to three main requirements. First, the PZT stack must be placed under an initial compressive stress of around 20 MPa, hence the use of a preload bolt. Second, the stack is capable of a 1000 microstrain deflection, therefore the preload mechanism must stretch this amount after being preloaded without significantly increasing the stress on the PZT; an increase of ~5 MPa is acceptable. This requirement translates to a preload mechanism with a low stiffness. The final requirement is that the preload mechanism must be able to supply the return force necessary to pull the head mass back after it has reached its full displacement. Calculations were performed using the known material properties to satisfy these requirements.

The design process for the PZT resonator begins with a characterization of the piezoelectric stack actuators and calculation of a head mass. The spring constant of the PZT stack is calculated using Equation 4.1,

$$k = \frac{AE}{L} \tag{4.1}$$

where k is the spring constant, A is the area of the piezoceramic, E is the Young's modulus, and L is the length; values of A=4.5x10^{-5} mm^2, E=70 GPa, and L=30 mm result

in a spring constant of 105 MN/m for one PZT stack. Knowing the spring constant allows a head mass to be calculated using Equation 4.2.

$$m = \frac{k_T}{(2\pi f)^2} \tag{4.2}$$

In this equation, k_T is the total spring constant, which is the sum of the three PZT stack spring constants and the preload spring constant, and f is the desired frequency in Hertz. A three stack arrangement was chosen because three stacks in parallel operating at 20 kHz required a head mass of approximately 20g. This mass was a manageable value rather than the 6.6g result from using one stack.

One of the requirements deals with the preload mechanism having the necessary force to keep the stacks in contact with the head mass. This force was calculated by determining the peak acceleration of the mass. Equations 4.3 and 4.4 illustrate this calculation.

$$x = \delta \sin(\omega t) \tag{4.3}$$

$$\left\| \frac{d^2 x}{dt^2} \right\| = \delta (2\pi f)^2 \tag{4.4}$$

In these equations, x is the head mass displacement, δ is the peak displacement, and f is the desired frequency, in Hertz. The necessary return force was then calculated by multiplying the peak acceleration by the head mass. The preload system must be able to provide the necessary return force because the PZT stacks were not rigidly attached to the head mass. This was necessary because the stacks will fail if placed in tension. Therefore the bolts must be able to carry the return load to avoid "floating" the head mass at high frequency and hammering the stacks.

After determining base requirements, it was concluded that there was no combination of readily available materials that would provide the necessary return force at the maximum strain of the PZT material. The system would either be quite large or require a very high initial preload, which would reduce the performance of the piezoelectric material. Therefore, it was decided to decrease the maximum strain of the stacks to approximately 300 microstrain by reducing the drive voltage. Using this deflection, a single threaded rod made of 18-8 stainless steel size 6-32 was chosen as the preload mechanism. Because the maximum deflection was reduced, a manageable thread size was available. The length of the threaded rod was made five times the length (150 mm) of the PZT stack actuator; this allowed for a lower spring stiffness, while still providing the necessary return force at maximum deflection. The spring stiffness of the preload rod was calculated using Equation 4.1, where A is the threaded rod effective tensile area and E is the Young's modulus for steel.

4.3 Calculations Using Chosen Hardware

The design calculations began with the initial preloading of the stack actuators. The initial preload desired was 22 MPa, which corresponds to a 2970N preload on the single threaded rod. This load was acting on a tensile area of 5.87 mm^2, which produced a stress of 506 MPa in the rod. This preload was acceptable for a rod that is grade 5 or better (Norton 2000).

The next system requirement was to determine the effect the preload bolt had on restraining the actuators. At the full operational displacement of the stack there was an

increase of 72N on the stacks over the initial preload; this additional load corresponded to 540 kPa in additional stress on the PZT, which was an acceptable value.

The third requirement that was satisfied was for the bolt to supply the necessary return force for the mass to operate at 20 kHz. This was because a higher deflection would require a higher return force due to the increase in peak acceleration. This cannot be accomplished with common materials because of the initial preload that would be required to achieve the necessary return force. The preload that is necessary would place an unacceptable load on the stack actuators. A 300 microstrain deflection corresponds to a displacement of .009 mm for a 30mm long stack. Using Equation 4.4, this displacement operating at 20 kHz results in a peak acceleration of 142 km/s^2. Multiplying this value by the head mass of 20g results in a return force of 2840 N. The bolt must be able to supply this return force at maximum deflection, otherwise the stack actuators will be moving faster than the head mass. The spring constant of the preload rod is 8.09 MN/m, calculated using Equation 4.1. The force at maximum deflection was calculated by adding the deflection from preload to the maximum strain of the stacks. This value resulted in a return force of 3042 N. Therefore, a preload of 22MPa allowed the bolt to supply the return force necessary for a 300 microstrain deflection. Figure 4.2 shows the completed PZT resonator.

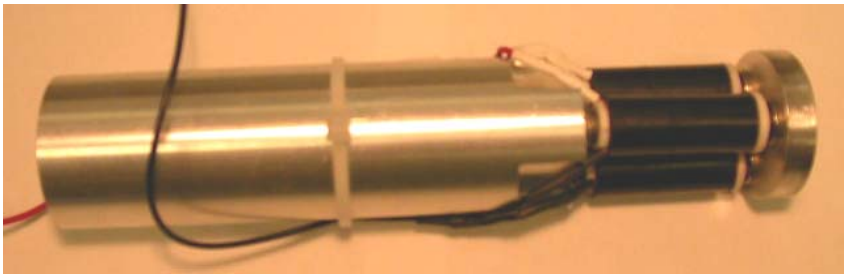

Figure 4.2: Three Stack PZT Resonator

4.4 Testing and Results

Testing of the three stack PZT resonator was performed using a Polytec laser Vibrometer (Model OFV 55) and accompanying data acquisition system. The schematic of the experimental setup is shown in Figure 4.3. The laser vibrometer uses a laser pointed at the head mass to measure the vibration of the head in order to characterize the frequency response of the resonator. The data from the vibrometer passed through signal conditioners and was input to a software package that allowed the user to view the information in different bases and time scales. A voltage reference input was connected to the data acquisition system from the output of the amplifier used to drive the PZT actuators. This normalized the vibration data and accounted for any fluctuation in driving voltage. A function generator was connected to a power amplifier (Krohn Hite model 7500) to drive the stacks. A 1V peak to peak sine wave was used to drive the resonator. Low voltage was used because the resonant frequencies are not dependent on the level of excitation. A frequency sweep from 1-30kHz was performed, and the maximum velocities were monitored. The resonant frequency of the resonator system was narrowed down to approximately 10kHz; this result was much less than the 20kHz desired frequency. Figure 4.4 shows a graph of the magnitude of velocities around the 10 kHz

range. Having a lower than expected resonant frequency was attributed to the design calculations not taking the mass of the stack actuators and preload rod into account. The overall light weight of the system exacerbated the effect that these masses have on the system, resulting in a resonant frequency which is approximately one half the value that was anticipated.

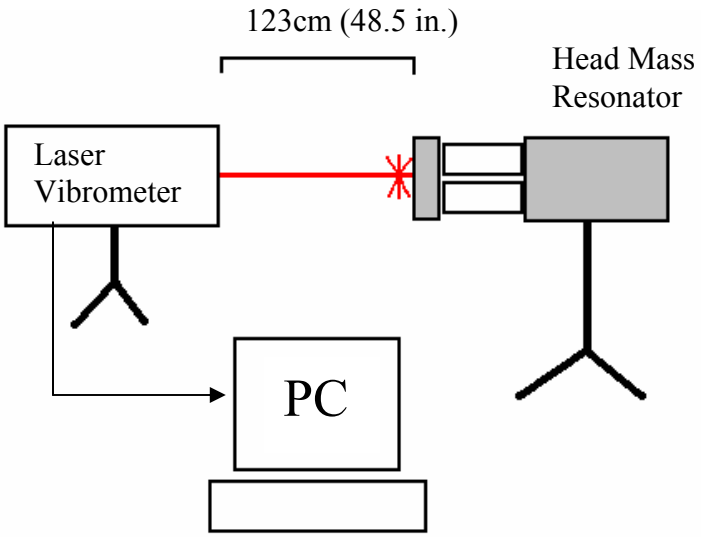

Figure 4.3: Experimental Setup of Laser Vibrometer

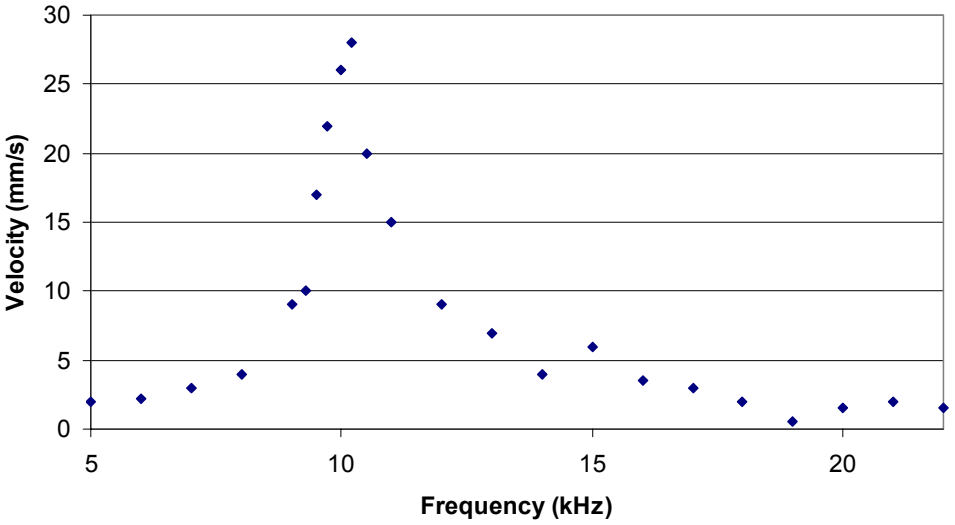

Figure 4.4: Velocity Magnitude at First Natural Frequency

4.5 Discussion

The purpose of designing a PZT resonator was to test a mechanical resonant system using piezoceramic stack actuators. An important result of testing the system was that the mass of the stack actuators had a great effect on the resonant frequency of the system. The head mass must be made much lighter than originally calculated in order to compensate for this extra mass and raise the resonant frequency. Removing material in non-critical areas of the mass geometry may also change the frequency. The type of resonating system discussed was being developed for use in a resonating fluid piezo-hydraulic pump. The design and construction of this resonant system was important because the mechanical side of the resonant pump must be investigated before addressing the increased complexity of the coupled fluid-mechanical system.

CHAPTER 5

Design of Piezo Driven 20kHz Fluid Cavity Resonator

5.1 Introduction

The reason for designing a fluid resonator was to explore the concept that piezo ceramic stack actuators may be used to drive a fluid cavity in resonance and possibly pump a fluid. The main objective of this investigation was to build a high-pressure wave in a fluid cavity and use small check valves to relieve some of the pressure and create positive fluid flow. Designs of two prototype resonating fluid pumps are discussed. The first design was developed around an operating frequency of 20 kHz. This frequency would produce a system with an inaudible operation noise. Due to difficulties associated with rectifying the fluid flow at these frequencies, a second pump system was also developed with an operating frequency of 1kHz.

The resonators consisted of cylindrical fluid cavities with a diaphragm at one end that was vibrated using cofired actuators. This chapter discusses the design of a driving system, diaphragm, and fluid cavity capable of producing the desired pressure waves in a fluid. An investigation into the rectification of fluid flow is also discussed. The hardware of the previous designs, including pistons and check valves, limited the operating frequency to approximately 100 Hz (Oates 2001). Using a resonating fluid bypassed these limitations. The next section details the design and construction of the vibrating diaphragm, which was used to create the pressure waves.

5.2 Diaphragm Design

5.2.1 Diaphragm Design Characteristics

There are many factors to consider when designing a high frequency vibrating diaphragm. For example, the mass of the diaphragm plays an important role in the operation of the resonant system. In the previous chapter, it was found that the PZT stack actuators contribute considerable mass to the mechanical resonance system. In order to have a system that resonates at the desired frequency of 20kHz, a head mass on the order of a 4-6 grams is necessary. This low mass must be maintained in order to meet the frequency response requirements of the PZT material.

In order to have such a light head mass, a diaphragm design was selected which used a thick diaphragm (1.59 – 3.175mm thick) as a separation between the stack actuators and the liquid. A thick diaphragm was chosen because the system required a wall that was lightweight, yet very stiff to keep up with the frequency response. The stacks were preloaded against the diaphragm by bolting them into an outer housing instead of directly to the diaphragm. Since the diaphragm must be very light, preloading the stacks against the diaphragm itself would be difficult.

In designing the driving portion of the fluid resonator, the response of the PZT actuators was investigated in conjunction with the diaphragm. The displacement function of the ends of the PZT stack actuators was calculated to determine the peak velocity of the vibrating wall. This was performed using the maximum displacement of the actuators. The stacks have a free displacement of 1000 microstrain, which for a 30mm stack corresponds to a displacement of .03mm (.00118 in.). Therefore, the position function of the end of the actuator is of the form $x=D\sin(\omega t)$, where D is half the maximum free

displacement. The peak velocity is then the derivative of position or $v=D\omega\cos(\omega t)$. If ω is the frequency, in radians, then the peak velocity of the end of the stack actuators is 1.88m/s at 20 kHz. Taking the derivative of the velocity function yields the acceleration function, $a= -D\omega^2\sin(\omega t)$. The peak acceleration is then computed as $D\omega^2$, which results in a value of $474 km/s^2$. The peak acceleration of the diaphragm must be greater than or equal to the peak acceleration of the stack actuators in order to avoid separation.

The next consideration dealing with the design of the diaphragm was the material. The diaphragm must be stiff enough to provide a good reflection surface for the pressure waves. However, it must also be flexible to allow the actuators to excite the fluid through the diaphragm without placing an unacceptable stress on the actuators. For this design, aluminum was chosen as the diaphragm material due to its relatively low stiffness (71.8 GPa) as well as its ease of machinability.

5.2.2 *Diaphragm Construction*

For experimentation purposes, three aluminum diaphragms were fabricated; the diaphragm thicknesses were 1.588mm (.082in.), 2.54mm (.10in.), and 3.175mm (.125in.). Figure 5.1 shows a picture of one of the completed diaphragms. Three diaphragm thicknesses were used to determine how each affected the system's response. The diameter of the resonating column was chosen as 50.8mm (2in.). This dimension was chosen arbitrarily to allow three stack actuators to be arranged in a symmetric pattern near the middle while still allowing enough area so bending of the diaphragm would occur. The symmetric three-stack arrangement was chosen to promote uniform vibration of the diaphragm. A finite element analysis was performed on the diaphragm to

determine the force necessary to deflect the diaphragm an amount which equals the full free displacement of the stack actuator.

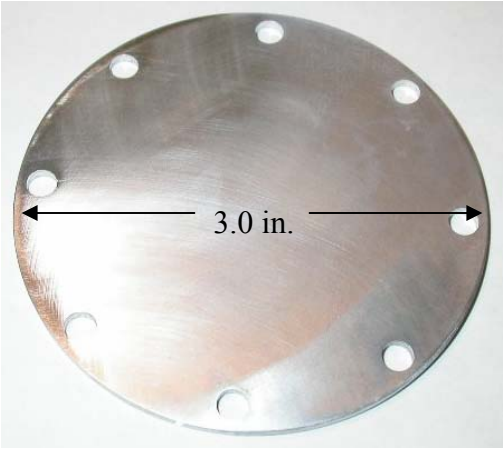

Figure 5.1: Aluminum Diaphragm

5.2.3 Diaphragm Finite Element Analysis

The I-DEAS solid modeling and finite element package was used to model and analyze the diaphragm. For the analysis, a 2.54mm (.1in.) thick parabolic triangle shell element was used. The diaphragm was meshed using 2.54mm (.1in.) maximum element size. The outer surfaces of the 76.2mm (3in.) diaphragm that were clamped in the fluid chamber were constrained by placing displacement restrictions on the individual elements. This left a 50.8mm (2in.) area which was free to move. The distributed load was placed on three 12.7mm (.5in.) circles near the center of the diaphragm. These circles were where the driving system contacts the diaphragm. Material properties such as the Young's modulus, density, and poisson's ratio were entered into the software package so the program can simulate the material properly.

The purpose of the finite element investigation was to determine how much additional stress was placed on the stack actuators purely from the diaphragm deflection. Another objective was to calculate how much force was required to displace the diaphragm the full allowable displacement. If the additional stress exceeds ~8-10MPa, then the diaphragm may be made thinner. Subsequent analyses were performed until the load applied to the diaphragm resulted in a deflection that equaled the maximum free displacement of the stack actuators. Figure 5.2 shows the results of this investigation. A larger version of this illustration is also shown in Appendix H. The simulation predicts a maximum displacement of .03mm (1.18×10^{-3} in.). This is the maximum free displacement of the stack actuators at 1000 microstrain. The total load placed on the diaphragm was 311N (70 lb.). This load distributed across the areas of the three stack actuators, each with an area of 4.5×10^{-5} m^2, resulted in an added stress of only 2.31 MPa. This added stress was acceptable and still allowed the actuators to function normally, which satisfied one of the requirements of the mechanical resonant system.

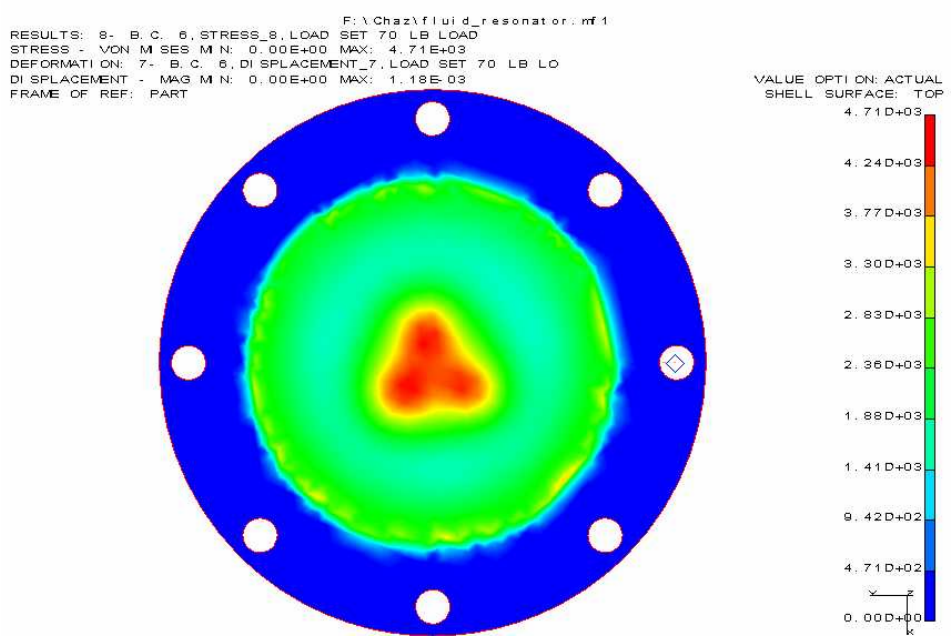

Figure 5.2: Finite Element Model of Diaphragm (values in psi)

Another simulation that was performed was to determine the deflection of the diaphragm when the stack actuators are at their maximum stress levels. For the PZT used in the experiments, the maximum compressive stress that was considered safe was 35 MPa. When the three stacks are placed at this stress level, it corresponds to a 4725N (1062 lb.) load on the diaphragm. When this load was placed on the diaphragm, the finite element model predicted a maximum deflection of .457mm (.018 in.).

Another requirement that must be satisfied was that the end of the stack actuators must remain in contact with the diaphragm. Therefore, there must be sufficient return force in the diaphragm to attain a peak acceleration higher than that of the stack actuators. Using Newton's law, F=ma, the acceleration of the diaphragm with an assumed mass of 5g is 62.20 km/s^2. The 5g mass was assumed because the actual vibrating mass was distributed between the center and the clamped edges of the diaphragm. When comparing

this value to the stack actuators' peak acceleration of 474 km/s^2, the diaphragm accelerates 7.6 times slower than the stacks. Therefore, in order to use the diaphragm at this frequency, the peak displacement must be lowered to avoid separation. If high displacements are desired, the operating frequency must decrease or the diaphragm must become lighter and stiffer. The stack actuators could also be preloaded further into the diaphragm, which would increase the return force by adding an initial deflection to the diaphragm.

From this analysis it may be seen that a 2.54mm (.10 in.) thick diaphragm was suitable for two reasons. First, the maximum deflection of the stacks only added 2.31 MPa stress to the piezo material, which meant the diaphragm did not hinder the stacks from performing their function. Second, since the diaphragm was not distorted even at the maximum stress level for the stacks, the diaphragm was a suitable barrier for preloading the stacks in compression. Three different diaphragms were tested with the system to account for any assumptions or nonlinearities experienced with the resonant cavity.

5.3 Piezoelectric Driving System

The driving system of the resonating fluid pump consisted of a rear housing, PZT actuators, backing plate, and various hardware. The rear housing incorporated a bolt flange to allow connection to the fluid chamber through the diaphragm. The diaphragm was sealed against the fluid chamber using a confined o-ring. The rear housing itself had a recess to allow the flexible diaphragm to vibrate. The end of the housing had three

holes which were approximately the size of the PZT actuators. These holes contained the actuators and kept them properly aligned.

The actuators used were three cofired EPCOS PZT actuators wired in parallel. The actuators were 30mm in length with a 6.7x 6.7mm PZT stack encased in soft plastic. Figure 5.3 shows a picture of one bare EPCOS stack. The actuator has a diameter of 12.7mm (.5in.). Each stack had a 1.78mm (.070 in.) piece of alumina ceramic glued at each end. Attached to these pieces were stainless steel spherical washers. The alumina ceramic functioned as a hard barrier between the bare PZT and the irregularly shaped spherical washers. The alumina has a high compressive yield strength of 2.07 GPa (300 ksi) which prevented the spherical washers from pushing into and cracking the PZT under the high loads experienced. The spherical washers were used on each end to prevent bending moments on the actuators, which would crack them. Figure 5.4 shows the piezo stack array ready for testing. On the free end of the stack actuators, there was another piece of alumina ceramic which contacts the diaphragm. Figure 5.5 shows an exploded view of the 20 kHz resonator. On the rear of the housing, there was a backing plate that screws into the rear housing. This backing plate was held in place using four 8-32 cap screws. These screws allowed adjustment of the preload on the stacks against the diaphragm.

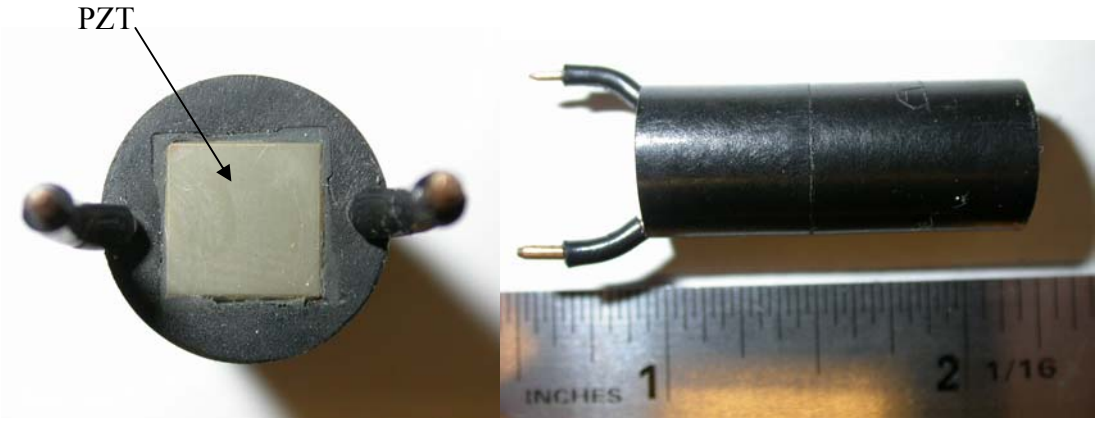

Figure 5.3: EPCOS Stack Actuator Top and Side View

Figure 5.4: EPCOS PZT Array

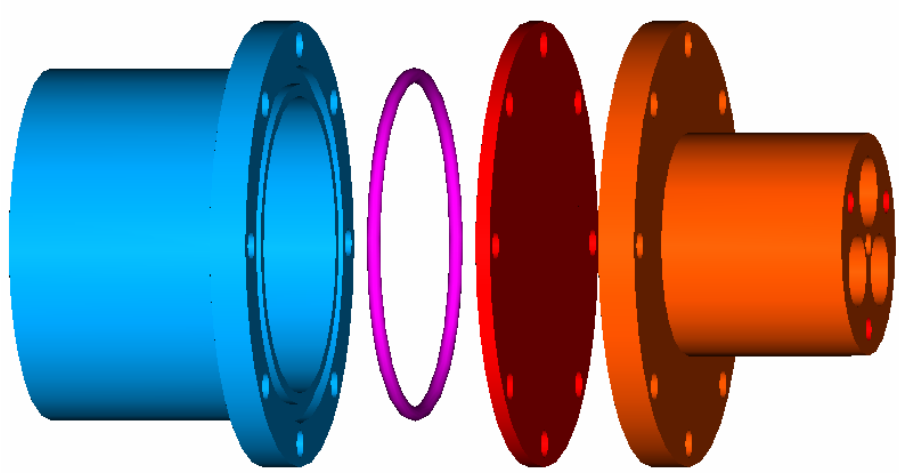

Figure 5.5: Fluid Resonator Assembly

5.4 Fluid Cavity Design – 20 kHz Operation

The design of the fluid cavity resonator involved selection of the fluid that will be used, wave speed calculations, and construction issues. The fluid which was used in the resonator pump was the same as was used in the aluminum check valve pump, Dow Corning 200. This light silicone oil has a viscosity of .65cSt which is comparable to the viscosity of water. Because of its similarity, water was used in the preliminary experiments, and a sound speed of 1500 m/s was used in the wave speed calculations.

One of the most critical dimensions of the resonating fluid cavity was the chamber length. As stated earlier, the cavity was cylindrical in shape with the wave traveling between the two flat ends. The 20kHz operating frequency corresponds to a period of 50μs. Therefore, in this period of time the wave must travel from one end of the cavity to the other and back. This type of chamber is known as a half-wave system. Equation 5.1 shows the calculation of the fluid cavity length, L.

$$2L = 1500m/s \cdot 50\mu s \tag{5.1}$$

This equation yielded a cavity length of 37.5mm. This size produced a very compact resonator. Figure 5.6 shows a wireframe model of the resonator fluid cavity. The resonator body and rear housing were constructed out of stainless steel because of its high stiffness. In order to get good wave reflection and with minimal losses, a stiff material and relatively thick walls were deemed necessary. The compact resonant system, along with an inaudible excitation frequency would produce a compact pump design.

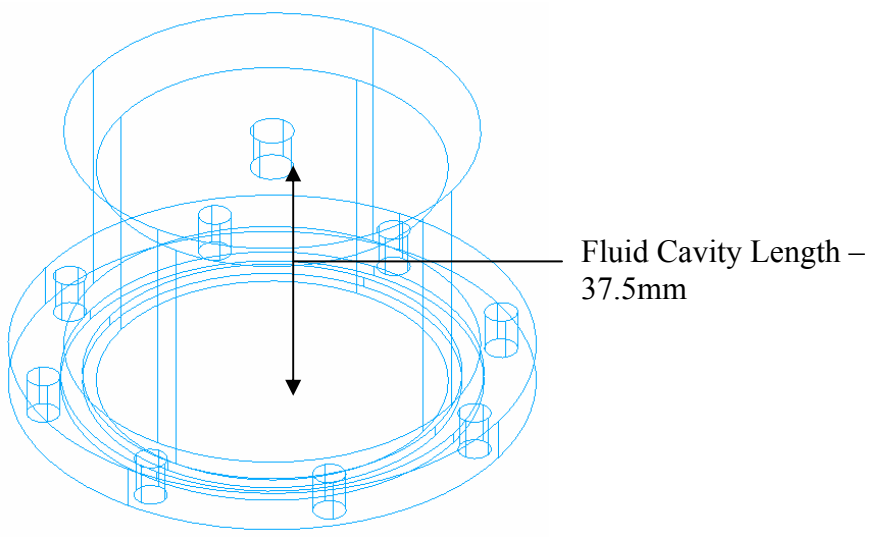

Figure 5.6: Resonating Fluid Cavity

5.5 Experimental Setup- Closed Chamber

Once the fluid cavity had been filled and there were no air bubbles in the system, the resonator was sealed and the fluid chamber, diaphragm, and rear housing were bolted together. A schematic of the system is shown in Figure 5.7. Figures 5.8 and 5.9 show the completed resonator assembly. The stack actuators were driven by a power supply capable of producing the necessary 20V at the selected frequency. The experiments were run at 20V peak to peak excitation to prevent diaphragm separation. In the first

experiments performed, the fluid chamber only had provisions for a pressure sensor. This setup was used to measure the pressure fluctuations in a solid column of water, and investigate the system response at resonance. Pressure in the fluid was measured using a fast response pressure sensor (Omega Model DPX 101) capable of measuring pressure transients with a rise time of 1 microsecond or more. The pressure sensor was connected to a battery operated signal conditioner (Omega Model ACC-PS1). Notice in Figure 5.9 the three holes where the stacks were installed. The backing plate is not shown in these figures. Once the fluid cavity was assembled and all the air removed, the piezoelectric actuators were preloaded into the diaphragm. They were then driven with a frequency sweep to find the frequency of the driving system that induced resonance in the fluid. The experiments were repeated for different diaphragm thicknesses. Also, pressures were measured both at the center and the edge of the reflecting wall to determine any deviations in pressure response. From this data, the peak pressure in the fluid was determined.

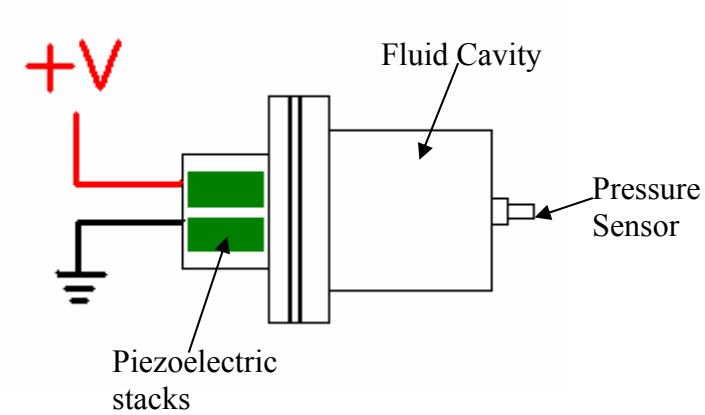

Figure 5.7: Schematic of Closed Chamber 20 kHz Resonator

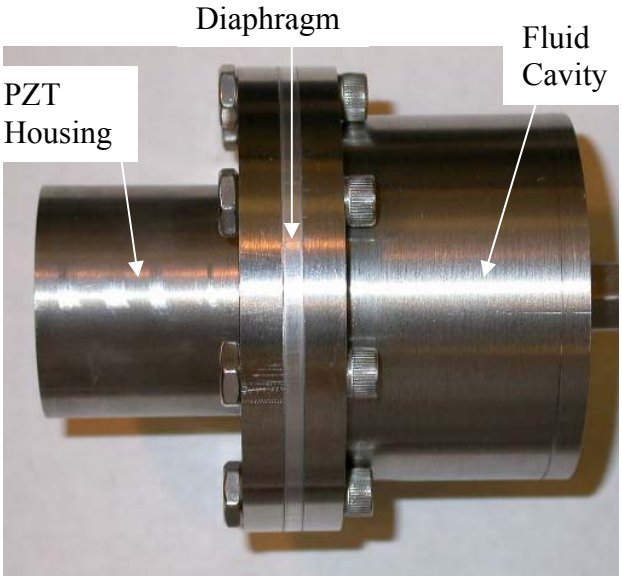

Figure 5.8: Resonator Assembly (side view)

Figure 5.9: Resonator Assembly (end view)

5.6 Results – Closed Chamber

Resonant data was obtained using the closed resonant chamber. The pressure sensor has a sensitivity of 5.1mV/psig, therefore the readings required a simple calculation to convert them to pounds per square inch. Figure 5.10 shows the results of the closed chamber test. As can be seen in the figure, there were definite resonances occurring at 17.4kHz and 22.2kHz. Changing the diaphragm thickness only shifted where the maximum amplitude occurred between these two values.

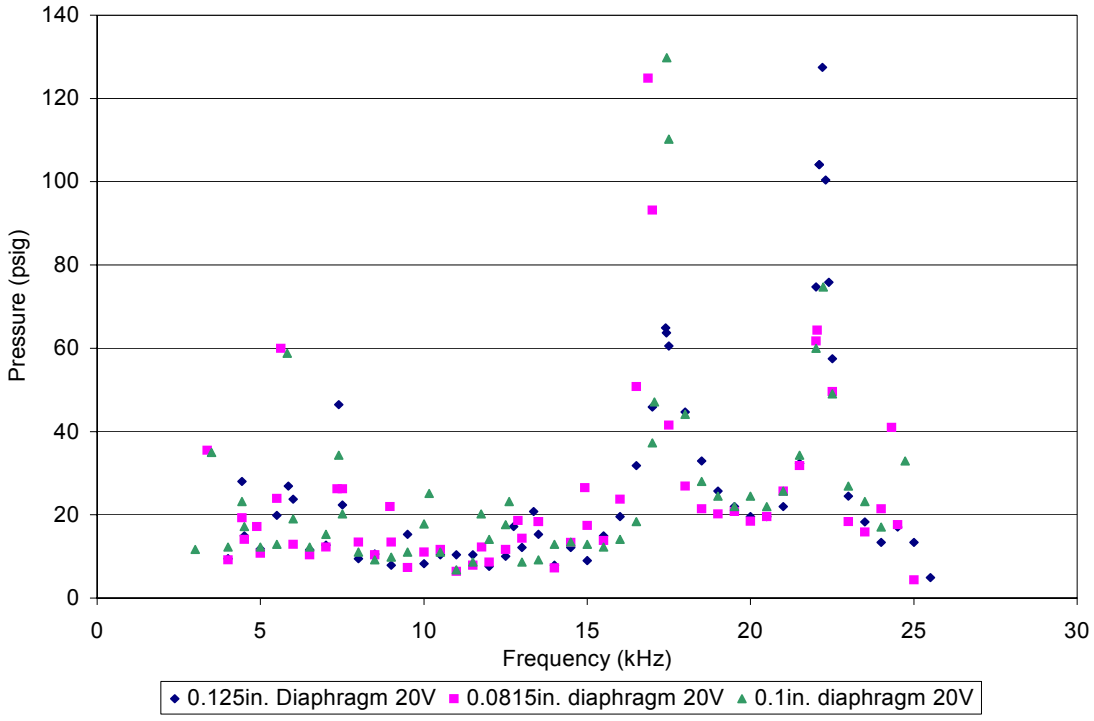

Figure 5.10: Pressure vs. Frequency for Closed Chamber

The placement of the pressure sensor in the fluid cavity was also tested. The purpose was to determine where the highest pressure fluctuation exists on the end wall of the fluid cavity. The pressure sensor was placed in the center and at the edge of the end

of the fluid cavity. Pressure data was taken as a function of frequency. This data is shown in Figure 5.11.

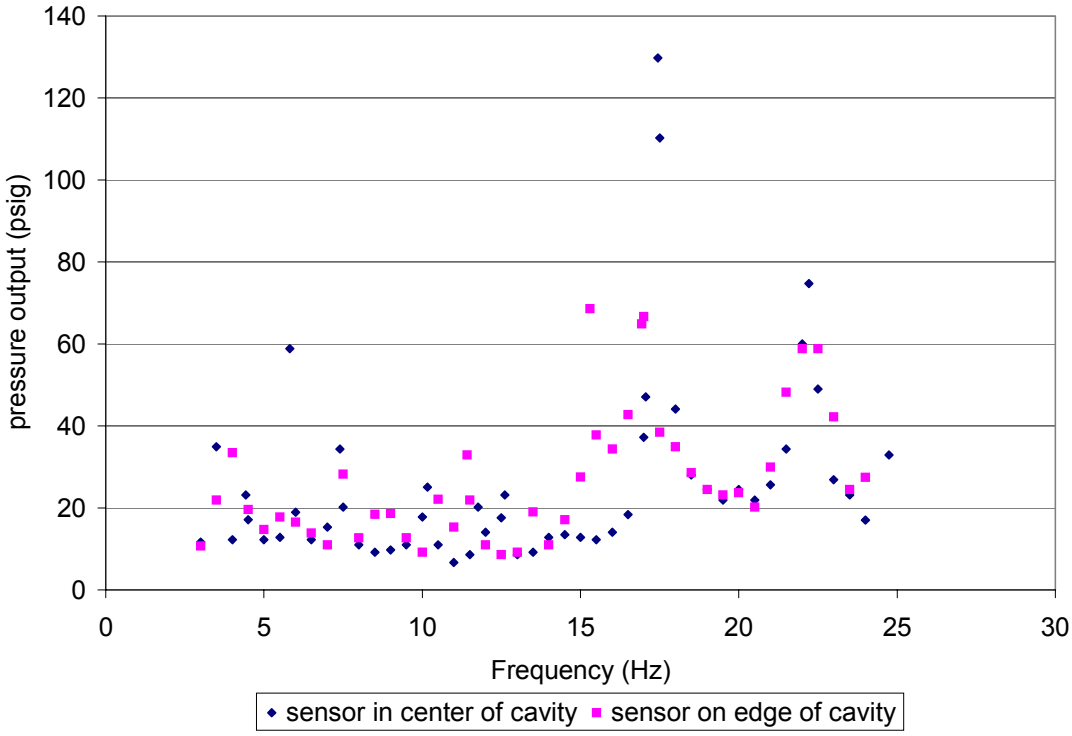

Figure 5.11: Pressure Sensor Location Data for .1 in. Diaphragm

As can be seen in this graph, the location of the pressure sensor showed that the resonance of the system occurred at the same frequencies across the end of the chamber. The relative amplitudes of the pressures at resonance, however, were slightly different. The pressure amplitude at both resonant frequencies were lower when the sensor was located on the edge of the chamber versus when it was in the center. This is most likely due to radial pressure fluctuations. The length of the chamber is not much larger than the diameter, therefore the pressure waves cannot be assumed to travel in only one direction.

This experiment demonstrates the value of resonating a column of water. Pressures in excess of 130psig were attained with only a 20V input voltage. This performance is quite promising, however the challenge of how to rectify these short pressure pulses into a constant, high pressure flow remains.

5.7 Rectification Investigation for Use in Piezohydraulic Pump

5.7.1 Introduction

One of the major challenges in designing a resonant fluid pumping system was how to rectify pressure pulses into positive flow. Conventional poppet check valves, such as those used in the aluminum piezopump described in Chapter 2, will not function at frequencies in the kilohertz range. Therefore, a high frequency alternative to the conventional check valve needed to be devised. The first approach was the design of a cantilever type reed valve. This type of valve is known for its high frequency response and ability to seal high pressures such as in a two-stroke engine. The second type of fluid rectifier that was considered was a vortex fluid diode. The fluid diode has no moving parts to fatigue; however it has no positive pressure holding capacity like a check valve. The last rectifier that was considered was the method of using nozzles and diffusers to rectify fluid flow. This method utilized fluid loss in a diffuser to promote flow in one direction. This method was also beneficial because there are no moving parts.

5.7.2 Reed Valve - Frequency Response

In order to operate a pumping system at a frequency in the tens of kilohertz, the reed valves must have a natural frequency in the same range, preferably higher than the maximum operating frequency. The valves were assumed to be a cantilevered beam

fixed at one end. They are rectangular in shape with a length, width, and thickness. For the calculations, spring steel thicknesses of .254mm (0.010in.), .381mm (0.015in.), and .508mm (0.020in.) were used. The equation for the natural frequency of the beam with its mass distributed along its length is shown in Equation 5.2

$$\omega_n{}^2 = (3.52)^2\left(\frac{EI}{ml^3}\right) \tag{5.2}$$

where I is the second moment of inertia in the form of Equation 5.3.

$$I = \frac{bt^3}{12} \tag{5.3}$$

In these equations, b is the width of the beam, l is the length, and t is the thickness. The calculations were performed for two natural frequencies, 10kHz and 20kHz. Using the given thicknesses and a common width of 5 mm, Equation 5.2 was solved for the length of the beam. Table 5.1 shows the results of these calculations. All the necessary lengths required for the desired natural frequencies were manageable. The lengths of the reed were also long enough to easily cover a machinable inlet or outlet hole. The only questionable valve length was the .254mm thickness operating at 20kHz. A length of 3.25mm did not leave much room for a fluid passage underneath. The inlet and outlet holes needed to be of sufficient size as not to choke the system with excessive fluid resistance.

Table 5.1: Natural Frequency Calculations for 10kHz and 20kHz

Natural Frequency (Hz)	Thickness (mm)	Required Length (mm)
10000	.254	4.60
10000	.381	5.63
10000	.508	6.50
20000	.254	3.25
20000	.381	3.98
20000	.508	4.60

5.7.3 Reed Valve - Fatigue Investigation

Now that the basic calculations had been performed to attain geometry, the investigation into fatigue resistance may ensue. A more in depth look into the operation of the reed valves suggested that fatigue must be considered in their design. Because of their high operating frequency, the valves have to be designed for infinite life. In order to have infinite life, the maximum alternating stress must be below a minimum value, as defined by one of the standard fatigue criterion. This alternating stress value is directly affected by how far the reed valve bends in operation. The calculations will result in a maximum allowable displacement; the feasibility of the reed valve design was made using these values.

The fatigue calculations began with the determination of the endurance limit. According to Norton (2000), the uncorrected endurance limit for steels with an ultimate tensile strength of less than 200ksi is one half the ultimate tensile strength. For the

calculations in this thesis, 1095 carbon steel quenched and tempered at 200 °F was used. Table 5.2 illustrates some of the properties of this material. Using the value of the ultimate tensile strength, the uncorrected endurance limit was 448 MPa.

Table 5.2: Properties of 1095 Carbon Steel Q&T at 200 °F (Norton)

Density (kg/m^3)	7800
Modulus (Pa)	207x10^9
Yield Strength (Pa)	552x10^6
Ultimate Tensile Strength (Pa)	896x10^6

Once the uncorrected endurance limit is calculated, a series of correction factors are calculated to account for size, surface, and other conditions during the loading cycle. Equation 5.4 shows the correction factors according to Norton.

$$S_e = C_{load} C_{size} C_{surf} C_{temp} C_{reliab} S_e' \tag{5.4}$$

Because the valve was in a bending mode, C_{load} equals 1; similarly, C_{size} equals 1 due to the small size of the valves. For the surface effect correction factor, a ground finish was assumed. Therefore, the correction factor was calculated in Equation 5.5.

$$C_{surf} = 1.58(S_{ut})^{-0.085} \tag{5.5}$$

This calculation resulted in a surface correction factor of 0.89. The temperature effects were assumed negligible, therefore C_{temp} equals 1. For reliability, a 99.9% value was desired, which resulted in a correction factor of 0.753. These correction factors were combined in Equation 5.4 to produce a corrected endurance limit of 299 MPa. This value

was then input into the desired failure criterion to determine the maximum possible alternating stress.

The failure criterion used was the modified Goodman criterion. This criterion relates the mean and alternating stresses to experimental evidence of failure. Equation 5.6 illustrates the failure line of the modified Goodman criterion.

$$\sigma_a = S_e\left(1-\frac{\sigma_m}{S_{ut}}\right) \tag{5.6}$$

In this equation σ_a and σ_m are the alternating and mean stresses, respectively; S_e is the corrected endurance limit and S_{ut} is the ultimate tensile strength. In the case of the reed valves, the mean stress was equal to the alternating stress, resulting in Equation 5.7.

$$\sigma_a = \frac{S_e}{\left(1+\frac{S_e}{S_{ut}}\right)} \tag{5.7}$$

With this equation, a maximum possible alternating stress was calculated to be 224 MPa. The maximum stress experienced by the reed valve was the mean stress plus the alternating stress, in this case $\sigma_{\max} = 2\cdot\sigma_a = 448MPa$. This was the maximum stress that may be experienced by the reed valves and still maintain infinite life. The deflection of the reeds themselves was then calculated using Equations 5.8 through 5.10. Equation 5.8 is the deflection of a beam under applied force.

$$y_{\max} = \frac{FL^3}{3EI} \tag{5.8}$$

Equation 5.9 is the maximum stress on a beam due to a force applied

$$\sigma_{\max} = \frac{FLt}{2I} \tag{5.9}$$

Solving Equations 5.8 and 5.9 for *FL/I* and combining results in Equation 5.10

$$y_{\max} = \frac{2L^2\sigma_{\max}}{3tE} \tag{5.10}$$

In Equation 5.10, the stress is the maximum stress the beam can withstand and still retain infinite fatigue life. Using Equation 5.10 to calculate the tip deflection, it was noticed that the L^2/t terms are the same for each thickness and length for a given resonant frequency. Therefore the maximum allowable tip displacement was only a function of frequency. The maximum tip displacement to maintain infinite fatigue life for the 10kHz and 20 kHz valves was 0.1204mm and 0.0602mm, respectively, regardless of thickness. The calculation sheet used is located in Appendix I.

5.7.4 Reed Valve - Discussion

The results of this investigation into the use of high speed reed valves to operate a fluid resonating pump yielded interesting results. Making a beam vibrate at frequencies in the tens of kilohertz made fatigue a dominating factor in its operating life. Infinite fatigue life was necessary to have a useful part under these conditions, and this constraint limited the amount of stress that can be placed on the material. The tip displacement of .1204mm for 10kHz was mediocre at best, but the .0602mm displacement for 20kHz was unacceptable. Such a small displacement would put an undesirable amount of fluid resistance in the system. The problem with the cantilevered beam reed valve is the fatigue life. If the valve could be modified to operate on a hinge, the stresses on the valve material would be minimal, satisfying the fatigue constraint. The tradeoff would be that the valve would no longer have a return force. The flow of the system would have to be routed around the reed flap to promote the opening and closing of the valve.

The cantilevered reed valve did have a valuable characteristic over the other methods discussed. When the pump is not running the valve will continue to hold

pressure. This allows the pump to run in energy efficient duty cycles, as opposed to continuously. This was not possible with the other two methods discussed because they allowed the high pressure fluid to bleed across to the low pressure side when the pump was not energized. Cantilever type reed valves would be feasible on a pumping system that operated at a lower frequency. This would allow for a larger displacement of the reed tip and less fluid resistance.

5.7.5 Vortex Fluid Diode

Another method for rectifying fluid flow was the use of a vortex fluid diode. This method restricted flow in the throttling direction by forcing the fluid to spin in a circular chamber before exiting. Figure 5.12 shows an illustration of the internal passages in a vortex diode. When fluid passed through the top passage, it fills up the circular cavity and flows easily out the side tube. When the flow was reversed, however, the liquid must enter the side tube and spin in the cylindrical chamber to the middle where it can exit. The fluid had to do this all while inertial effects on the liquid try to keep the fluid away from the center. This effect of creating a vortex is what causes the high restriction in the reversed direction. The vortex diode is a simple design that would be an elegant solution to the problem of rectifying flow. There are no moving parts to fatigue or to move at extremely high frequency. The diode was easy to construct.

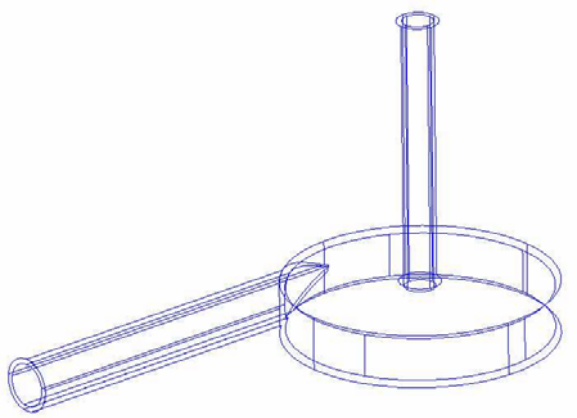

Figure 5.12: Vortex Fluid Diode

The disadvantages to this method were that there has not been much detailed work performed on the subject of designing these devices. Researchers such as Haakh (2003) only give rules of thumb for dimensioning the inlet and outlet as well as the vortex chamber itself. The fluid restriction works as a transient flow problem, and as a result, the head loss in the throttling direction takes time to set up. In larger systems the time to reach a steady state head loss can take as long as seven seconds (Haakh 2003). The fluid restriction is based on the forming of a vortex inside the diode. The time required to set up this vortex was an important factor in whether or not the diode became a viable alternative in the rectification of flow in the resonant fluid pump. The diodes have been used in the past as buffers against pressure fluctuations in water piping systems.

Two sizes of vortex fluid diodes were constructed for testing. Figure 5.13 shows a drawing of one of the fluid diodes. For each size, there were two identical diodes constructed; one for an inlet and one for an outlet. One set of diodes had a vortex chamber diameter of 15.4mm (.6075 in.) while the other had a diameter of 3.1mm (.123 in.). Figure 5.14 shows a picture of the larger of the two diodes. The other dimensions

were scaled proportionally such as the entrance and exit passage sizes. One of the diodes was fabricated out of aluminum, while the other three were made out of Plexiglas. Making the diodes out of Plexiglas gave the experimenter a view of fluid flowing through the diode. This was helpful in diagnosing problems. After machining, all surfaces were polished using a rotary polisher. The mating surfaces were made flat and all distortions from machining were polished away. Threaded rod fasteners were used to attach the two halves of the diode together. The two halves were thick enough to allow the installation of a threaded pipe fitting for installation into a fluid system.

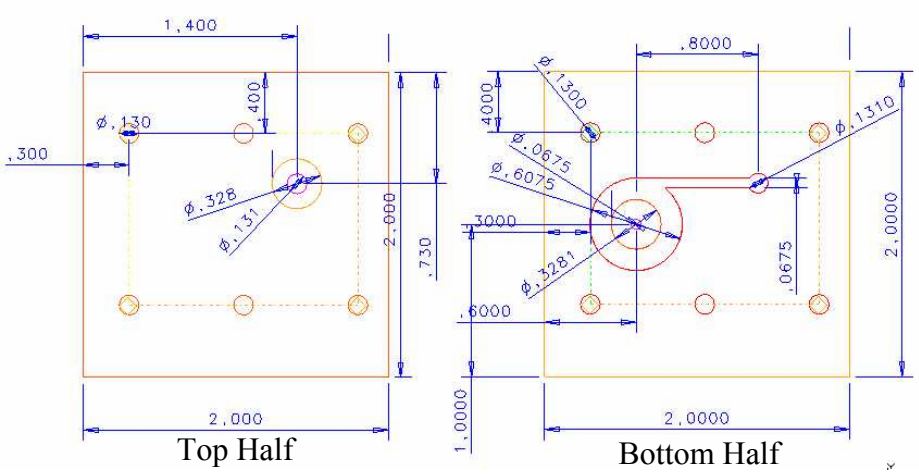

Figure 5.13: Dimensional Drawing of Fluid Diode (Dimensions in inches)

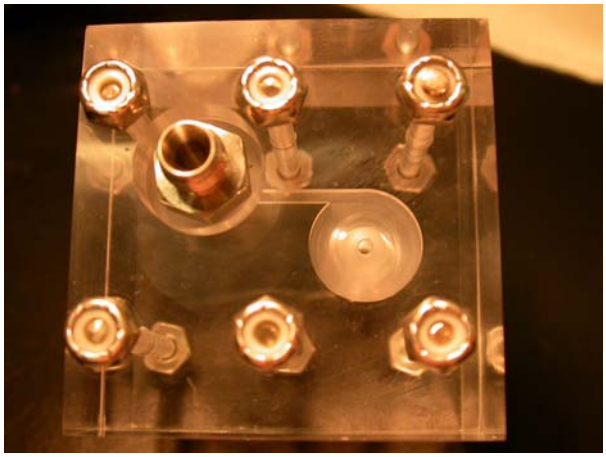

Figure 5.14: Large Vortex Fluid Diode

5.7.6 Flow Testing

The two different size vortex diodes were installed in line with a water faucet. The amount of flow restriction was measured by noting the amount of time it took to fill a 600mL beaker. The time to fill the beaker was measured without the diodes installed to account for restrictions in the lines. The flowrate measured was 16.7cc/s. Each size diode was then installed in each direction, for a total of four positions. The flowrates measured are shown in Table 5.3. Table 5.4 quantifies these readings as a percent reduction in flow from when the diode is not installed. This data shows that the diodes performed well at restricting flow in one direction. The question is whether this technology can be applied to restricting a high frequency pressure pulse.

Table 5.3: Measured Flow Rates for Vortex Diodes

	No diode installed	Large diode with flow	Large diode against flow	Small diode with flow	Small diode against flow
flowrates cc/s	16.7	14.9	9.6	6.8	2.9

Table 5.4: Percent Reduction in Flow versus Free Flow

	Large diode with flow	Large diode against flow	Small diode with flow	Small diode against flow
% Reduction in flow	-10.71%	-42.68%	-59.18%	-82.35%

The reason for making one set of diodes with a very small vortex chamber was because of the high frequency at which they operate. Since the vortex diode works by a swirling effect in the chamber, there is a time constraint that must be met. The pressure fluctuations from the resonator may be as short as 50μs, therefore the vortex must build and produce a flow restriction in this short amount of time.

5.7.7 Nozzle/ Diffuser Fluid Rectification

There has been research performed in the field of piezo pump technology using valveless nozzle/ diffuser cone technology. This type of system is similar to the vortex diode in that there are no moving parts. The system uses a diffuser and nozzle at the inlet and outlet of the compression chamber of the piezo pump. With each stroke, the fluid loss through the inlet orifice is more than the exit opening, thus causing positive fluid flow. As stated before, a rectification system that relies on a fluid loss mechanism to restrict flow has certain drawbacks. Researchers such as Ullman and Fono (2002) and L.S. Pan et al. (2001) have performed research in the area of valveless piezo pumps. Ullman and Fono have presented a dynamic model that details the nozzle and diffuser arrangement. They predict pump systems using this method would have an efficiency on the order of 1% (Ullman and Fono 2003). Another disadvantage is that the pump has to run continuously. There is no physical barrier to prevent backflow of the pump, like

when a check valve is used. Efficiencies in the range predicted by Ullman and Fono would not allow the technology to be used in engineering applications. Rigorous analytical fluids analysis of the fluid flow would be necessary to perfect the fluid loss rectification system. This type of rectification system was not implemented in testing.

5.8 Results – 20kHz Resonator Using Fluid Diodes

Testing of the resonant fluid system was performed using both sizes of vortex fluid diodes. Two holes were tapped into the fluid chamber; one hole in the end of the chamber and one on the side nearest the diaphragm. The diodes were attached to the chamber using 3.175mm (.125in.) stainless steel tubing and fittings. The diodes were placed as close to the chamber as possible to reduce fluid momentum losses in the lines. Connecting the diodes together and creating a closed loop was a typical hydraulic cylinder (Clippard model H9D-1D). Bias pressure was applied to the system using an accumulator and water was used as the working fluid.

After the system was assembled and bled of any air, it was pressurized and connected to a Krohn Hite (model 7500) amplifier. A 20V peak to peak sine wave was used with a 10V positive bias voltage. A low excitation voltage was used because of the high frequencies being investigated, and because the driving voltage should not have as much effect on the system once resonance was reached.

The system was run at 20V excitation and a frequency sweep performed. No positive fluid motion was observed. Resonance was achieved at a frequency of 17.5 kHz, which is consistent with the readings recorded with a closed chamber. The pressure at resonance was only around 10 psig, which was much less than that observed with a

closed chamber. Changing the position of the actuator manually also had an effect on the system resonance. Moving the actuator shifted the resonance point and the frequency had to be modified to compensate for the position of the actuator. Because of this observation, it was assumed that if the fluid beyond the diodes was affecting the response in the chamber, then there was not sufficient resistance in the diodes. It was thought that the very small displacement of fluid into the diode cavity did not allow the swirling effect to occur. Therefore the momentum of the fluid was not building quickly enough, which directly affected the operation of the diode to restrict flow. The decision was then made to construct the fluid diodes with a much smaller vortex chamber. Using the smaller set of fluid diodes produced the same results as the larger diodes, except the actuator was harder to move manually.

5.9 Discussion – 20 kHz Resonator

One of the goals set forth in this system was to determine if a half wave resonator driven by piezoelectric materials could be developed to pump a fluid at high pressure. A system was developed which produced high pressure, however, complications in the hardware of the system prevented this successful operation from being turned into a pumping system. The challenge of rectifying the very short pressure pulses, which were on the order of 50 μs, was a challenge which must be met with in-depth fluids research and analysis. Methods of fluid rectification explored were using reed valves, vortex fluid diodes, and nozzle/diffuser technology. The system which was designed was compact and operated in an inaudible frequency range. If the rectification of the acoustic pressure

pulses can be attained, the feasibility of the acoustic wave piezoelectric pump will grow as a viable application of these materials.

CHAPTER 6

Design of 1 kHz Fluid Resonator

6.1 Introduction

This chapter discusses the design of a resonating fluid cavity with a target frequency of 1 kHz. Operation at 1kHz allows the use of a cantilever type reed valve system. The 1 kHz resonator was similar to the 20 kHz version discussed in the last chapter, except it is longer and heavier. The design of a reed valve system was discussed in Chapter 5, and will be summarized here for a lower operating frequency.

The 1kHz resonator consists of a drive element, diaphragm, long tube and end cap. The main advantage gained from the lower frequency design is that a reed valve system can be readily designed and fabricated to operate in this frequency range. The use of reed valves prohibits backflow of the pump, unlike the valveless systems discussed in Chapter 5 which provided no such physical barrier. The fluid cavity was much longer than on the 20kHz fluid resonator in order to resonate at 1000Hz. The increased size and weight was detrimental to one of the goals of the project. However, a laboratory scale pump system designed to operate at 1kHz was ideal for testing the technology prior to miniaturization. This chapter discusses the calculation of resonant frequency based on wave speed, reed valve design, experimental setup, and testing of the 1 kHz resonator.

6.2 Resonant Frequency Calculations

The resonant frequency calculations were the same as for the 20 kHz resonator detailed in the last chapter. For testing purposes, water was used as the medium in the 1

kHz system. A 1 kHz oscillation corresponds to a period of 1 ms. Therefore, for a half wave resonator, the chamber length is calculated using Equation 6.1 (Same as 5.1)

$$2L = 1500m/s \cdot .001s \tag{6.1}$$

In this equation, L is the length of the chamber in meters. The result of this calculation was a chamber length of .75 m or 29.5 in. The speed of sound in the fluid is dependent on temperature, so the frequency was adjusted to achieve resonance.

Since the same drive element was used as the 20 kHz resonator, the fluid cavity had an inner diameter of 50.8mm (2 in.). A chamber that is almost 15 diameters in length promotes good wave propagation in the direction desired. In a chamber that is this slender, the wave propagation can be assumed axial, and the radial pressure effects ignored.

6.3 Reed Valve Design – 1 kHz Operation

The design of the passive reed valves for operation at 1 kHz followed the same procedure outlined in the last chapter. The first step dealt with the frequency response of the cantilevered valves. The natural frequency of the valves must be higher than the operation frequency. For the calculations, spring steel thicknesses of .127mm (0.005in.), .254mm (0.010in.), and .381mm (0.015in.), are used. Following the equations used in the last chapter, the maximum lengths of valves were calculated. These lengths are shown in Table 6.1 for a first natural frequency of 2 kHz. Operation at this frequency offers more flexibility than at 20 kHz. Each valve length may be easily produced and should cover an easily machined hole. A valve width of 5mm was chosen. The resistance to fatigue was the next requirement that must be explored.

Table 6.1: Maximum Valve Lengths

Natural Frequency (Hz)	Thickness (mm)	Required Length (mm)
2000	.127	7.27
2000	.254	10.3
2000	.381	12.6

6.3.1 Reed Valve Fatigue Investigation

The fatigue calculations followed the same pattern as for the 20 kHz resonator. The main concern was that the valves must be designed for infinite life. In order to have infinite life, the maximum deflection of the valves must be calculated through the use of the modified Goodman fatigue criterion. The same material was used in the design of these valves, 1095 carbon steel quenched and tempered at 200 °F.

After applying the correction factors for the type of oscillation experienced by the reed valves, the corrected endurance limit for this material was 299 MPa. Using the modified Goodman failure criterion, the maximum alternating stress was calculated using Equation 6.2,

$$\sigma_a = \frac{S_e}{\left(1 + \frac{S_e}{S_{ut}}\right)} \tag{6.2}$$

where σ_a is the maximum allowable alternating stress, S_e is the corrected endurance limit, and S_{ut} is the ultimate tensile stress. The result of this calculation was a maximum alternating stress of 224 MPa. Therefore, the maximum stress experienced by the reed valve was the mean stress plus the alternating stress, in this case

$\sigma_{\max} = 2 \cdot \sigma_a = 448MPa$. This was the maximum stress that may be experienced by the reed valves and still maintain infinite life. The maximum deflection of the reed valves to obtain infinite life was then calculated using Equation 6.3 (same as Equation 5.10)

$$y_{\max} = \frac{2L^2\sigma_{\max}}{3tE} \tag{6.3}$$

where y_{max} is the maximum deflection of the reed tip, L is the length of the reed, σ_{max} is the maximum stress allowed, t is the thickness, and E is the Young's modulus. The result of this calculation was .60 mm (.024 in) for all three thicknesses of reed material. This maximum displacement was much larger than the value calculated for the 20 kHz resonator. This allowed much more design flexibility with the construction of the reed valves and allowed for less fluid restriction across the valves.

For the experiments, the most conservative valve dimension was chosen. The reed valve was fabricated using a wire EDM process to accurately cut a 7.27 mm x 5 mm reed. The reed length of 7.27 mm was chosen because it was the shortest predicted reed dimension. Therefore, if the reed operation in a liquid lowers the resonance dramatically, because of the denser fluid, a thicker reed may be used. The calculations performed were assumed to be in air, therefore the valve operation in liquid may have a dramatic effect on the resonant frequency. A thicker reed valve has a higher resonant frequency, and may have an effective resonance in liquid that is higher than the 1kHz operation frequency.

6.4 1 kHz Resonator Construction

The 1kHz resonator assembly consisted of a driving element, diaphragm, fluid cavity, reed valves, end cap, and reed valve covers. The driving element was the same PZT housing and actuation system used in the 20 kHz resonator. The same diaphragms

were also used. The main difference was the larger fluid cavity and introduction of the reed valves. The fluid cavity was manufactured out of a 2 in. inner diameter aluminum tube which is .75m long. The inlet valve was placed as close to the diaphragm as possible. The outlet valve was placed at the end of the chamber in a steel end cap, sealed with a confined o-ring. The end cap was machined out of stainless steel for added rigidity. Figure 6.1 shows a detailed picture of the end cap. Note the reed valve and the pressure sensor installed.

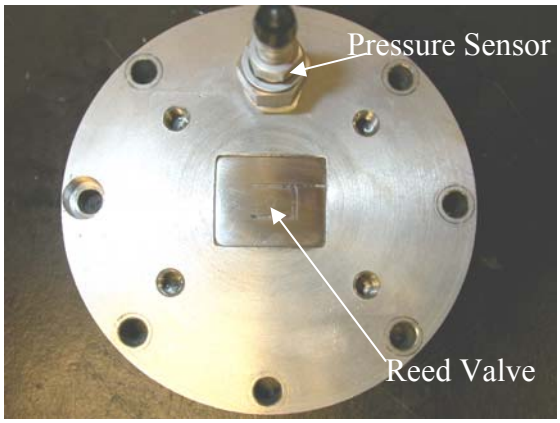

Figure 6.1: End Cap, Valve Cover Removed

A pressure sensor was installed in the end cap to monitor pressure and tune the operating frequency. A valve cover was bolted on top of the reed valve and constrained it to the valve seat as well as providing an o-ring seal. The valve cover also contained a fitting for attaching tubing. On the inlet side of the system, there was a similar valve cover. Figure 6.2 shows the inlet port of the fluid cavity along with the valve cover. A detailed picture of the reed valve is shown in Figure 6.3. The side of the reed valve that contacted the valve seat was polished using a rotary polisher. The reed valve was

constrained around its perimeter, and the flap in the middle was the part that deflected as fluid was passed.

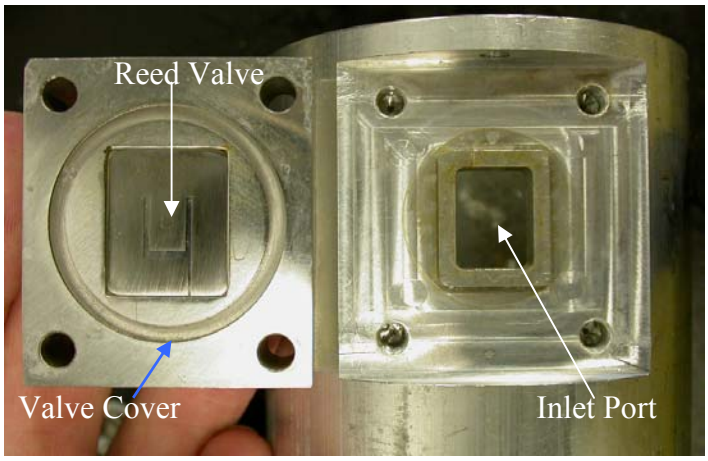

Figure 6.2: Inlet Port and Valve Cover

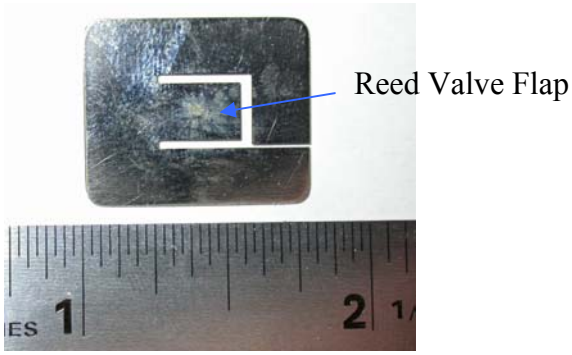

Figure 6.3: Reed Valve Detail

Assembly of the system consisted of filling the fluid cavity, attaching necessary lines and fittings, and bleeding air from the system. Tests were performed with a closed chamber to measure resonance with no flow; lines and a hydraulic actuator were then installed to test flow performance.

6.5 Experimental Setup

Tests of the 1 kHz resonator were first performed with a closed chamber, then with a hydraulic actuation system installed. A schematic of the experimental setup is shown in Figure 6.4. The assembly of the 1kHz resonator system for testing included preloading the stack actuators against the diaphragm. The wires to the stacks were then attached to a power amplifier. The amplifier used in the experiments is an Instruments Inc. model L6 kilowatt amplifier. The experimental setup was similar to the setup for the 20 kHz resonator. In the figure, the low pressure flow is represented by the color blue and the high pressure flow in red.

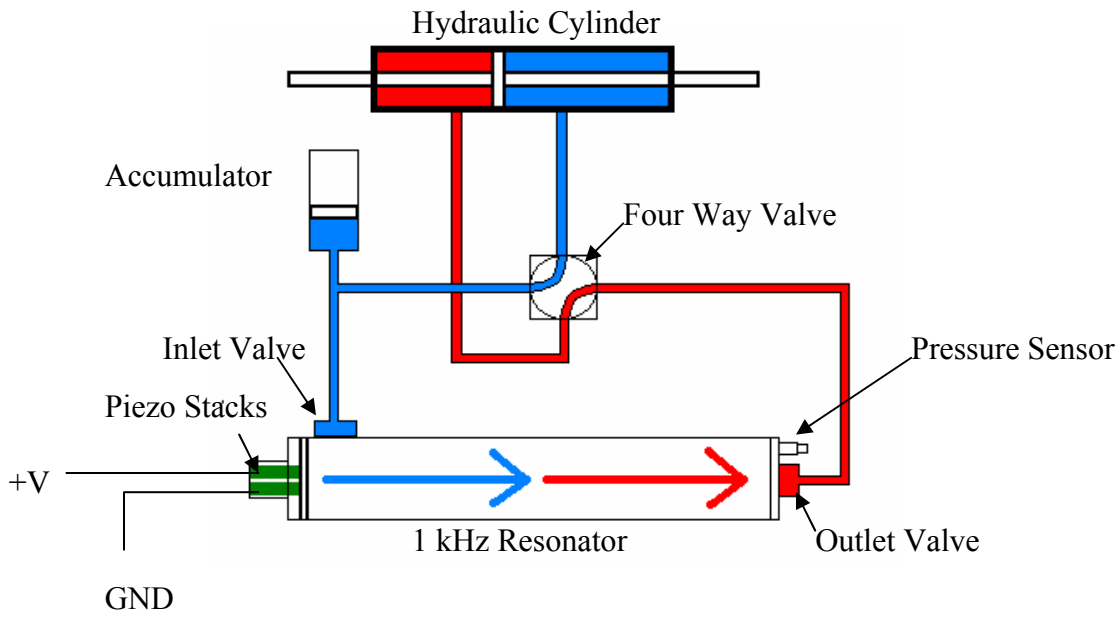

Figure 6.4: Experimental Setup of 1 kHz Resonator

For the closed chamber experiments, the inlet and outlet valves were blocked. Tests were performed by inputting a sine wave from a function generator into the power amplifier which was connected to the stack actuators. Several voltages were used, but the

output of the amplifier was not to exceed 150 Vpp to avoid damaging the stacks. The frequency of the sine wave was varied to attain resonance of the system. The peak pressures in the chamber were then recorded. Once the closed chamber experiments were complete, the hydraulic actuation system was installed. This consisted of a four way valve, reed valves, and hydraulic actuator. The same input voltage was used, and the frequency was tuned to achieve resonance. Any fluid flow present was measured by observing the motion of the hydraulic actuator.

6.6 Results and Discussion – 1kHz Resonator

Tests on the 1 kHz resonator were performed with both a closed chamber and open chamber, meaning with and without hydraulic lines installed. In the closed chamber experiments, a hydraulic accumulator was installed to apply a bias pressure of 100 psig. The inlet and outlet of the fluid chamber were capped off beyond the accumulator. The system was connected to the Instruments Inc. model L6 amplifier and input a $100V_{pp}$ sine wave with a positive bias. The frequency was then tuned to achieve resonance. A maximum pressure of 200 psig over the bias pressure was recorded at 963 Hz. This output with only 100V input was very promising.

In the next set of experiments, the hydraulic actuator and control system were installed. A range of excitation frequencies and voltages were input into the system and no actuator motion was detected once resonance was achieved. The failure of this system to rectify the pressurized fluid was attributed to the valve system. The reed valves were designed for a resonant frequency of 2 kHz in air. Most likely the operation in water

reduced the resonant frequency by a factor of two or more. This may have caused the valves to not seal the pressure pulses at the 1kHz operating frequency.

The 1kHz resonator showed promise as a high pressure resonant system. Although the valves that were designed for this application kept it from producing positive flow, more analysis and optimization of the valve design may yield acceptable results. A system was designed in the next chapter to test the frequency response of the same high speed reed valves to determine their frequency threshold.

CHAPTER 7

Non-resonant Pump Utilizing Reed Valves

7.1 Introduction

A non-resonant piezoelectric hydraulic pump was developed which utilized the high speed reed valves originally designed for the 1 kHz fluid resonator. The reed valve technology showed promise with its sealing capability, and there was potential for a high frequency, non-resonant reciprocating pump system. A high speed, directly driven reed valve pump was designed to explore this alternative. A non resonant pump system does not require a large fluid cavity. A small fluid cavity was desired to reduce the effects of fluid compliance. Implementation of a non resonant pump allowed the characterization of the upper frequency limit of the reed valves. This chapter describes the design, fabrication, and testing of a high speed reciprocating piezopump using reed valves.

7.2 Reed Valve Pump Design

The reed valve pump was designed to use a non resonant pumping method. This design resulted in a pump system capable of high frequency without relying on resonance effects. The output of a non-resonant system is proportional to the drive frequency. The check valves used in the aluminum pump of Chapter 2 limited high frequency operation with an upper operational limit of 700Hz. Operation on the order of a kilohertz would dramatically increase performance. This section describes the reed valve pump similarities to the resonant systems as well as its design and construction.

The reed valve pump used the same driving system as the resonant fluid systems. This consisted of three cofired stacks in parallel pushing on a thick aluminum diaphragm. A thick diaphragm was again chosen because of its rigidity. The overall stroke of the stack actuators was small enough that although the diaphragm is quite stiff, it may be deflected the maximum amount without placing an unacceptable stress on the stack actuators. Other research has shown that the thin diaphragms used in pumps of this type have been the major contributor to fluid volume loss with each stroke (Lee et. al. 2002). The rigidity of the diaphragm prevented this fluid volume loss. The depth of the chamber where the fluid was compressed was kept to a minimum to reduce the bulk modulus of elasticity of the fluid, further reducing fluid loss. The compression chamber was two inches in diameter but only .020 inches deep.

The reed valve pump was constructed completely out of stainless steel with the exception of the diaphragm. The pump consisted of four main plates: the PZT housing, diaphragm, cylinder head base, and cylinder head top. The cylinder head base and top are shown in Figures 7.1 and 7.2. The reed valve seats were raised on the cylinder head base and top so they may be polished using a rotary polisher. The reed valves were also polished on the sealing side. This fine finish on the valves and seats was the reason for their sealing success. The precision finish allowed pressure to be held with a metal to metal seal.

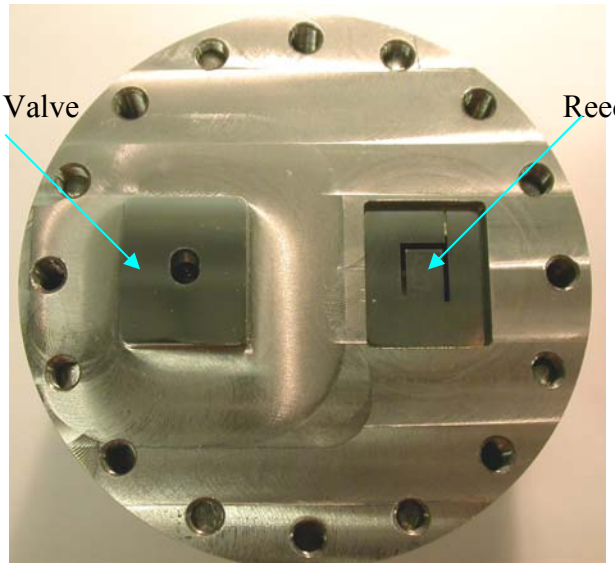

Figure 7.1: Cylinder Head Base

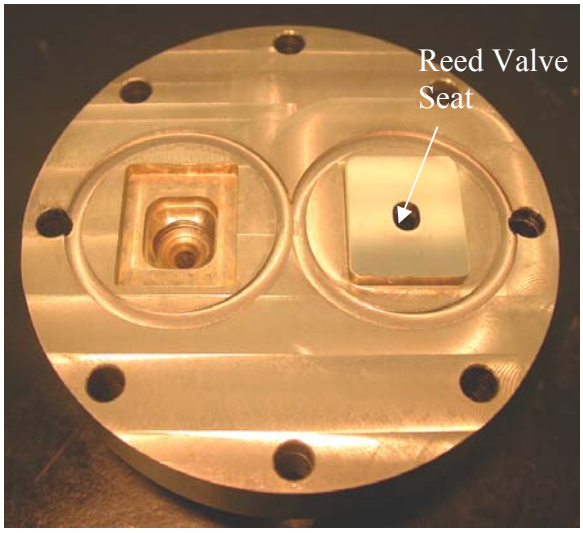

Figure 7.2: Cylinder Head Top

The reed valves were made using two different thickness materials. Identical sets of valves were fabricated out of .005 in. and .010 in. spring steel shim stock. An example of one of the reed valves is shown in Figure 7.3. They were manufactured using a wire EDM for accurate cutting of such a thin material. The reed flap was 5mm wide and 7.27

mm long. The two reed valves were placed in their respective recesses and the o-ring seals installed before the pump subsystem was bolted together. The assembled pump subsystem is shown in Figure 7.4. The pump was then bled of any air and assembled with the rest of the hydraulic system.

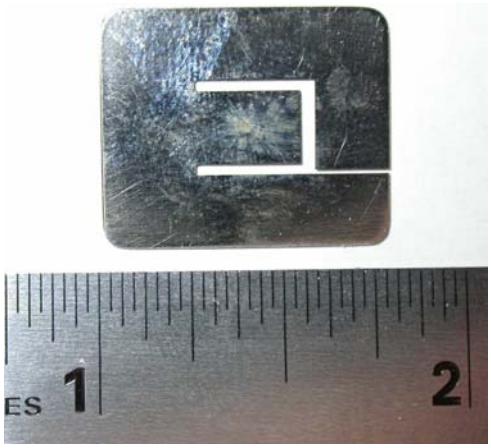

Figure 7.3: Reed Valve

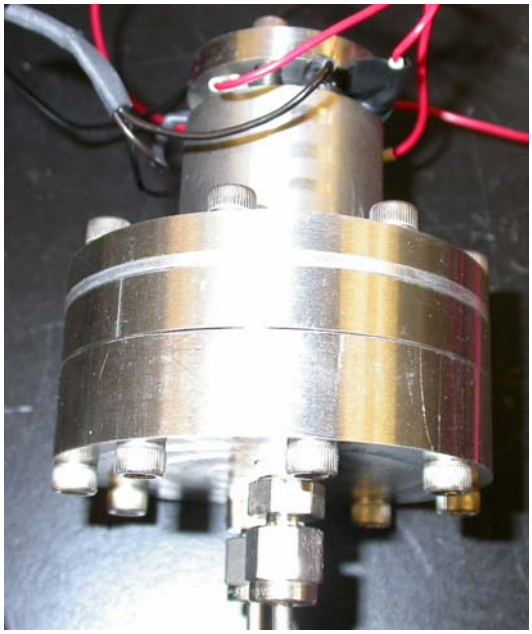

Figure 7.4: Reed Valve Pump Subsystem

7.3 Experimental Setup

A schematic of the experimental setup is shown in Figure 7.5. In this figure, red denotes high pressure and blue represents low pressure. A low pressure accumulator functioned to prevent cavitation, and a four way valve was installed to control the direction of flow. An analog pressure gauge was added in line with the high pressure side of the pump to measure blocked pressure. The time required for the hydraulic actuator to traverse its full range was measured to determine flow rate.

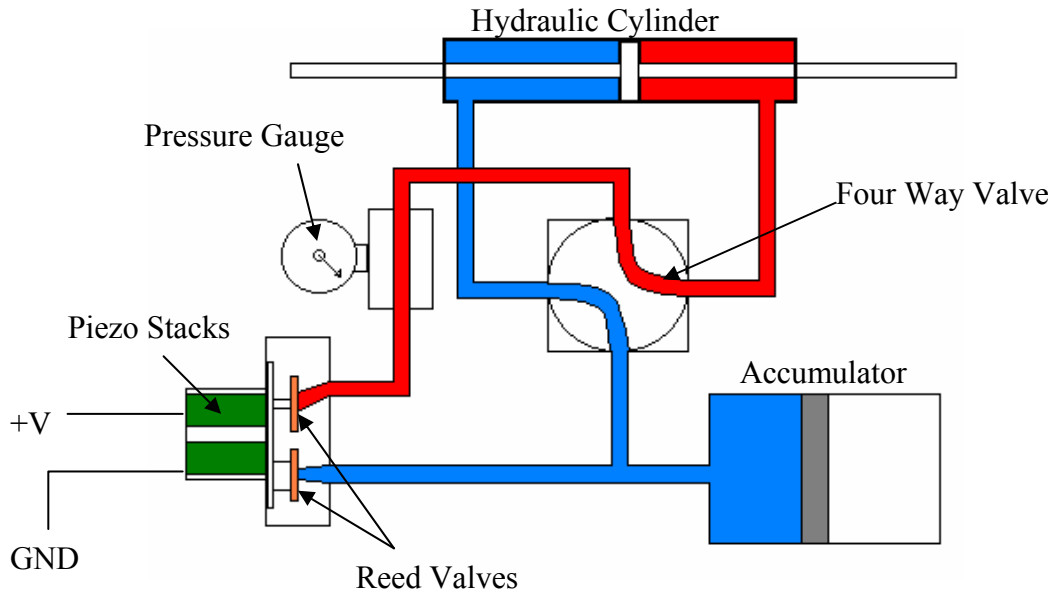

Figure 7.5: Schematic of Experimental Setup

For testing, a bias pressure of 125 psig was applied to the accumulator to prevent cavitation. A function generator was used to produce a sine wave which was input into the amplifier. Two different power amplifiers were used in testing. For frequencies below 50Hz, a Krohn-Hite (model 7500) power amplifier was used. For frequencies above 50 Hz, an Instruments, Inc. (model L6) amplifier was used to supply the needed

power. The output of the amplifier was connected to eight 9V batteries connected in series before going to the positive lead of the stack actuators. This produced the necessary positive bias required to drive the stacks. A positive bias voltage must be applied to keep from driving the stack actuators in the negative direction. A 100V peak to peak voltage level was used on the reed valve pump. A frequency sweep was performed at this voltage. The time necessary for the hydraulic actuator to traverse its entire range of travel was recorded. Then, knowing the fluid volume displaced in the actuator, flow rates were calculated.

Several arrangements of valve thickness and diaphragm thickness were investigated to determine the optimum setting. There were four thickness diaphragms to choose from. The thicknesses were 1.59mm (.0625 in.), 2.1mm (.082 in.), 2.5mm (.10 in.), and 3.18mm (.125 in.). There were two different reed valve thicknesses to choose from; they were .127mm (.005 in.) and .254mm (.010 in.).

The purpose of the first set of experiments was to determine which valve thickness produced the highest flowrate and which operated at the highest frequency. The 2.1mm (.082 in.) diaphragm was chosen for these experiments. Tests were performed and flowrates, frequencies, and blocked pressure were measured. The next set of experiments was to determine the optimum diaphragm thickness while keeping the reed valve thickness constant. This was performed using the .254mm (.010 in.) valves and varying the diaphragm thickness. Again, flowrates, frequencies, and blocked pressure were recorded. The blocked pressure was used to determine the blocked force on the hydraulic actuator.

7.4 Experimental Results

A picture of the pump assembly used in testing is shown in Figure 7.6. The results of the first set of experiments are shown in Figure 7.7. Recall that the purpose of this set of experiments was to determine the optimum reed valve thickness. The legend in Figure 7.7 shows the following information: the bias pressure used, the peak to peak voltage input, the reed valve thickness in inches, and the amplifier used. *K-H* represents the Krohn-Hite amplifier and *L6* means the Instruments, Inc. amplifier. It may be seen from the figure that the highest performance was attained using the .127mm (.005 in.) reed valves. The figure also shows where the Krohn-Hite amplifier began to overload and limit the current output at approximately 60 Hz. This was observed by the overload light illuminating on the amplifier. An assumed error of 4 cc/min was assumed to account for error in the stop watch readings.

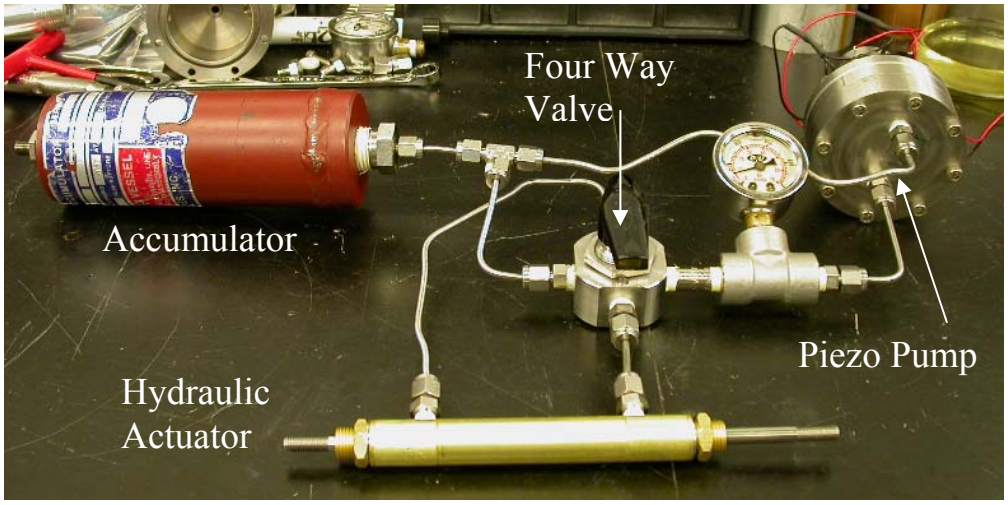

Figure 7.6: Reed Valve Pump Assembly

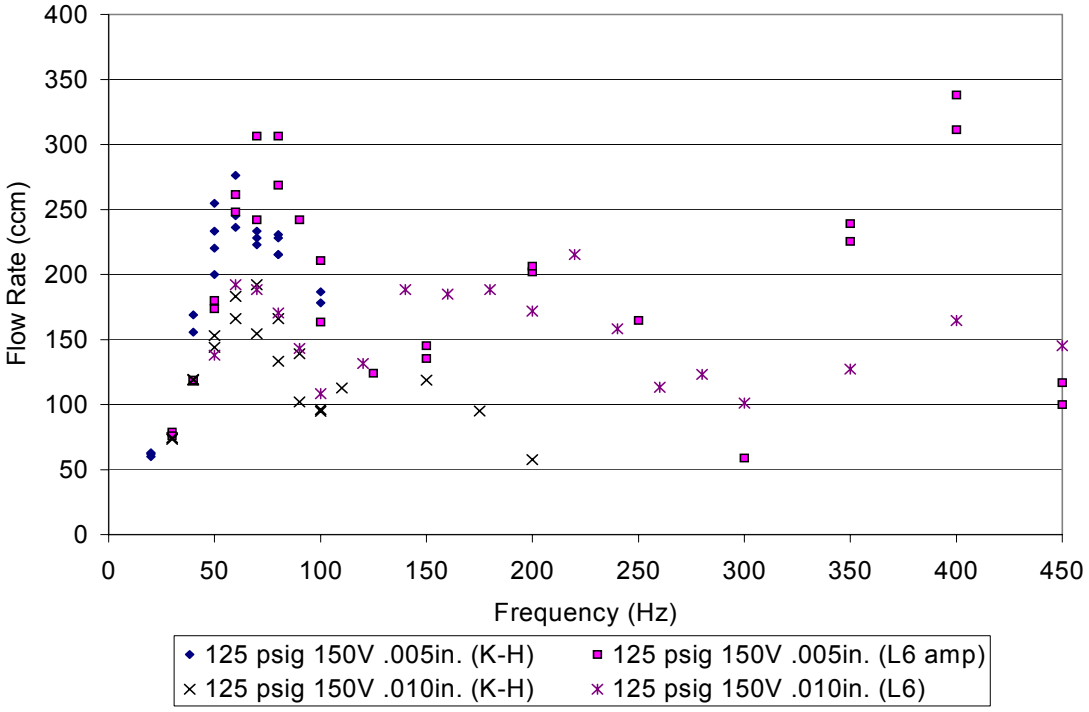

Figure 7.7: Flow Rate vs. Frequency for various reed valve thickness; 150V, 0.082in. diaphragm

.

As frequency was increased, the flowrate followed a very non-linear path. There were points at 75 Hz, 200 Hz, and 400Hz where the flowrate peaked. This result was attributed to a fluid/mechanical/electrical coupling of resonances. Although the reed valves were designed for a natural frequency of 2000 Hz in air, the introduction of the working fluid had a profound impact on their operation. The performance of the reed valves dropped sharply for frequencies greater than 400Hz and did not recover. Further analysis and optimization of factors such as valve thickness, dimensions, and shape could be used to tune the operating frequency into a higher regime.

An interesting phenomenon occurred while taking the flow data. The actuator was observed to travel in one direction faster than the other. This effect worsened as the

driving frequency increased. The faster direction flowrate is represented in the figures. The only difference between the forward and reverse direction was in the lengths of the steel lines that connected the four way valve to the hydraulic actuator. This effect was attributed to a mechanical/fluid resonance occurring between the outlet valve and the hydraulic actuator, or a damaged seal in the actuator.

The next set of experiments determined the optimal diaphragm thickness. The results of this experiment are shown in Figure 7.8. For these tests, the .254mm (.010 in.) reed valves were used. Flowrate and frequency tests were performed for each thickness diaphragm. The legend in Figure 7.8 shows the following information: the bias pressure used, the peak to peak voltage input, the diaphragm thickness in inches, and the amplifier used. This figure shows that the 2.1mm (.082 in.) diaphragm had the highest performance. The optimum diaphragm and valve thickness were then installed and measured. This optimum arrangement used the .127mm (.005 in.) reed valves and 2.1mm (.082 in.) diaphragm. A peak flowrate of 338 cc/min was recorded at 400Hz. The highest blocked force was recorded at a frequency of 350 Hz. This was a blocked force of 250 psig over the bias pressure. For the hydraulic actuator used, this corresponds to a force of 50 lb. As before, an error of plus or minus 4 ccm is assumed.

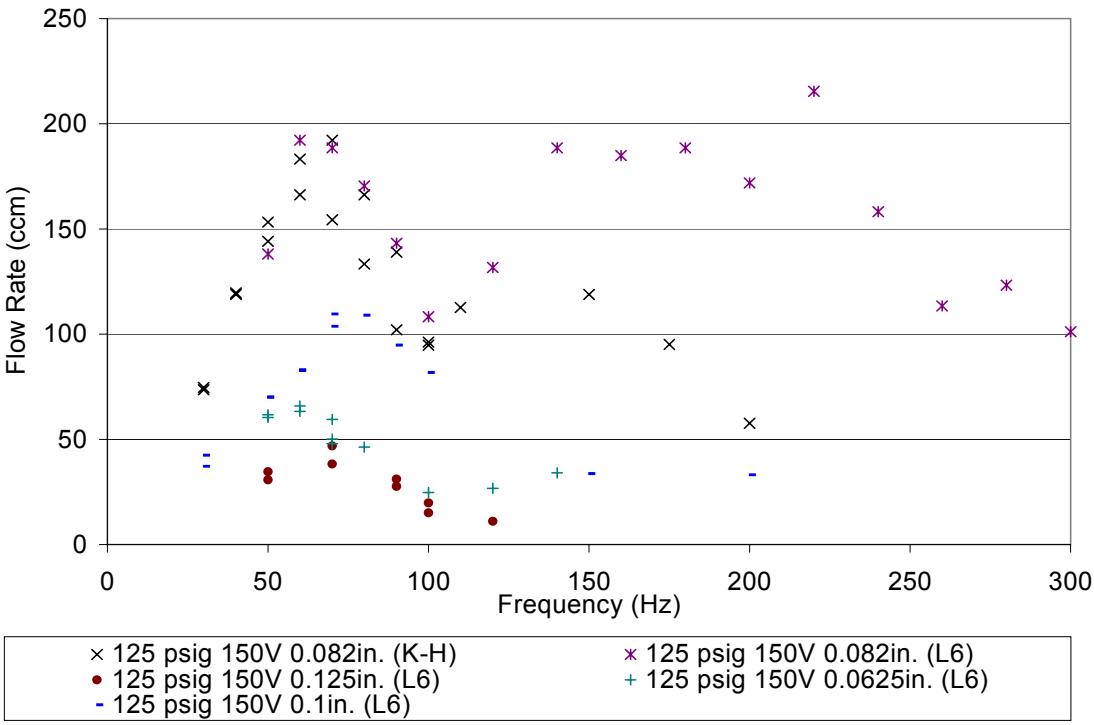

Figure 7.8: Flow rate vs. Frequency Diaphragm Thickness Variation; 150V, .010" Valves

7.5 Discussion

The non-resonant reed valve pump tested the capability of the newly designed reed valves. The maximum flow rate developed was 338cc/min at a frequency of 400Hz. The maximum blocked pressure was measured at 250 psig over bias at 350 Hz. This pump system performed better than the aluminum check valve pump described in Chapter 2. The reed valves had much less fluid restriction than the miniature check valves used in the aluminum pump. The actuator was easier to move manually on the reed valve pump than the aluminum check valve pump. The reed valves used in this pump system were originally designed for the 1 kHz fluid resonator. Analysis and testing of reed shapes could be used to increase the reed valve operating frequency from 400Hz

to over 1000Hz. When this is achieved, not only will the reed valve pump benefit, but the 1kHz resonator would also be a viable option for continued development.

CHAPTER 8

Concluding Remarks and Recommendations

This thesis details the design and testing of applications for piezoelectric materials. An aluminum piezohydraulic pump utilizing conventional check valves was constructed and tested. Fluid and mechanical resonant systems were also discussed; three models were developed, the head mass resonator, 20kHz resonator, and 1kHz resonator. These systems showed promise in their ability to reliably build pressure under closed chamber conditions. The difficulty was met when trying to rectify these resonant systems to produce positive fluid flow. A high speed reed valve system was developed and tested. Originally designed for the resonant systems, the reed valve system performed well in a non resonant, directly driven piezo pump which was developed and tested. This chapter discusses the future development of these systems and concluding remarks based on the research performed.

The aluminum check valve piezo pump described in Chapter 2 was the next generation of pump designed at Georgia Tech. The goal of this pump was to utilize the new cofired stack actuator and reduce the size and weight of the system. These goals were met, and the relative performance of the pump increased. This system is the closest to commercial development of all the systems described in this thesis. With a weight of only 625g and a simple design, this hydraulic fluid pump will perform well where high force light weight actuation is necessary. The tasks to be performed in the future development of this system are design of an impedance matched electrical system to most efficiently drive the capacitive load. Also, the low viscosity silicone oil did not seem to

be the best option for the hydraulic system. A fluid with more lubricating properties should be used to avoid stripping the hydraulic cylinder seals of grease. This simple, yet solid design has many possible applications in industry.

The design and development of the resonant fluid systems was the most challenging of the systems researched. It is well known that fluids set into resonance can produce high pressure. The difficulty was in taking the short pressure pulses and rectifying them into high pressure flow. Options such as active valves, vortex fluid diodes, and nozzle/ diffuser arrangements were discussed. The 20kHz system would produce a small and silent piezopump if a rectification system was devised which worked at its operating frequency. The 1kHz resonator was a more practical frequency for development of the technology. A reed valve system was designed and tested, but was not able to successfully operate at the 1kHz desired frequency. The peak operational frequency of the valves was measured at approximately 400Hz. There is confidence that optimization of the reed valve shape and dimensions can produce a reed valve that operates in the kilohertz range in liquid. Once this is achieved, the potential of the fluid resonator systems would be realized. At this point the mechanical resonant system may be employed to further increase amplitudes at resonance. There is much potential for these systems as a new technology in the application of piezoelectric materials.

The design and development of the high speed reed valve pump was an effort to prove the sealing capability of the newly designed reed valve system. A secondary goal was to determine the upper operational limit of the reed valves. Both of these goals were met with good results. The outcome was a piezohydraulic pump that used the same driving system, diaphragms and reed valves designed for the resonant systems. This

system was a conglomeration of different parts which resulted in a pump system that output 338 cc/min, which was higher than previous pumps designed at Georgia Tech. The upper limit of the reed valves was determined to be at a driving frequency of approximately 400 Hz. The output of the pump was proportional to driving frequency up to 60 Hz. Increasing the frequency introduced resonant effects which made the output very nonlinear with respect to frequency. These effects will have to be taken into account and the system design changed in order to take full advantage of the high frequency capability of the stack actuators. There is much future growth in the area of reed valve technology in relation to piezo pumps. Because the reed valves are custom they are also scalable. For example, the size of the reed valve pump could be shrunk dramatically by using smaller reeds, smaller diaphragm, and utilizing single crystal technology for the driving elements. Acceptable flow rates and pressures were attained using parts originally designed for the resonant fluid system. Therefore, designing specifically for a direct drive pump would produce even better results and allow for optimization of cavity and diaphragm dimensions. The rigid diaphragm was used instead of a thin shim stock diaphragm to fully transmit the small stroke of the cofired actuators to moving the fluid through the valves. Using a thick diaphragm did not have much of an effect on increasing stress on the stack actuators, but the increased rigidity did have an effect on fluid volume loss. There are many applications that could use a high pressure, high flow rate miniature pump to control small hydraulic systems. As the size of these pumps continues to shrink, it will open up even more possible applications.

APPENDIX A

Check Valve Pump Dimensional Drawings

Figure A.1 Pump Body Assembly

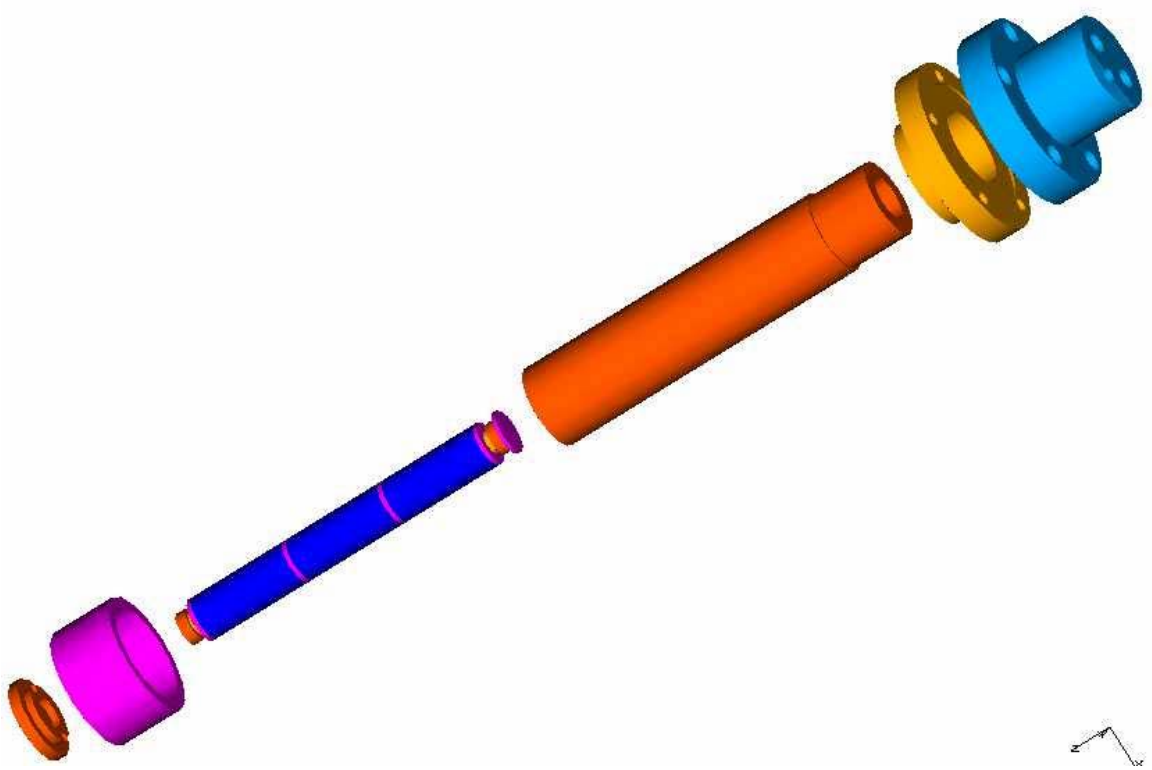

Figure A.2: Backing Plate (Dimensions in inches)

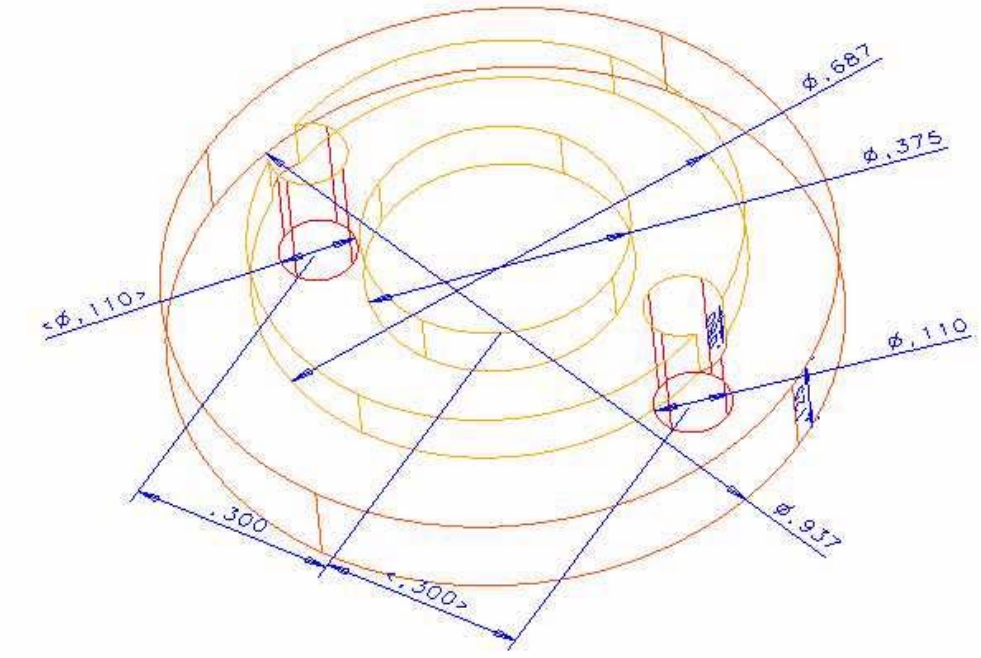

Isometric View

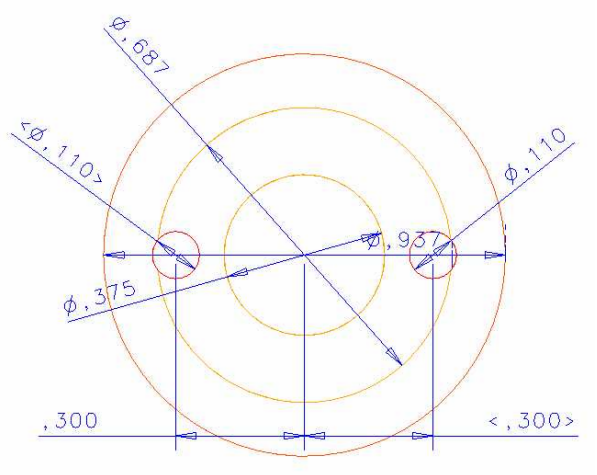

Top View

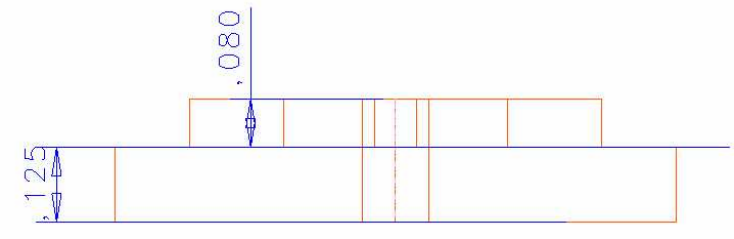

Side View

Figure A.3: End Screw Cap (Dimensions in inches)

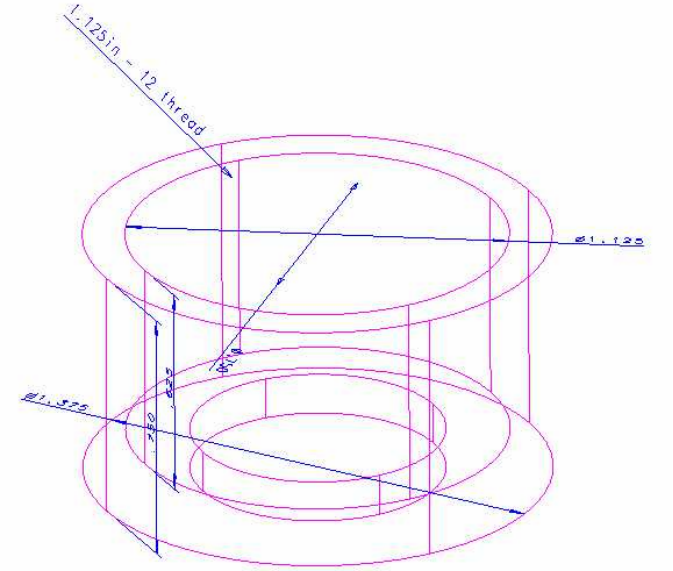

Isometric View

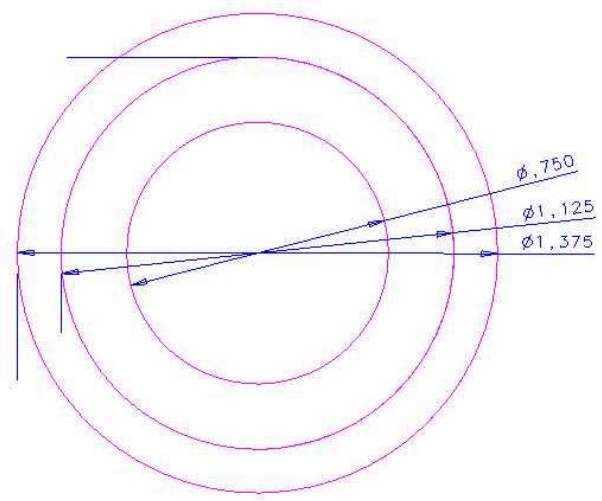

Top View

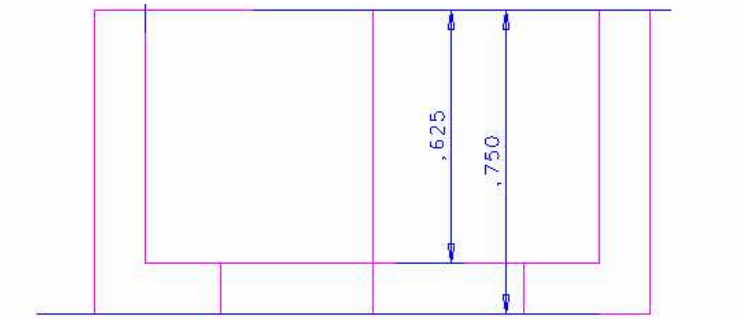

Side View

Figure A.4: PZT Housing (Dimensions in inches)

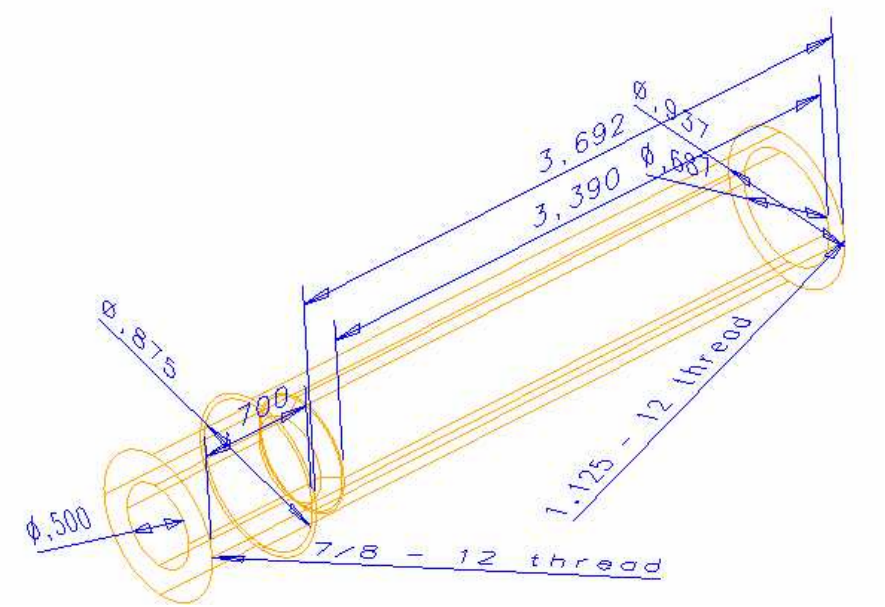

Isometric View

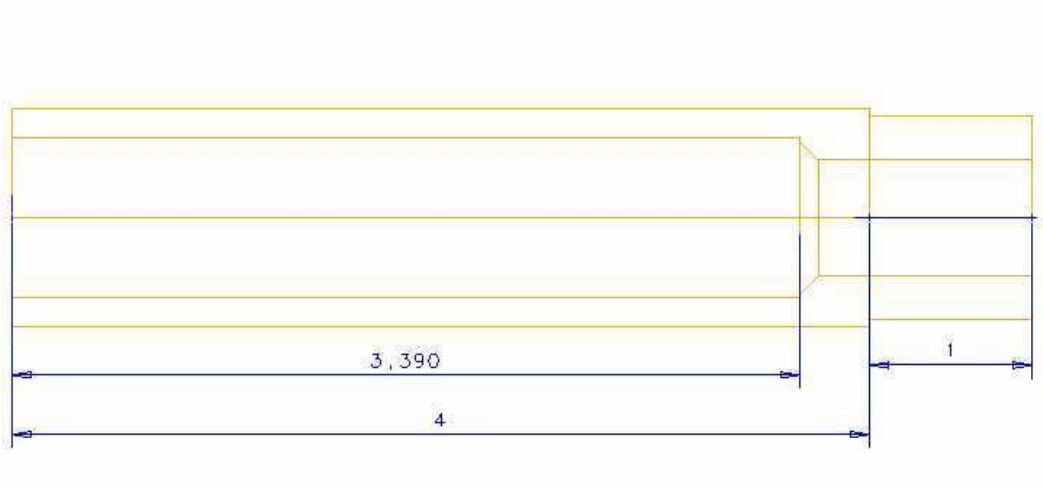

Side View

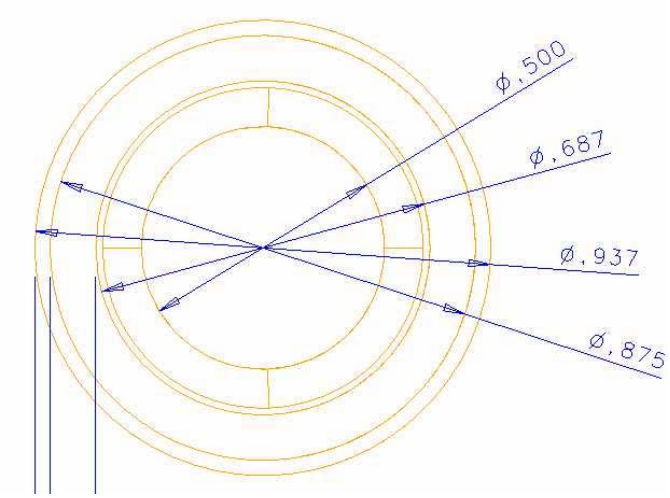

End View

Figure A.5: Cylinder Head Base (Dimensions in inches)

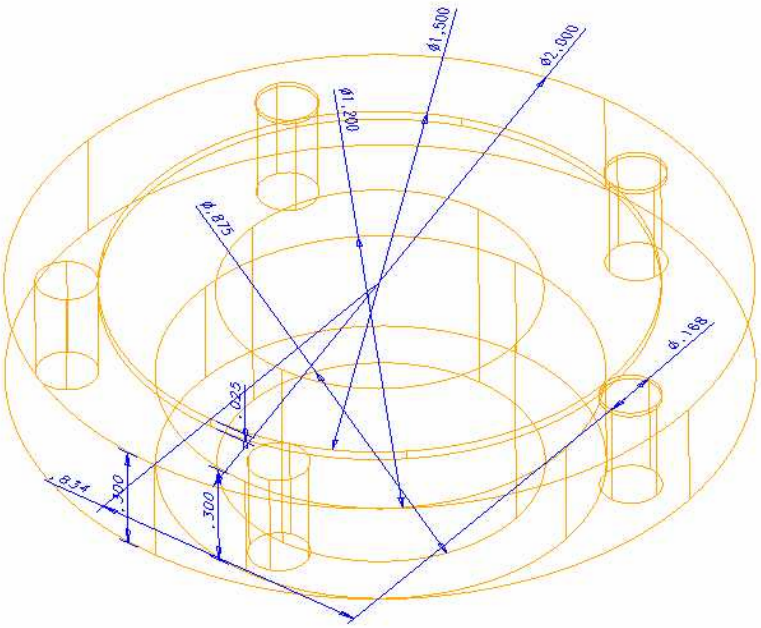

Isometric View

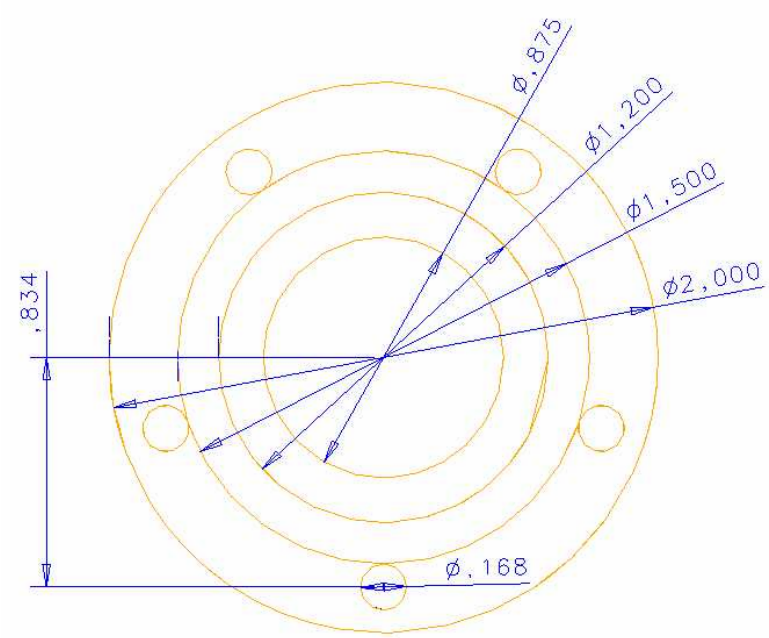

Top View

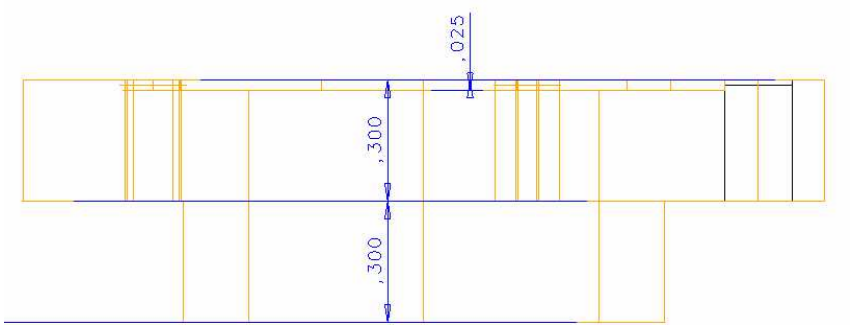

Side View

Figure A.6: Cylinder Head Top (Dimensions in inches)

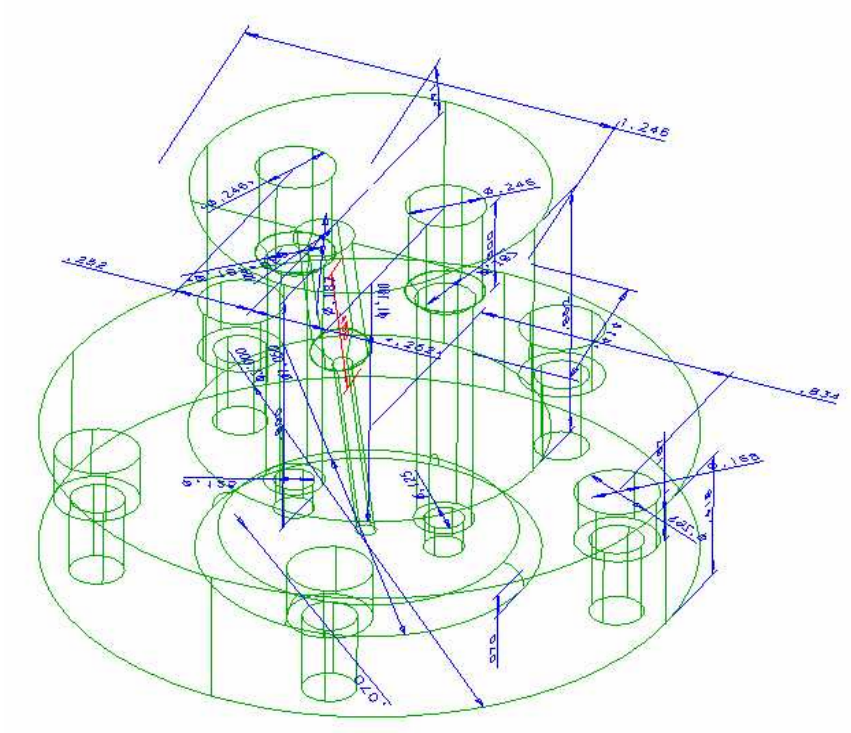

Isometric View

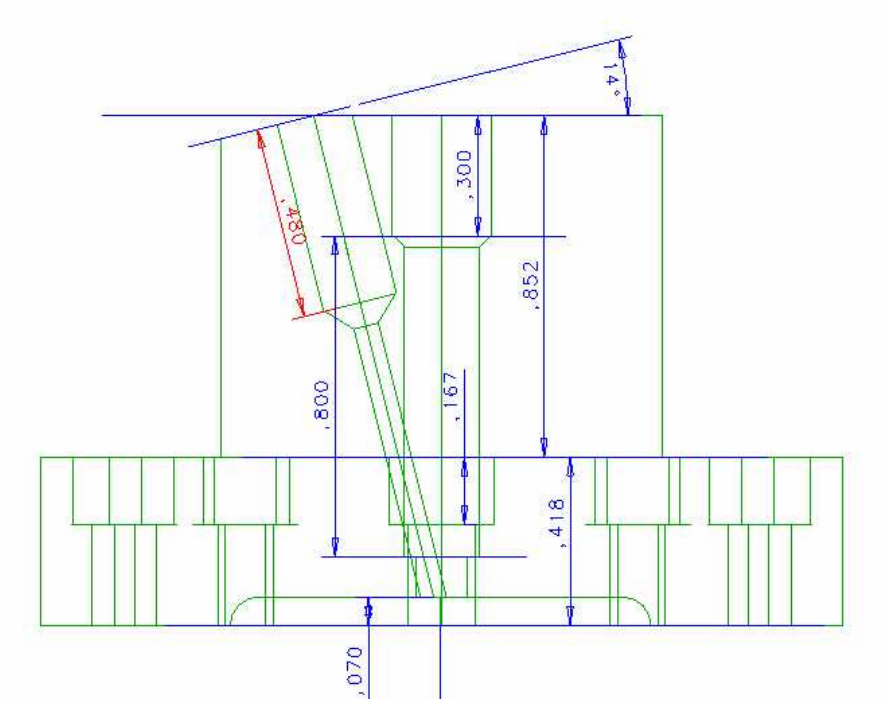

Side View

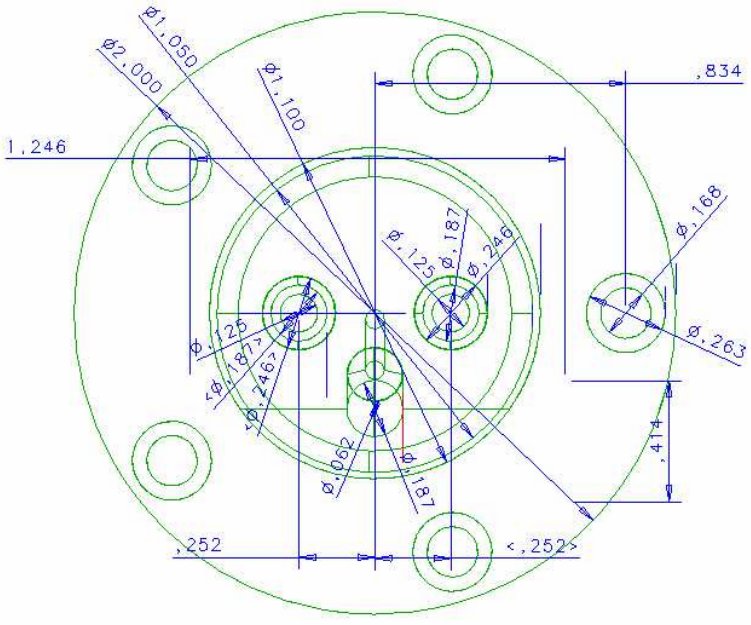

Top View

Figure A.7: Spool Valve Body (Dimensions in inches)

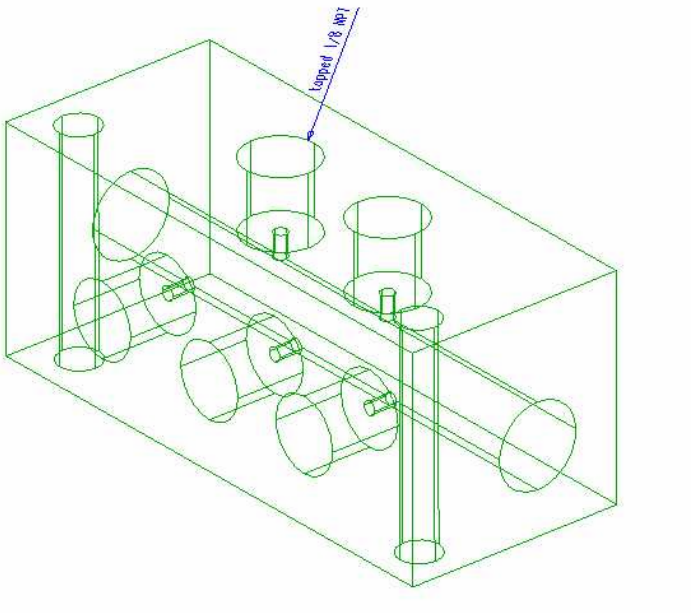

Isometric View

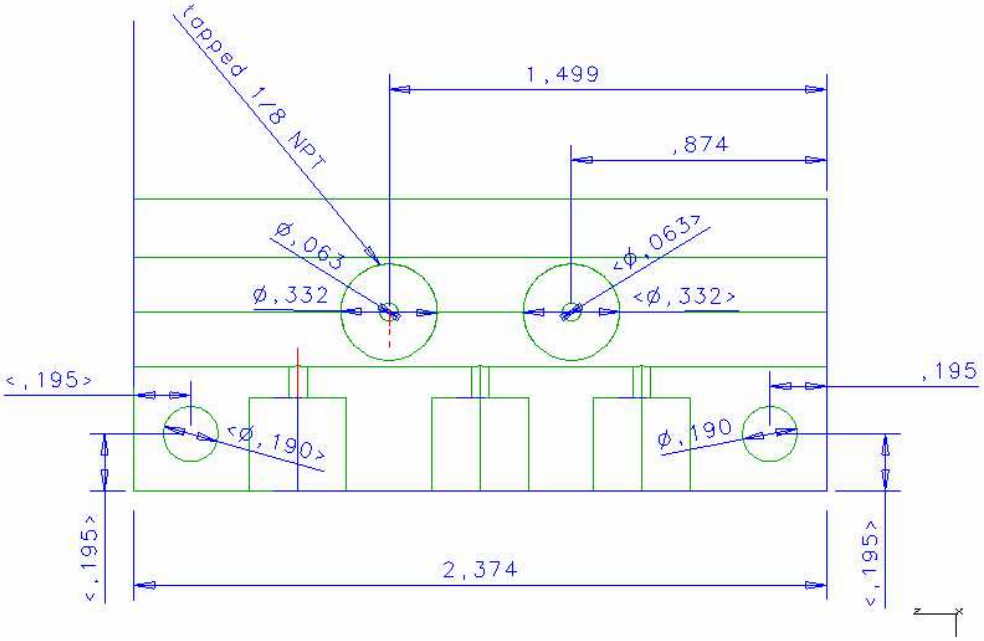

Side View (a)

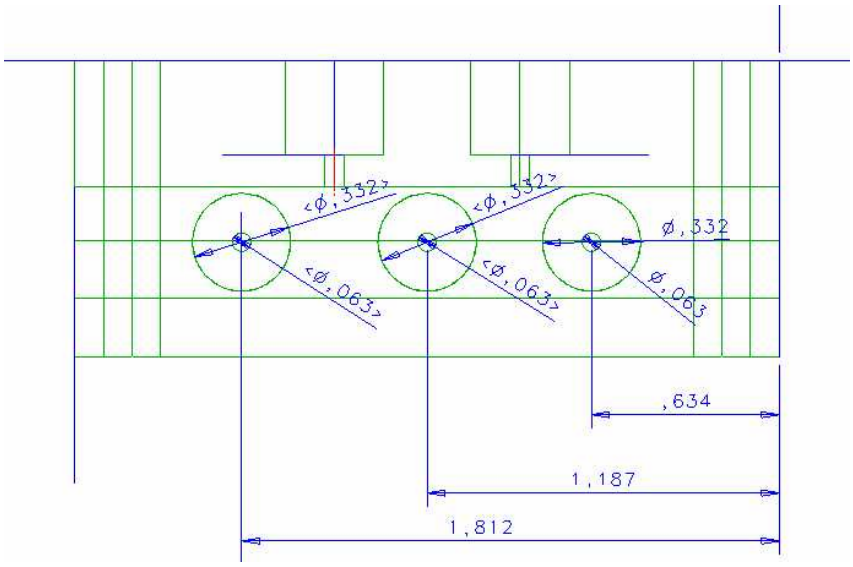

Side View (b)

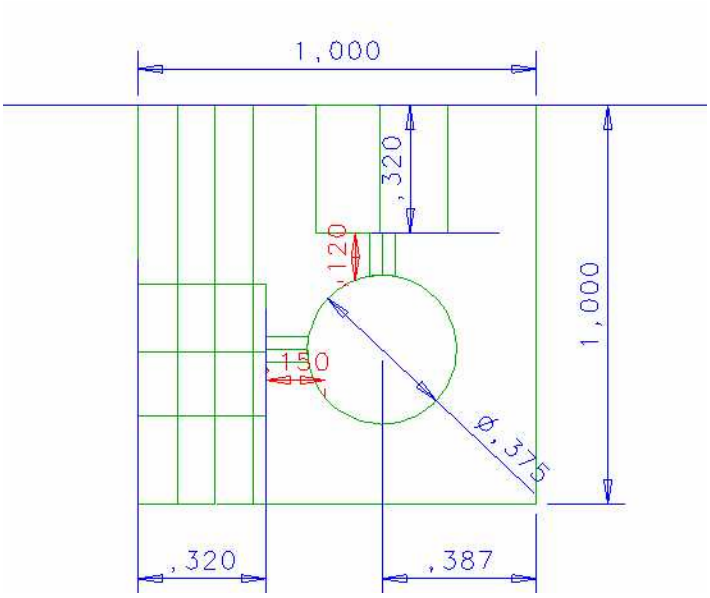

End View

Figure A.8 Spool Valve Rod (Dimensions in inches)

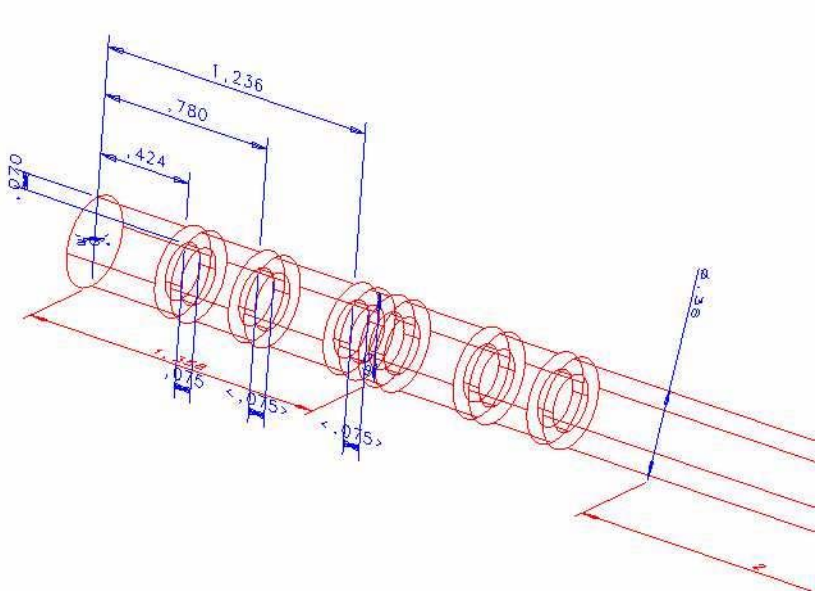

Isometric View

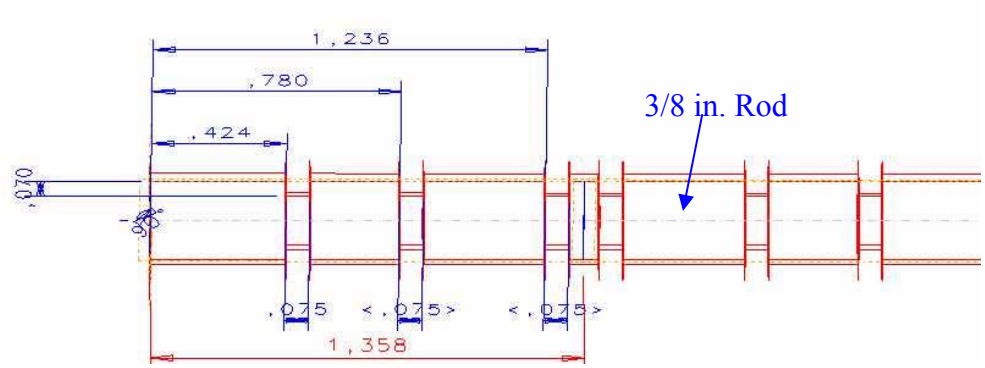

Side View

APPENDIX B

Head Mass Resonator Dimension Drawings

Figure B.1: Head Mass Resonator Assembly

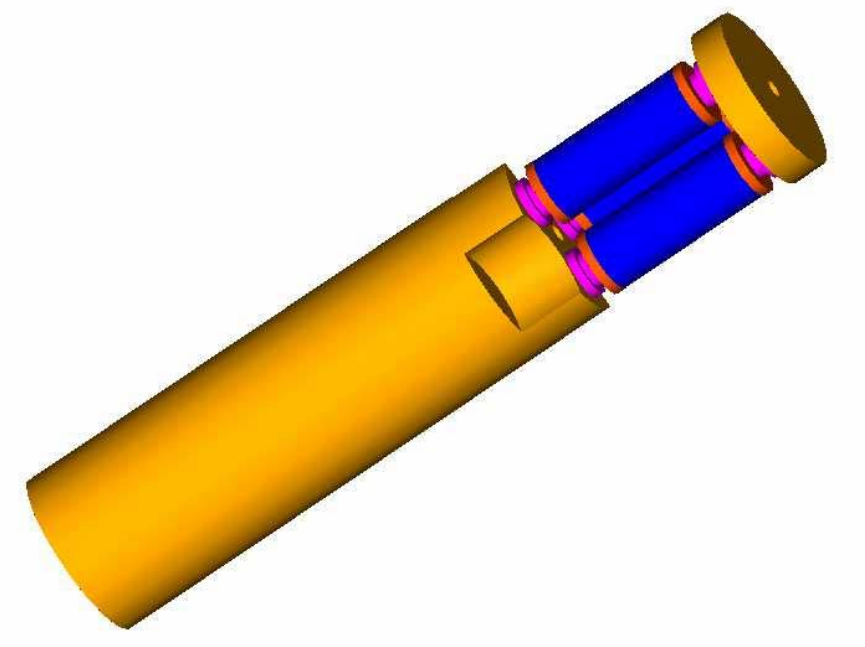

Figure B.2: Head Mass (Dimensions in inches)

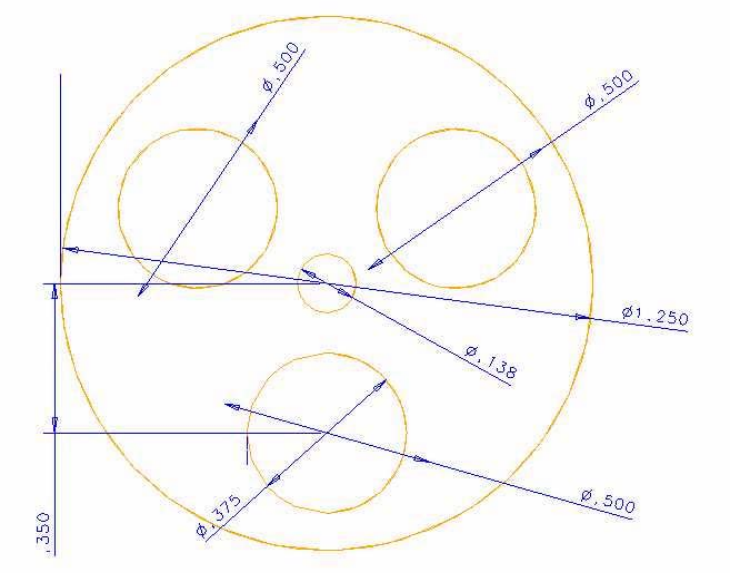

Top View

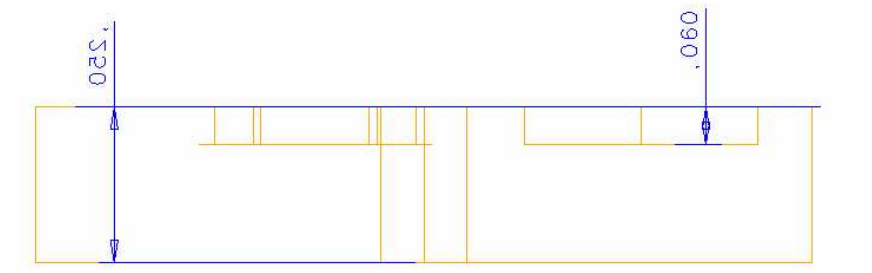

Side View

Figure B.3: Tail Mass (Dimensions in inches)

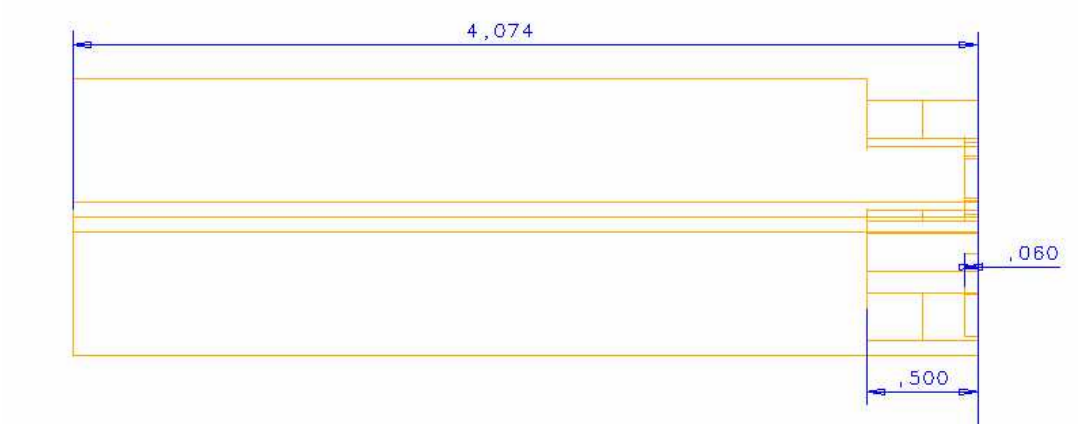

Side View

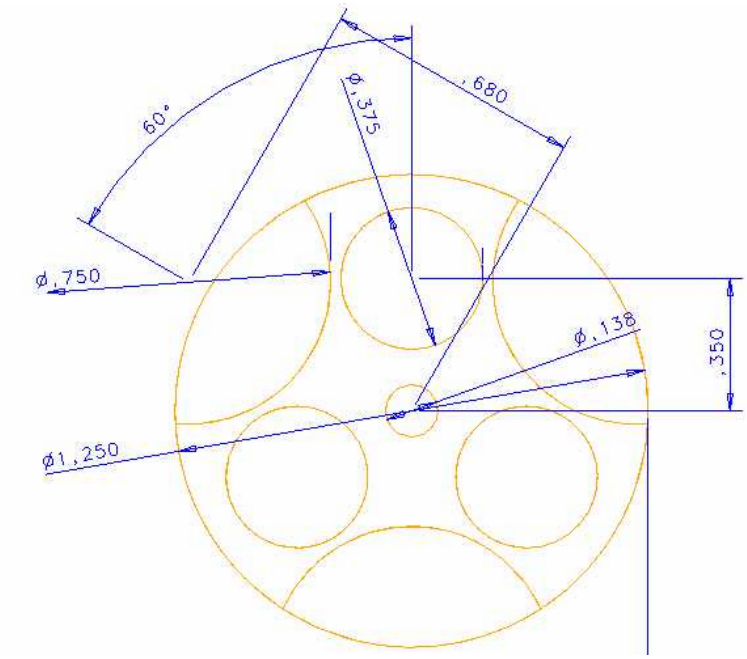

End View

APPENDIX C

20 kHz Fluid Resonator Dimension Drawings

Figure C.1: 20 kHz Resonator Fluid Cavity (Dimensions in inches)

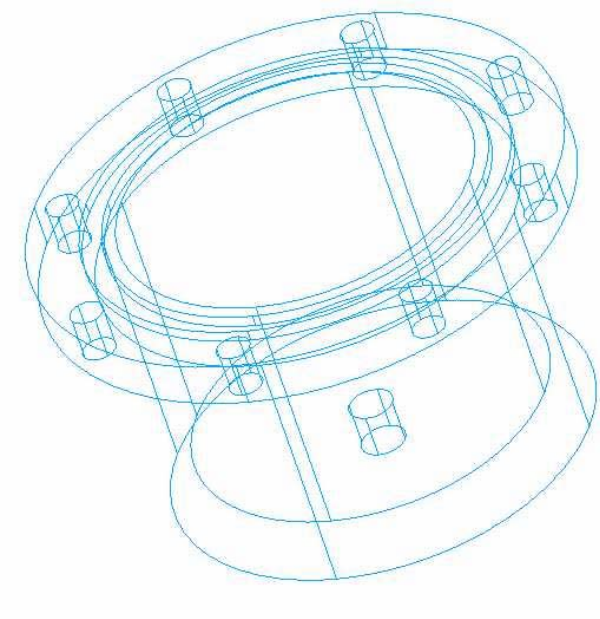

Isometric View

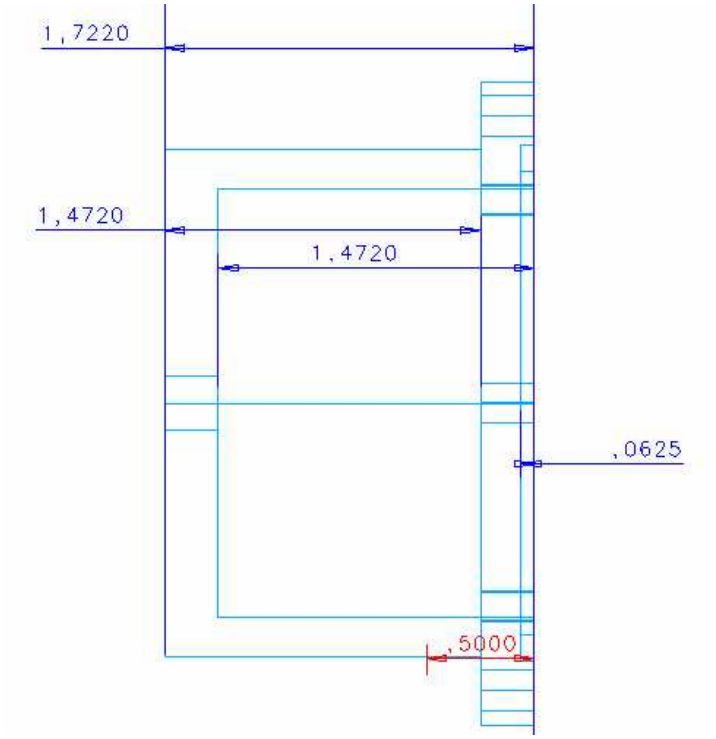

Side View

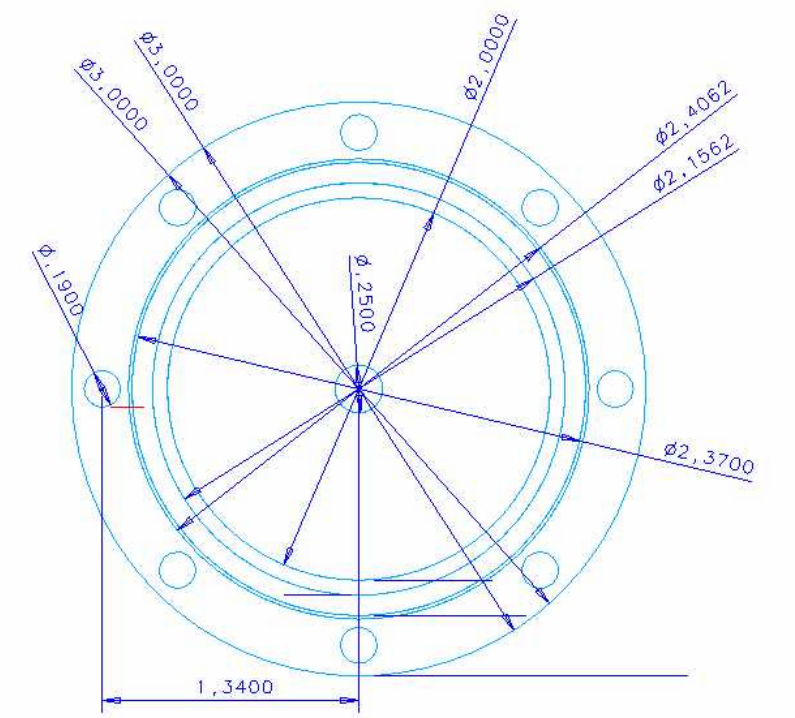

End View

Figure C.2: O-ring

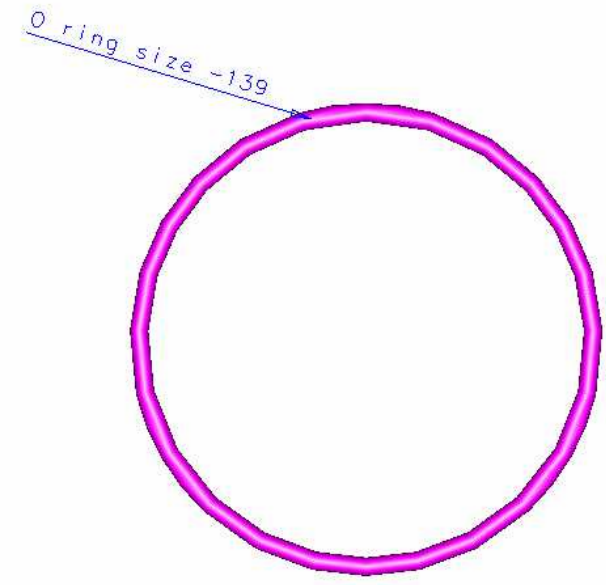

Figure C.3: Rear PZT Housing (Dimensions in inches)

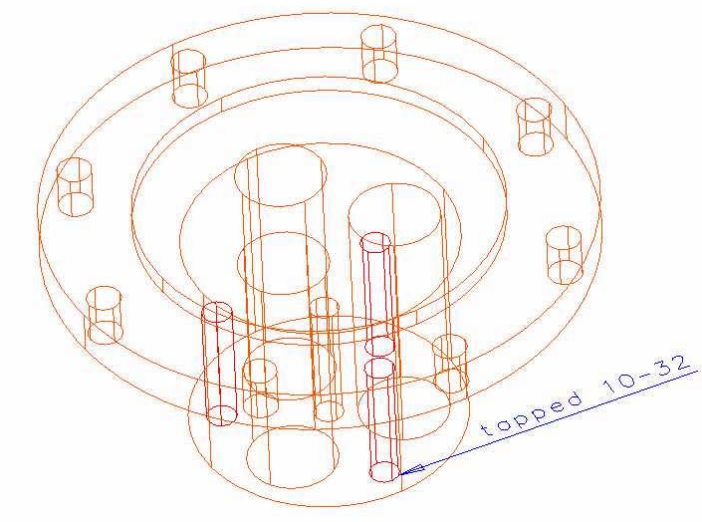

Isometric View

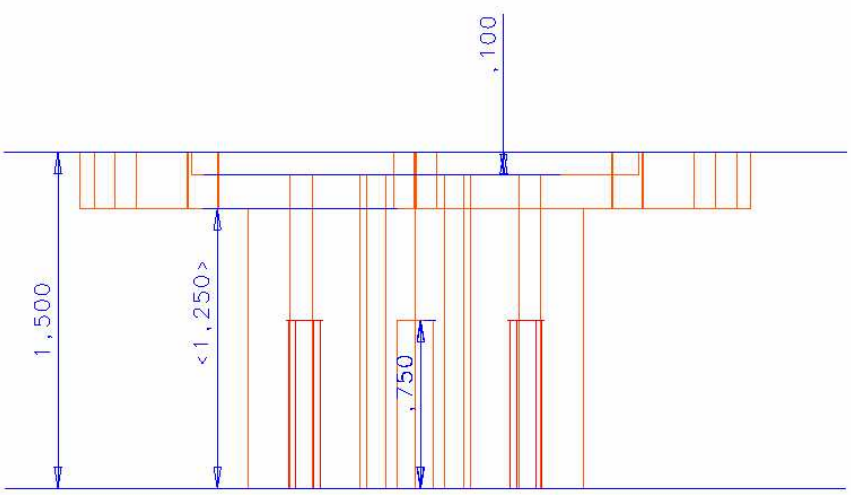

Side View

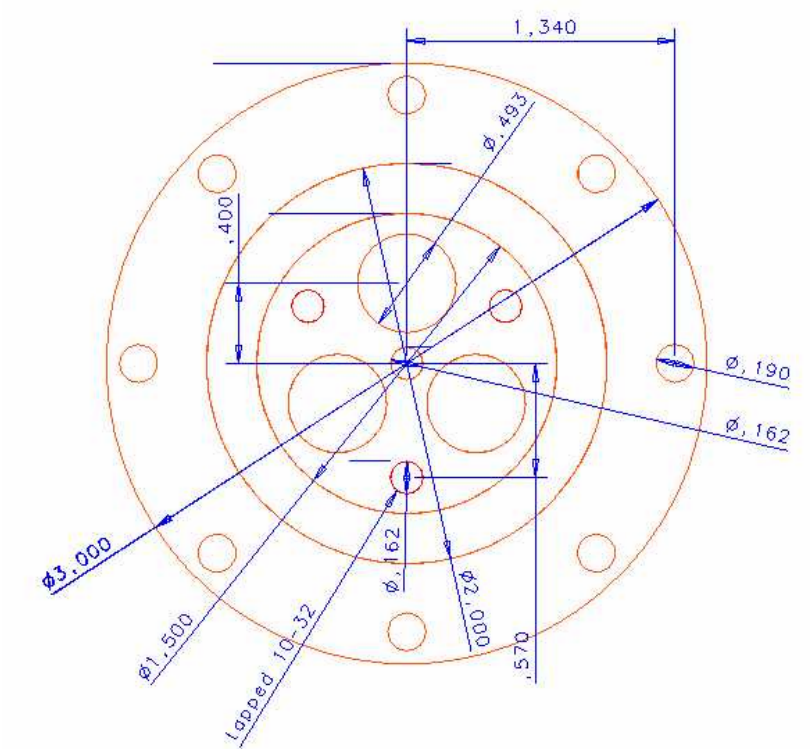
1,340
ø.493
.400
ø,190
ø,162
ø3,000
ø.162
ø2.000
ø1,500
.570
tapped 10-32

End View

APPENDIX D

Vortex Fluid Diode Dimension Drawings

Figure D.1: Large Fluid Diode (Dimensions in inches)

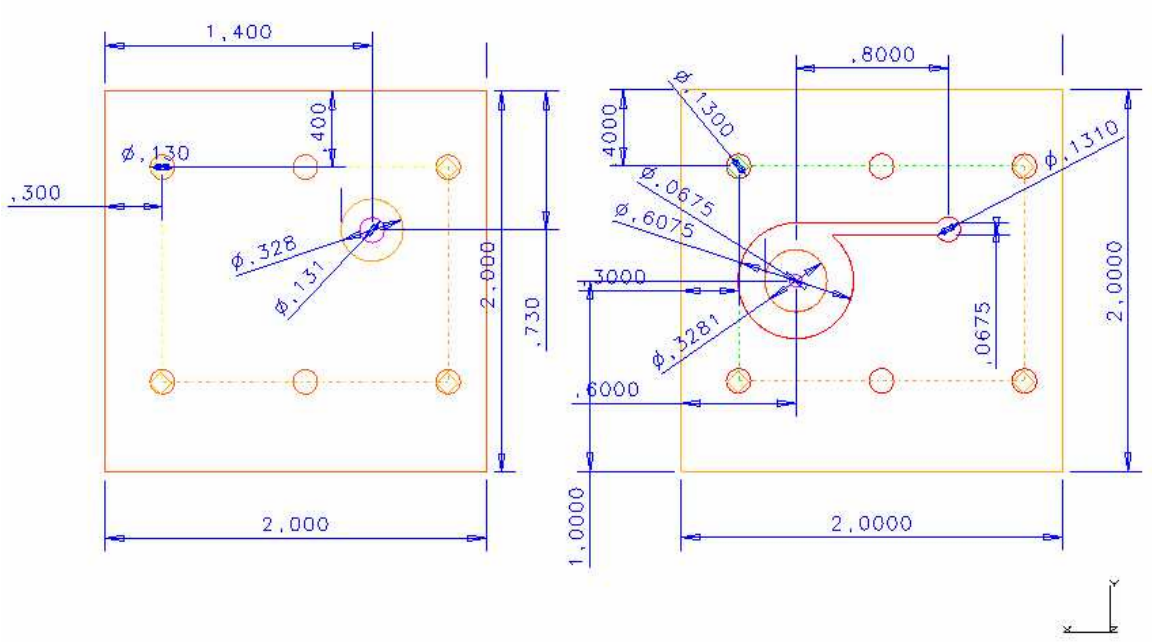

Figure D.2: Small Fluid Diode (Dimensions in inches)

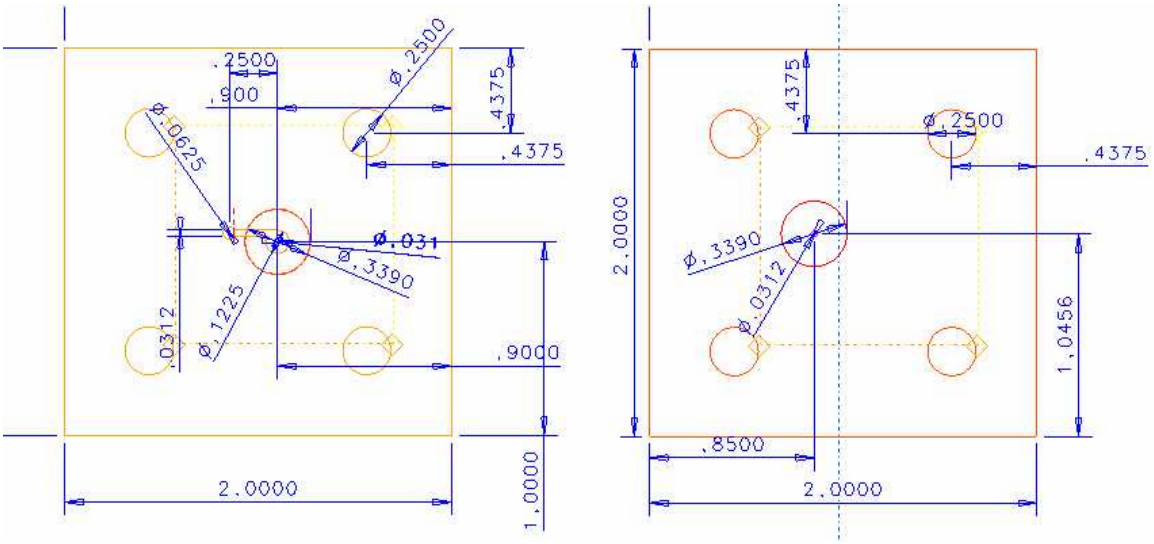

APPENDIX E

1 kHz Fluid Resonator Dimension Drawings

Figure E.1: Resonator Body (Dimensions in inches)

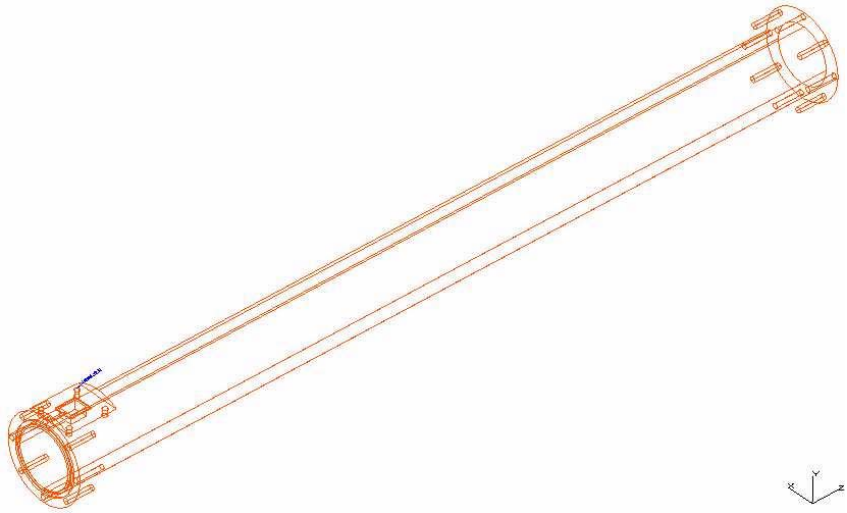

Isometric View

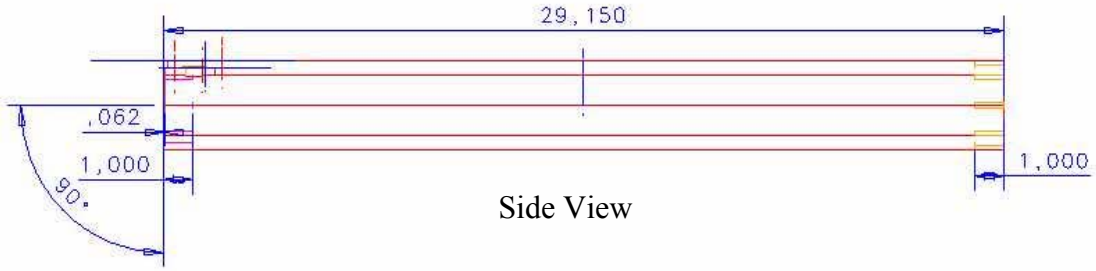

Side View

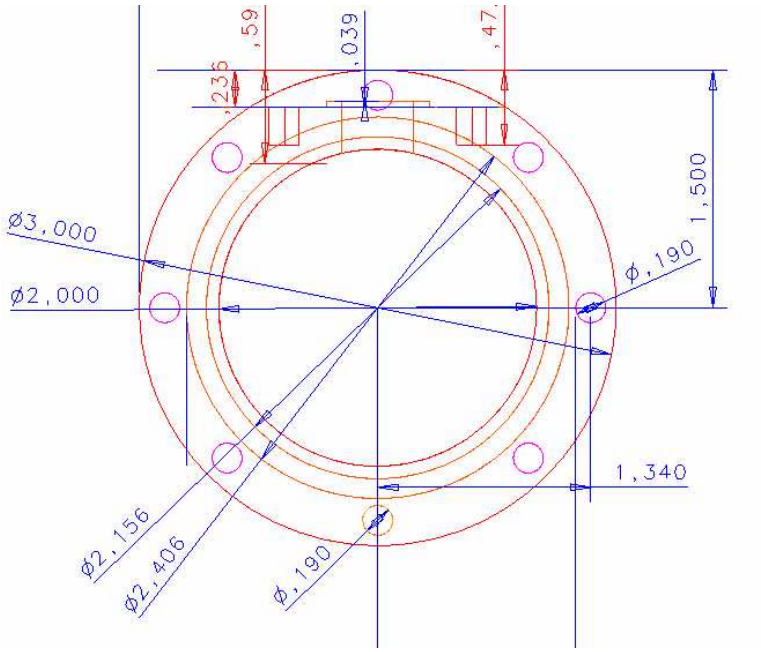

End View

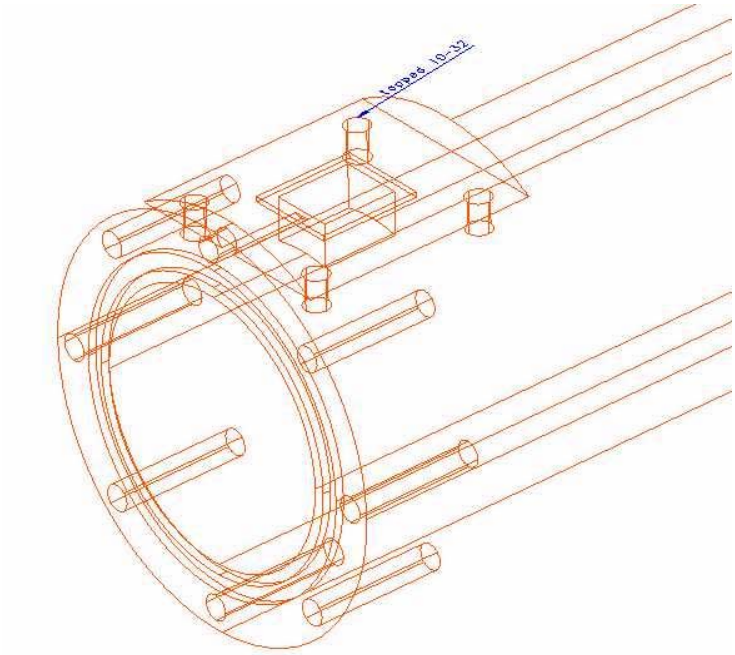

Detail of Inlet Valve End of Fluid Cavity

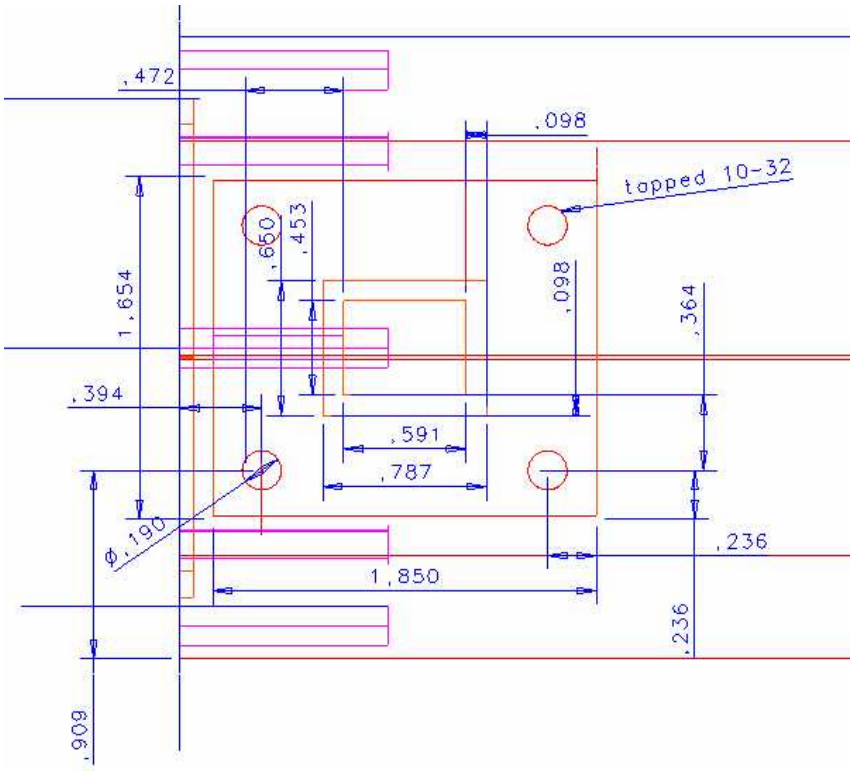

Dimensioned Detail of Inlet Valve End of Fluid Cavity

Figure E.2: Resonator Body End Cap (Dimensions in inches)

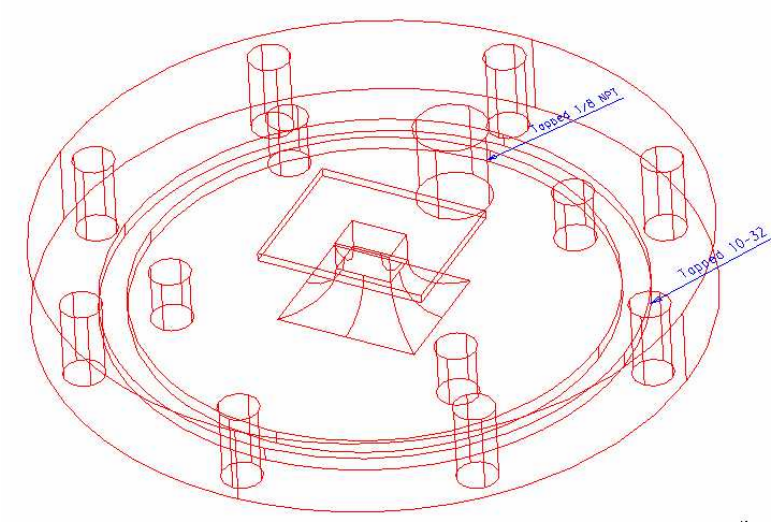

Isometric View

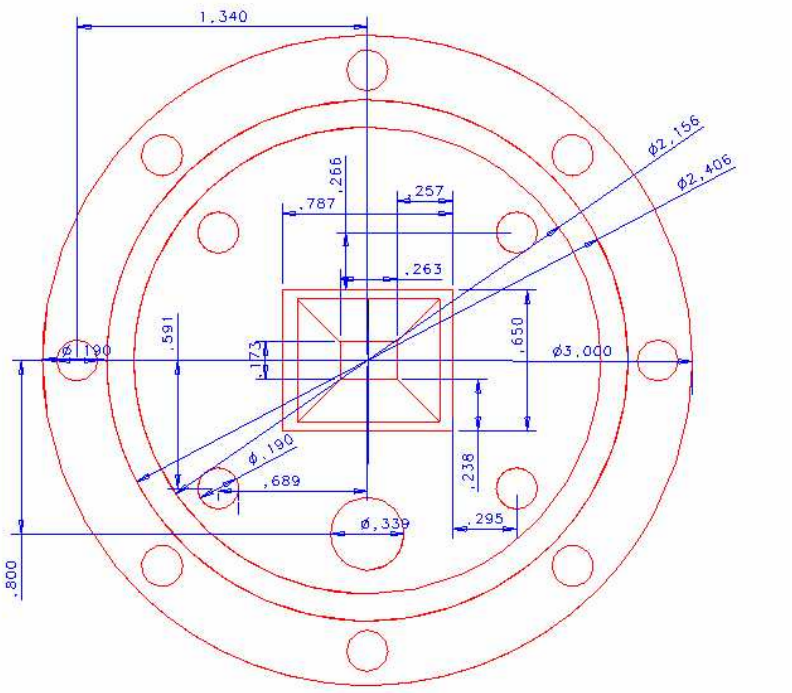

Top View

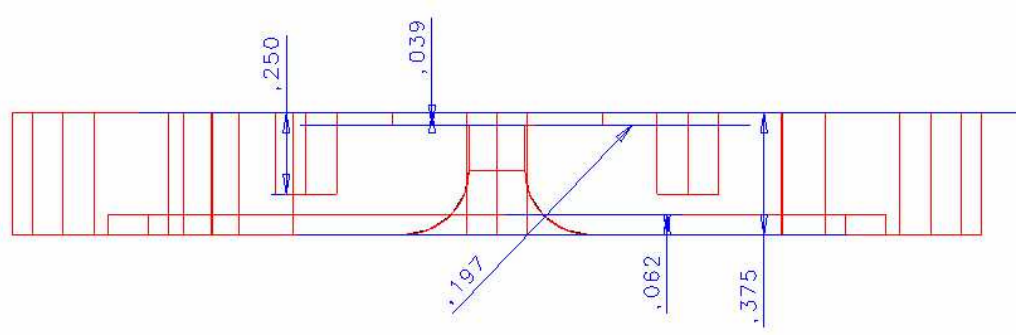

Side View

Figure E.3: Inlet Valve Cover (Dimensions in inches)

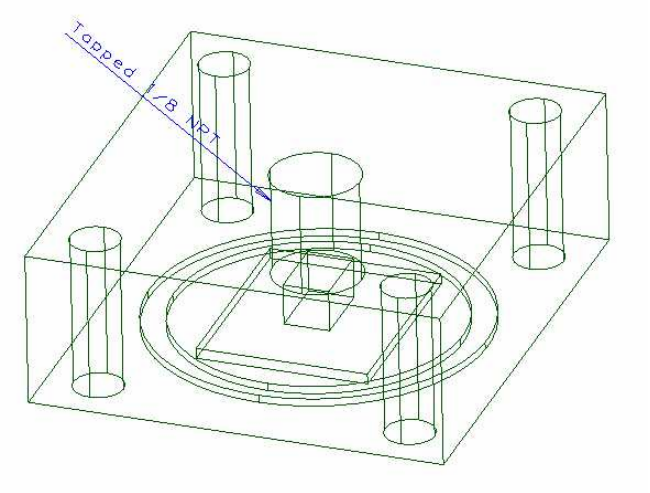

Isometric View

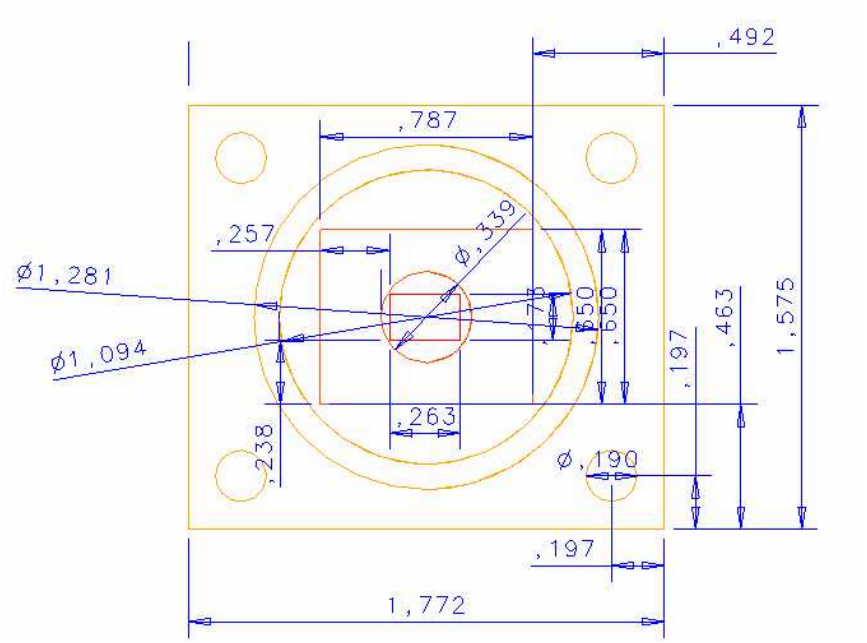

Top View

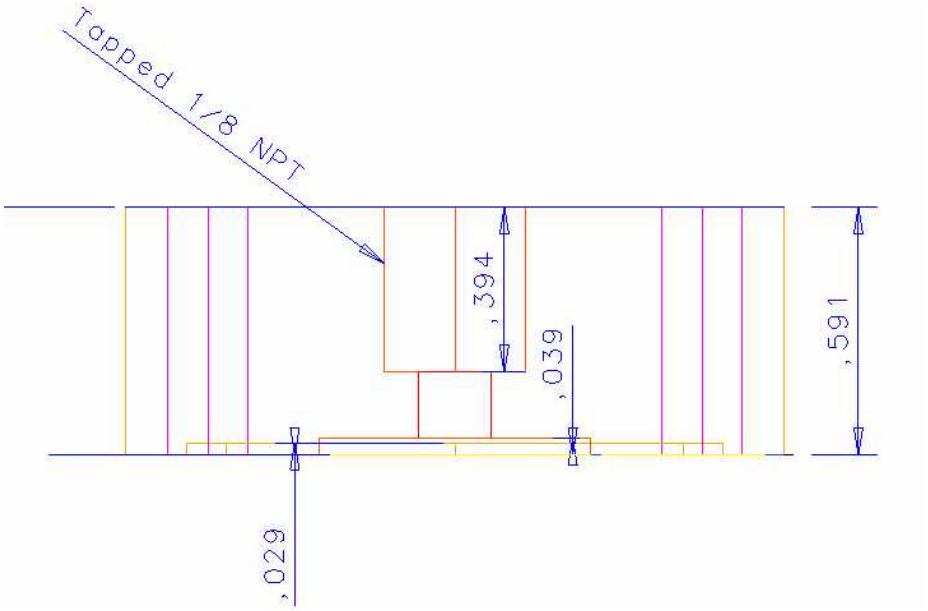

Side View

Figure E.4: Outlet Valve Cover (Dimensions in inches)

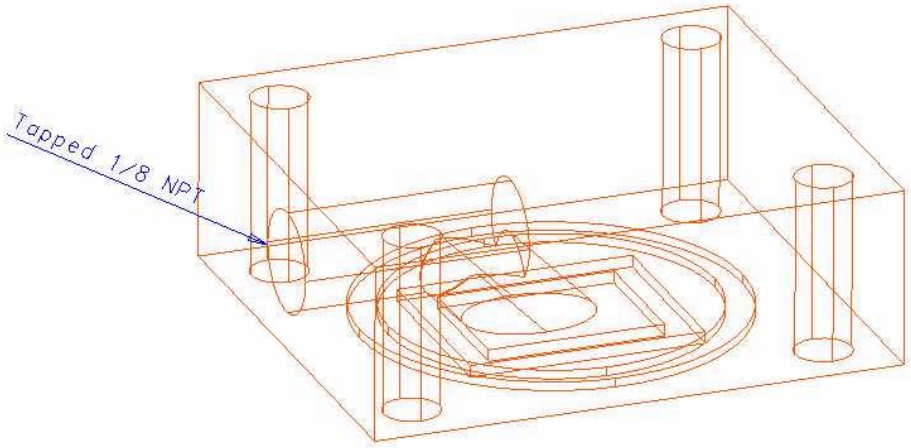

Isometric View

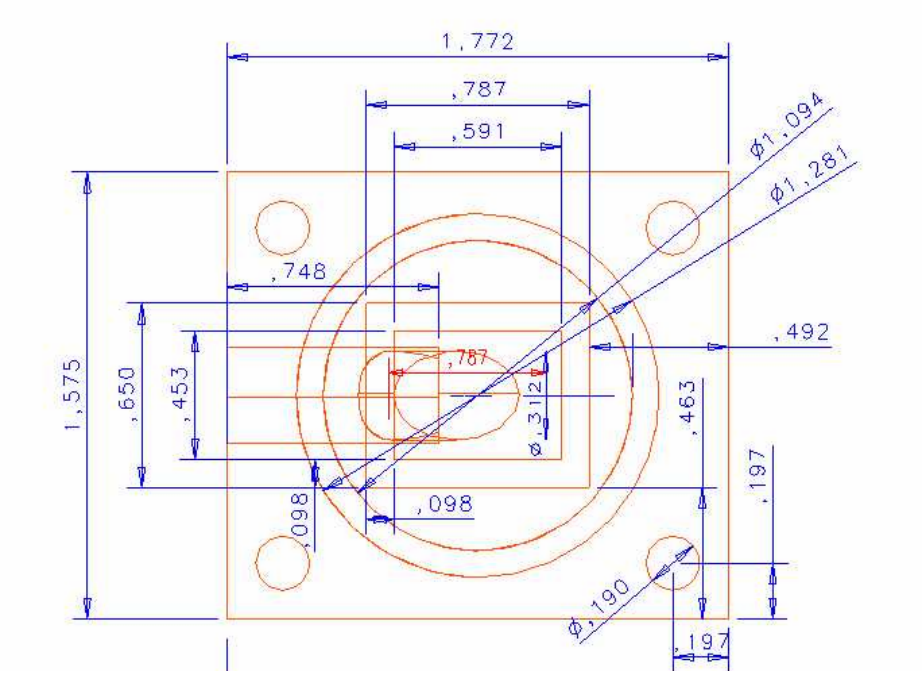

Top View

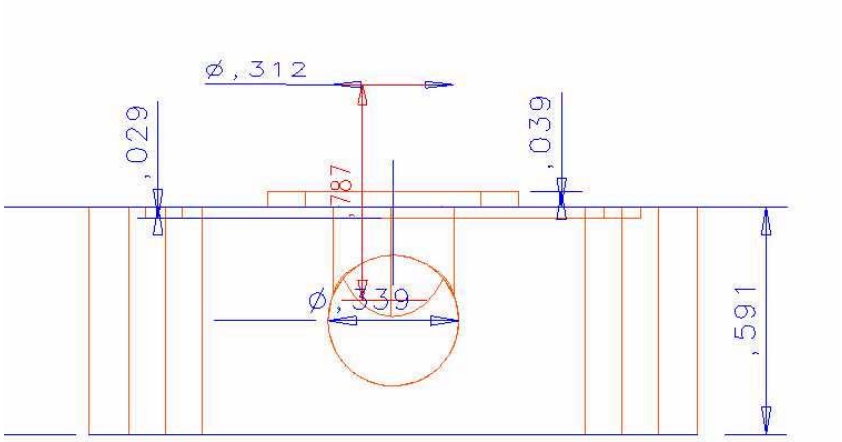

Side View

APPENDIX F

Reed Valve Dimension Drawings

Figure F.1: Reed Valve (Dimensions in inches)

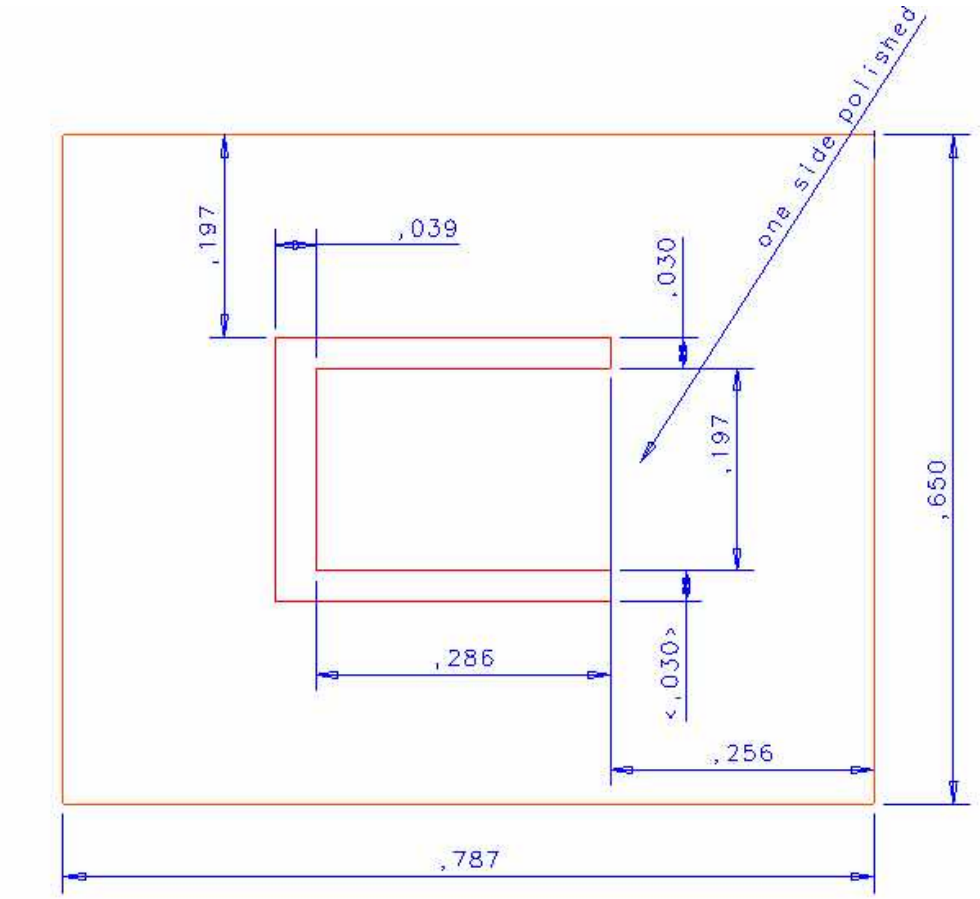

APPENDIX G

Reed Valve Pump Dimension Drawings

Figure G.1: Pump Head Base (Dimensions in mm)

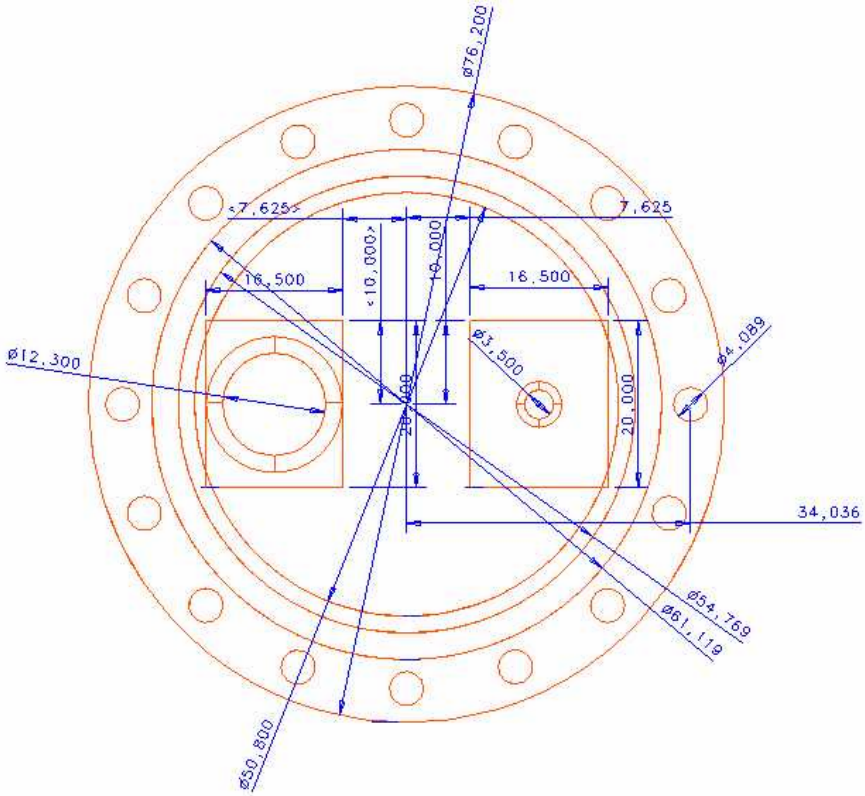

Top View

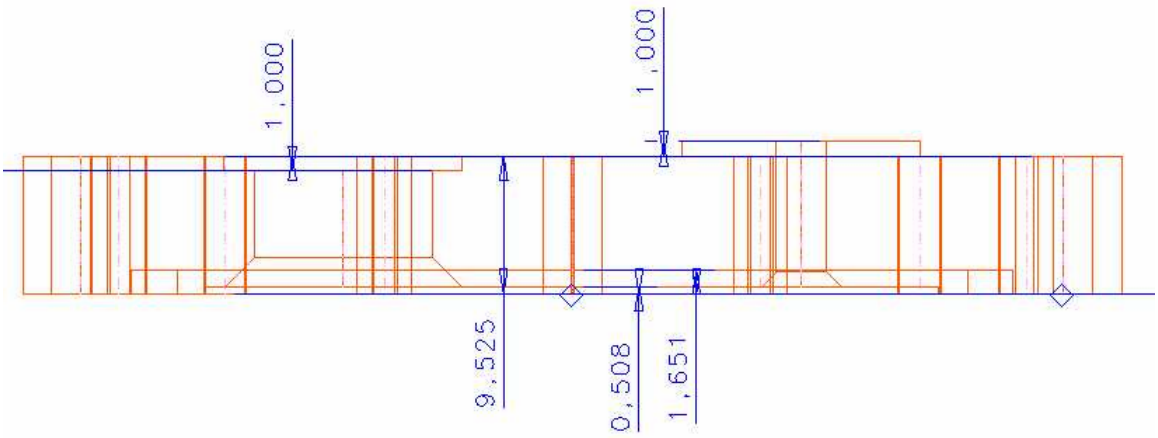

Side View

Figure G.2: Pump Head Top (Dimensions in mm)

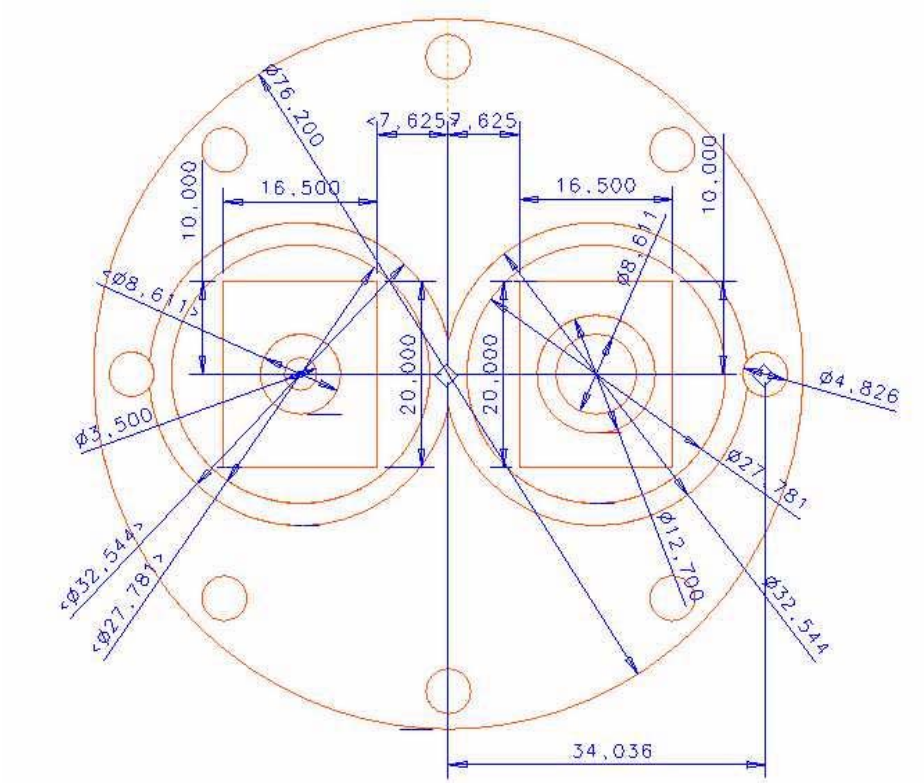

Top View

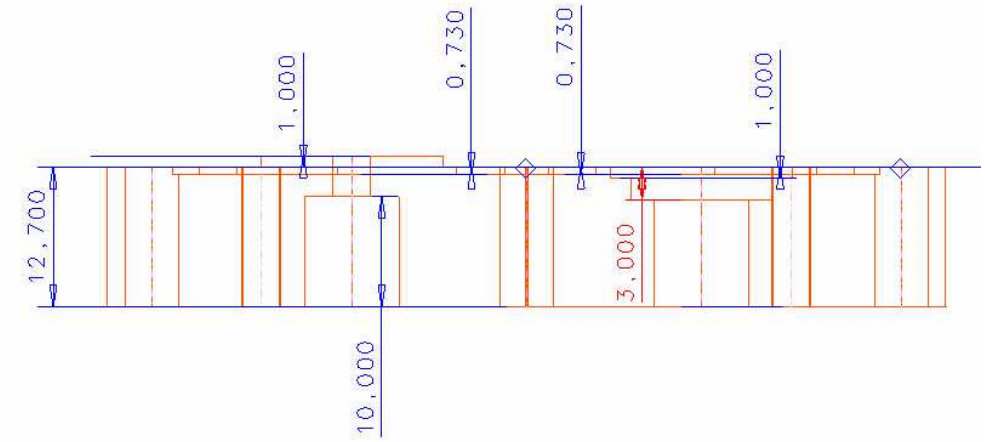

Side View

APPENDIX H

Finite Element Result for Aluminum Diaphragm

Figure H.1: Finite Element Result of .1 in. diaphragm (Top View)

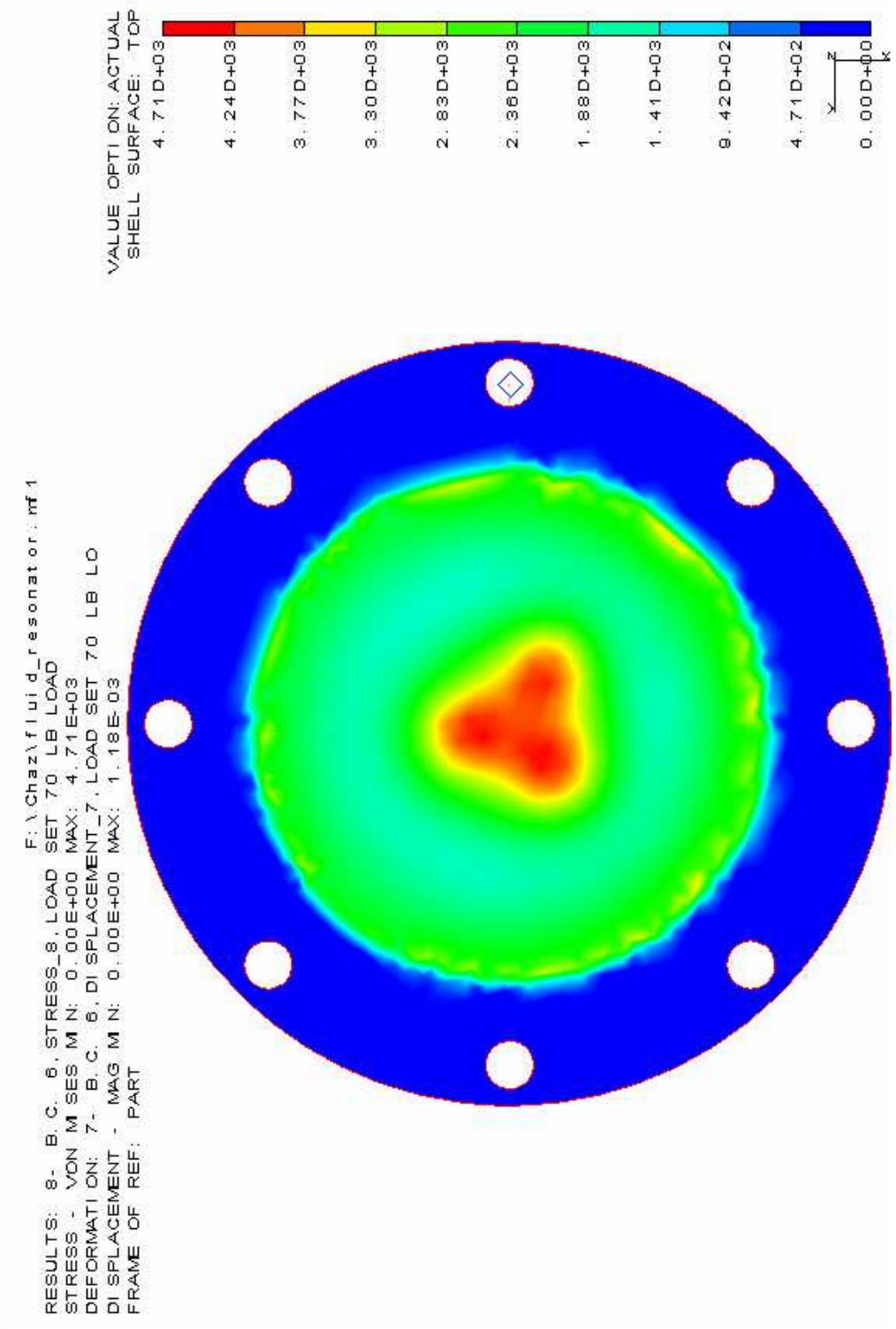

APPENDIX I

Spread Sheet Data

Figure I.1: Reed Valve Frequency Response for Fluid Resonators

Chaz Keller Reed valve design 7/25/03

steel properties (1095 carbon steel Q&T @ 200 F			chosen geometry		
density	7800	kg/m^3	t = thickness		
modulus E	2.07E+11	Pa	b=	5	mm
Sy	5.52E+08	Pa	length =		mm
Sut	8.96E+08	Pa			

possible spring steel C1095 thicknesses

0.005	in.	=	0.127	mm
0.01	in.	=	0.254	mm
0.015	in.	=	0.381	mm
0.02	in.	=	0.508	mm

dynamic equation
Not including damping from fluid

1st natural freq	10000	Hz	62831.9	rad/s
thickness (mm)	length (mm)			
0.127	3.25201			
0.254	4.59904			
0.381	5.63265			
0.508	6.50402			

1st natural freq	20000	Hz	125664	rad/s
thickness (mm)	length (mm)			
0.127	2.29952			
0.254	3.25201			
0.381	3.98288			
0.508	4.59904			

1st natural freq	2000	Hz	12566.4	rad/s
thickness (mm)	length (mm)			
0.127	7.27172			
0.254	10.2838			
0.381	12.595			
0.508	14.5434			

Figure I.2: Reed Valve Fatigue Calculations (All Applications)

Fatigue calculations

Se' = 448000000 Pa

fatigue correction factors			for valve thicknesses .005in., .010 in., .015 in., .020 in.	
C_load =	1	d_equiv =	0.64381	mm
C_size =	1		0.91048	mm
C_surf =	0.89	Ground finish	1.11511	mm
C_temp =	1		1.28762	mm
C_reliab =	0.753	99.90%		

Corrected endurance limit
Se = 2.99E+08 Pa

Maximum alternating stress allowed for infinite life by the modified Goodman criterion

sigma_a = 2.24E+08 Pa

Max stress experienced
2* sigma_a 4.48E+08 Pa MAXIMUM

Resultant displacement of reed tip (10000Hz)

0.1204	mm	MAXIMUM DISP.	for	.005 in. thk. Valve
0.1204	mm	MAXIMUM DISP.	for	.010 in. thk. Valve
0.1204	mm	MAXIMUM DISP.	for	.015 in. thk. Valve
0.1204	mm	MAXIMUM DISP.	for	.020 in. thk. Valve

Resultant displacement of reed tip (20000Hz)

0.0602	mm	MAXIMUM DISP.	for	.005 in. thk. Valve
0.0602	mm	MAXIMUM DISP.	for	.010 in. thk. Valve
0.0602	mm	MAXIMUM DISP.	for	.015 in. thk. Valve
0.0602	mm	MAXIMUM DISP.	for	.020 in. thk. Valve

Resultant displacement of reed tip (2000Hz)

6.02E-01	mm	MAXIMUM DISP.	for	.005 in. thk. Valve
6.02E-01	mm	MAXIMUM DISP.	for	.010 in. thk. Valve
6.02E-01	mm	MAXIMUM DISP.	for	.015 in. thk. Valve
6.02E-01	mm	MAXIMUM DISP.	for	.020 in. thk. Valve

REFERENCES

Elmore, William C. et al. Physics of Waves. Dover Publications, Inc.: New York, 1969.

"piezein" The American Heritage Dictionary of the English Language, Fourth Edition, 2000. Houghton Mifflin Company

Piezo Systems, Inc. www.piezo.com Cambridge, Massachusetts, 2002.

Haakh, Dr.-Ing Frieder, "Vortex Chamber Diodes as Throttle Devices in Pipe Systems. Computation of Transient Flow." Journal of Hydraulic Research, Vol. 41 No. 1 (2003): 53-59.

Hopkinson, David P. "Development of Stress Gradient Enhanced Piezoelectric Composite Unimorph Actuators." Master's Thesis. Atlanta, Georgia. Georgia Institute of Technology, 2003.

Hwang, S.C., C.S. Lynch, and R.M. McMeeking. "Ferroelectric/ferroelastic Interactions and Polarization Switching Model. Acta metall. mater. Vol. 43, No. 5, (1995): 2073-84.

Jaffe, B., W.R. Cook, and H. Jaffe. Piezoelectric Ceramics. Marietta, OH: Academic Press Limited, 1971.

Kinetic Ceramics. http://www.kineticceramics.com , 2002.

Lee, Dong Gun, Siu Wing Or, Conal O'Neill, and Gregory P. Carman. "Piezoelectric Hydraulic Pump with Innovative Active Valves." Smart Structures and Materials 2002: Smart Structures and Integrated Systems, Proceedings of SPIE Vol. 4701, (2002): 530-36.

Lynch, C.S. "The Effect of Uniaxial Stress on the Electro-mechanical Response of 8/65/35 PLZT" Acta mater Vol. 44, No. 10, (1996): 4137-4148.

Mauck, L.D. "The Role of Rate Dependence and Dissipation in the Constitutive Behavior of Ferroelectric Ceramics for High Power Applications." Ph.D. Thesis. Atlanta, Georgia, Georgia Institute of Technology, (2002).

Mauck, L.D., W.S. Oates, and C.S. Lynch, "Piezoelectric Hydraulic Pump Performance", presented at Smart Structures and Materials 2001: Industrial and Commercial Applications of Smart Structures, Proceedings of SPIE Vol. 4332, (2001): 246-253.

Mauck, L.D., Lynch, C.S., "Piezoelectric Hydraulic Pump Optimization", presented at 10th International Conference on Adaptive Structures and Technologies ICAST '99, Paris, France (1999)

Mauck, Lisa D. and Christopher S. Lynch. "Piezoelectric Hydraulic Pump Development", Journal of Intelligent Material Systems and Structures Vol. 11 (2000): 758-64.

Norton, Robert L. Machine Design: An Integrated Approach, Second Edition. Prentice-Hall. New Jersey, 2000.

Oates, William S. "Piezoelectric Pump Design and System Dynamic Model." Master's Thesis. Atlanta, Georgia, Georgia Institute of Technology, 2001.

Pan, L.S., et al. "Analytical Solutions for the Dynamic Analysis of a Valveless Micropump – A Fluid-membrane Coupling Study." Sensors and Actuators A 93 (2001): 173-181.

Park, Jung-Ho, Kazuhiro Yoshida, and Shinichi Yokota. "Resonantly Driven Piezoelectric Micropump, Fabrication of a Micropump Having High Power Density." Mechatronics 9. (1999): 687-702.

Physik Instrumente (PI), GmbH & Co. KG, Auf der Roemerstrasse, D-76228 Karlsruhe/Palmbach, Germany

Tan, Honghui, William Hurst, and Donald Leo. "Performance of a Piezohydraulic Actuation System with Active valves." Smart Structures and Materials 2002: Smart Structures and Integrated Systems, Proceedings of the SPIE. Vol. 4701 (2002): 537-51.

Ullmann, Amos, and Fono, Ilan. "The Piezoelectric Valve-Less Pump – Improved Dynamic Model." Journal of Microelectromechanical Systems Vol. 11, No. 6 (2002): 655-664.